Mechanotransduction of Head Impacts to the Brain Leading to TBI: Histology and Architecture of Subarachnoid Space

by

Parisa Saboori

A dissertation submitted to the Faculty in Engineering in partial fulfillment of the requirements for the degree of Doctor of Philosophy,
The City University of New York

2011

This manuscript has been read and accepted for the
Graduate Faculty in Engineering in satisfaction of the
dissertation requirement for the degree of Doctor of Philosophy.

	Prof. Ali Sadegh
Date	Chair of Examining Committee
	Prof. Mumtaz Kassir
Date	Executive Officer

Prof. Yiannis Andreopoulos

Prof. Peter Ganatos

Prof. Luis Cardoso

Prof. Barclay Morrison

Supervisory Committee

THE CITY UNIVERSITY OF NEW YORK

ABSTRACT

Mechanotransduction of Head Impacts to the Brain Leading to TBI: Histology and Architecture of Subarachnoid Space

by

Parisa Saboori

Advisor: Professor Ali Sadegh

Traumas involving vehicular collisions, contact sports or falls could cause relative motion between the brain and the skull leading to Traumatic Brain Injury (TBI). It has been shown that subarachnoid space (SAS) trabeculae play an important role in damping and reducing the relative movement of the brain with respect to the skull, thereby reducing traumatic brain injuries (TBI), (Zoghi and Sadegh 2010). The histology, architecture and mechanical properties of the SAS are not well established in the literature. A few investigators have estimated the mechanical properties of trabeculae based on the collagen's properties, i.e. Zhang et al (2001-2002) and Jin X et al. (2006). There is a wide range of reported values of the elastic modulus of the trabeculae up to three orders of magnitudes. Previous investigators have over simplified the complex architecture of the SAS trabeculae and have employed soft solid materials for the SAS which may have led to unreliable results.

The goal of this thesis was to investigate the mechanotransduction of head impacts to the brain with the emphasis on the role of material modeling of the subarachnoid space. This was accomplished through three aims. The first aim of this study was to investigate the histology and architecture of the SAS and in particular the trabeculae. This step was accomplished through several experimental studies including, Micro CT Scan, Histology sectioning, Two- Photon Microscopy (TPM), Scanning Electron Microscopy (SEM) and Transmission Electron Microscopy (TEM). It was concluded that the trabeculae are collagen based Type I, Kierszenbaum 2007, Van Der Rest (1991), and their architectures are in the form of tree-shaped rods, pillars, plates and, in some regions, in the form of a complex network.

The second aim of this study was to determine the stress/strain changes in the brain as a function of the material properties of the SAS. The 2D and 3D local models of the SAS were created and the effect of the SAS material properties on transferring the external load to the brain was investigated. A wide range of the mechanical properties of the trabeculae were employed and based on the validation of the models with experimental results of Sabet et al. (2009), the mechanical properties of the SAS trabeculae were determined. The result indicated that when we use soft material properties for the trabeculae the meningeal layers absorb and damp the impact load. It is also concluded that the trabeculae can be simulated as tension elements since they buckle with minimal compressive load. In addition, the mechanotransduction of the external load to the brain, through two basic local models was investigated. It was shown that, the tree-

shaped orientation of the trabecula provides more protection (less strain) for the brain tissue when the head in subjected to impacts.

The third aim of this study was to create a 3D head model and study the effect of external head impacts on the strain in the brain, leading to traumatic brain injury. A three-dimensional (3D) model of the head-neck was created and was validated against the experimental study of Feng et al (2010). The results indicate that the elastic modules of E=1000 Pa is a realistic value for the SAS. The effect of the different types of material modeling of SAS on transferring the load to brain was studied and was compared with the experimental study of Feng et al (2010). Finally, the 3D head model was subjected to a series of impact velocities and the strain in the brain as a function of applied velocity impact were determined. It has been concluded that, for the impact velocity range of 17-27 MPH, the strain in the brain varied 12-17%. The strain range is less than the 20% threshold of Traumatic Brain Injury (TBI) addressed in the literature, Meany et al. (1995) and Bayly et al. (2003). In addition, the strain in the brain is proportional to the applied impact velocity and the severity of TBI. This thesis reveals that the choice of material modeling and material properties of the meningeal layers are significant factors in determining the strain in the brain and therefore understanding different types of the head/brain injuries.

Indicated to

To my husband, my daughter and my parents
who gave me enough curiosity to learn.

ACKNOWLEGMENT

I would like to express my deep and sincere gratitude to my supervisor, Professor Ali Sadegh. His wide knowledge and logical way of thinking have been great value for me. His understanding, encouraging and personal guidance have provided a good basis for the present thesis. It was a privilege for me to study and do my research in his care.

His valuable guidance helped me to overcome any difficulty and discover new aspects in my research. He was the most encouraging people in my research to assist me to become a creative and independent researcher.

I would like acknowledge great efforts of the entire Ph.D. examining committee: Professor Yiannis Andreopoulos, Professor Peter Ganato, Professor Luis Cardoso and Professor Barclay Morrison from Columbia University for their review of this thesis, discussions, and constructive comments.

I am deeply indebted to Prof. Delale the chair of the mechanical engineering department of The City College of New York for his support during my master and Ph.D. studies.

I would like to thank Professor Latif M. Jiji who has often advised me kindly and helped me in my career.

My sincere gratitude to Professor Stephen C. Cowin who has helped me in my study and career. I really enjoyed his classes and his great way of explaining problems.

I am so grateful to staff of the department of mechanical and biomedical engineering of The City College of New York.

My special thanks to my friend in City College for all the great help and support during my Ph.D. study.

I also wish to thank Mrs. Jo Russo for revising the English of my manuscript and for her non stopping advice in my life.

I would like to thank my family, my mother Sabiheh Askari, father Aziz Saboori, my brothers Omid and Navid and my lovely sisters Arezoo and Sara for their help in guiding me to the completion of this dissertation. Their support over the years has given me the strength to reach this achievement.

Most importantly, I would like to thank my true love, Mehran, for his unlimited love, constant patience and great deal of understanding.

My endless thank to my little angel, my daughter Misha who was patient enough during all these years. She will be always six month older than my Ph.D.

Table of contents

List of Figures

List of the Tables

CHAPTER 1 Introduction

1 INTRODUCTION

Traumatic Brain Injury (TBI) is mainly due to automotive accidents, contact sports, falls or blunt impacts to the head. In recent years, it has been reported that exposure to a blast from and improvised explosive device (IED) can cause TBI. Based on Centers for Disease Control and Prevention (CDC) report, TBI is a major public health problem in the US, especially among males young people, adults ages 15 to 24, and elderly people of 75 years and older. Children age 5 and younger are also at high risk for TBI (CDC) .

Traumatic brain injury (TBI) is generally caused by contact (blunt head impact) or non-contact (angular acceleration) to the head. The breakdown of the major causes of the TBI is shown in Figure 1.1. Symptoms of the TBI can be mild, moderate, or severe, depending on the extent of the damage to the brain. CDC reports further indicate that each year about 1.7 million people experience a type of TBI in USA. Approximately 52,000 people die from head injuries and about 1.365 million, nearly 80%, of head injured people are treated in hospital emergency rooms. TBI is a major contributing factor to a third (30.5%) of all injury-related deaths in the United States, Faul et al (2010). About 75% of TBIs that occur each year involve concussions or other forms of mild TBI. Figure 1.2 shows the comparison between selected health problems in the US, (http://www.ibiblio.org). This Figure indicates that TBI has the highest number of cases compare to other health related problems.

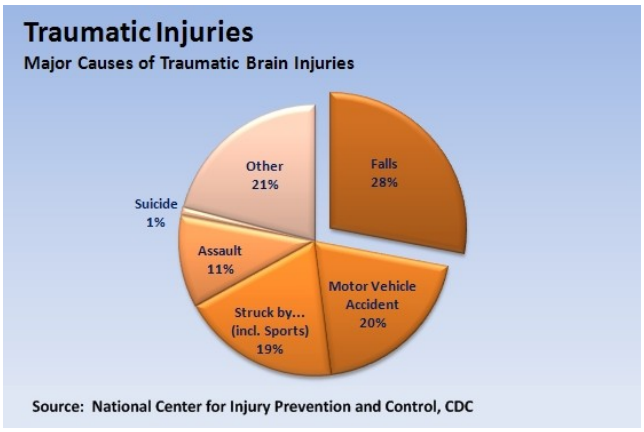

Figure 1.1 Major causes of Traumatic Brain Injury.

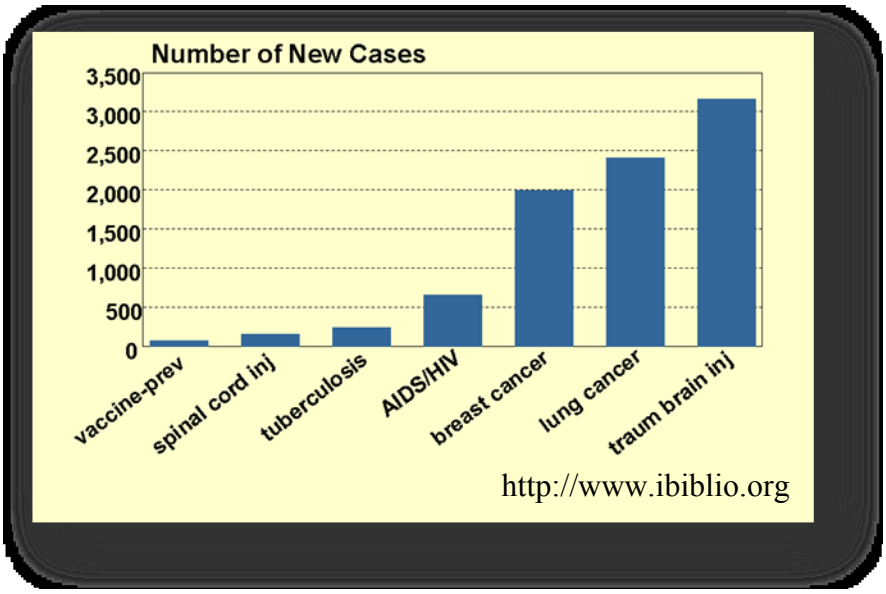

Figure 1.2 Comparison between selected health problems in the US.

Depending on the severity of the impact an injured patient with a mild TBI may remain conscious or may experience a loss of consciousness for a few seconds or minutes. Different symptoms of mild TBI may include headache, confusion, lightheadedness, dizziness, blurred vision or tired eyes behavioral and trouble with memory. A person with a severe TBI may show the same symptoms, but may also have

a continuous headache, repeated vomiting or nausea, and increased confusion, restlessness, or agitation.

Anatomically, human brain is encased in the skull and is suspended and supported by a series of fibrous tissue layers, dura mater and the three layers: arachnoid, trabeculae and pia mater, known as the meninges. In addition, cerebrospinal fluid (CSF) located in the space between the arachnoid and pia mater known as subarachnoid space (SAS) stabilizes the position of the brain during head movements. Blunt head impacts and/or non-contact angular acceleration of the head cause relative motion between the brain and the skull. This increases the normal and shear stresses in the skull/brain interface region, which leads to the rupture of cerebral blood vessels and in particular bridging veins. This may also increases the strain in the brain which causes TBI. Subarachnoid space (SAS) trabeculae play an important role in damping and reducing this relative movement of the brain with respect to the skull, thereby reducing traumatic brain injuries.

To explain the likely injury process of the brain and to quantify the response of the human head to blunt impacts, investigators have employed experimental, analytical and numerical methods. Many researchers have used the finite element (FE) method to study head/brain injuries, (Al-Bsharat 1999, Kleiven et al. 2002, Ruan et al, 1993, Zhang et al. (2001b, 2001c , 2002), Takhounts et al.(2008), Moss et al. (2009), Gupta et al (2009) and Feng et al (2010). The complicated geometry and architecture of the SAS and trabeculae makes it impossible to model all the details of the region. Thus, in these studies and other similar studies, the meningeal layers and the subarachnoid region have been simplified as a soft elastic material or in some cases as water (i.e. soft solid having

bulk modulus of water and very low shear modulus), e.g., (Kleiven et al. 2002, Zhang et al. 2001c and 2002). That is, the hydraulic damping (i.e. the fluid solid interaction) and the mechanical role of the fibrous trabeculae and the cerebrospinal fluid (CSF) in the subarachnoid space (SAS) were ignored. These simplifications, which are due to the complex architecture and random orientation of the trabeculae, could make the result unreliable.

In addition to the simplified models, the mechanical properties of SAS are not well established in the literature. A few studies (Jin X, et al. 2006, Zhang et al. 2001a and 2002), have reported a wide range of elastic modulus of trabeculae up to three orders of magnitudes. This wide range of the reported elastic modules (from $E= 59.81 \times 10^3$ Pa Jin X et al. (2006) to $E= 21.5 \times 10^6$ Pa Zhang et al (2002)) questioning the validity of these data.

The SAS that includes CSF and the trabeculae has a complex structure. This is due to abundance of trabeculae, which are in the form of rods (fibers), thin transparent plates, and tree-shaped that are extended from the arachnoid (subdural) to the pia mater. The pia mater adheres to the surface of the brain and follows all the brain contours including the folds of the cerebral and cerebella cortices. This gives the subarachnoid space a highly irregular shape and makes the flow of CSF around the brain non-laminar and complicated. The volume of CSF is highest within the cisterns regions of the brain where, due to the shape of the brain surface, the subarachnoid space is large. Arachnoid trabeculae are more concentrated in the subarachnoid cisterns, sometimes even coalescing into membranes that partially occlude the subarachnoid space. This interaction

between the CSF and the trabeculae suggests that their functions are not independent. The interaction between the fluid and solid phase mechanically support the brain.

While the functionality of the SAS is understood, the histology and biomechanics of this important region has not been fully investigated. It is understood, however, that the arachnoid is a thin vascular layer composed of layers of fibroblast cells interspersed with bundles of collagen. The trabecula is also a collagen based structure. Only the histology of the trabeculae of the optical nerves has been studied (Killer et al. 2003a). To the best of our knowledge the histology of the human brain trabeculae has not been addressed in the literature.

The goal of this thesis was to investigate the mechanotransduction of the head impacts to the brain with the emphasis on the role of material modeling of the subarachnoid space as it relates to Traumatic Brain Injuries (TBI). That is, to establish a criterion for the range external impacts magnitude to the head which causes concussion or TBI. This investigation was achieved through three aims. The first aim involved, histology and experimental study of the subarachnoid space, as it is explain in chapter 5. The second aim of this study was to determine the stress/strain changes in the brain as a function of the material properties and the material modeling methodology of SAS, as it is reflected in chapter 7, 8, 9and 10. The third aim of this study was to create a 3D head model and study the effect of impacts on the brain, leading to traumatic brain injury, as it is explained in chapter 11.

As the first aim of this study, the histology and the architecture of the trabeculae through in-vitro and in-vivo (animal) studies, were investigated by Saboori and Sadegh

(2009, 2010a). Specifically, in the first experimental study, we employed a Micro CT scan and Mimics Software and studied the 3D random structure of the trabeculae. In second in-vitro experiment, the solidified samples of the brain tissues were sliced using vibratome, and were dyed through standard procedure for fluorescent and con-focal microscopy. In our third in-vivo experimental study, we used a live Sprague-Dawley (SD) rat and Two – Photon Microscopy (TPM) to investigate the histology of the SAS. The fourth and fifth experimental studies were performed using the SD rat and electron microscopy to study the architecture and histology of the trabeculae. Our experimental studies reveal that the trabeculae are collagen based of Type I, Kierszenbaum (2007) , Van Der Rest (1991), and their architectures are in the form of tree-shaped rods, pillars, plates and in some areas in the form of complex network. The details of the experimental studies are presented in chapter 5.

The second aim of this study was to determine the stress/strain changes in the brain as a function of the material properties and the modeling methodology of SAS. This aim is explain through chapters 7, 8, 9 and 10. To achieve this aim, a wide range of the material properties of the trabeculae were examined through a series of modeling and the results were validated by the experimental results of Sabet et al.(2007). Through several models, it was shown that the material properties of the meningeal layer is a significant factor in determining the strain in the brain and therefore understanding different types of the brain/head injuries. While there have been many finite element studies of the brain/head models there are limited analytical models of SAS in the literature. One of the objectives of this aim was to mathematically model the subarachnoid space (SAS) and to

investigate the biomechanics of CSF flow through trabecular architecture in the subarachnoid space. Another objective of this aim was to study the mechanotransduction of the external load to the brain, through two basic local models. It was shown that, the tree-shaped orientation of the trabecula, where the branches are attached to the arachnoid mater, provides more protection (less strain) for the brain tissue when the head in subjected to impacts.

The third aim of this study was to create a 3D head model and study the effect of the various impacts to the brain, leading to traumatic brain injury, as it is explained in chapter 11. The 3D head model was created and validated against experimental study of Feng et al. (2010). The 3D model was used to investigate the material modeling for SAS. Finally the strain in the brain as a function of applied velocity impact was determined.

The details description of each chapter are as follow. In chapter two the anatomy of the human head and the brain is discussed. Background study of traumatic brain injuries (TBI) is presented in chapter 3. Some of the literature reviews consisting of experimental, analytical and finite element models are discussed in chapter 4. In the chapter 5, as the first aim, the histology and architecture of the SAS, and in particular the trabeculae, are investigated. This step was accomplished through five different experimental studies, micro CT Scan machine, Histology sectioning, Two- Photon Microscopy (TPM), Scanning Electron Microscopy (SEM) and Transmission Electron Microscopy (TEM). The specific material properties of the head/brain are presented in details in chapter 6.

In chapter 7 and 8, as the second aim, the stress/strain changes in the brain as a function of the mechanical properties and the modeling methodology of the trabeculae, when the loading and the boundary conditions of the model are kept the same, were investigated. This study was performed through several modeling steps. The 2D and 3D local models of the SAS was created to investigate the effect of the SAS material properties on transferring the external load to the brain. From the result of these analyses it was concluded that the load or the impact is directly transmitted to the brain if the material property of the trabecula reported by Zhang et al. (2002) , $E=21.5x10^6$ Pa, is used. That is, if the young modules reported by Zhang et al. (2002) is used, the SAS region is unable to absorb under the impact load and causes the direct transition of the load to the brain. In addition, the transverse, lateral and sagittal models of the human head using MRI images of an adult female patient were created. A wide range of the mechanical properties of the trabeculae were employed, and the transductions of blunt impact loads from the skull to the brain were investigated. Based on the validation of the models with the experimental results of Sabet et al. (2009) the mechanical properties of the SAS trabeculae were determined, i.e. Young's modules of 1150 Pa. The results indicated that when we use softer material properties for a trabecula the meningeal layers absorb and damp the impact load. It is also concluded that the material properties of the trabeculae can be simulated by only a tension element since the trabeculae buckles with minimal compressive load.

As a part of the second aim, the mechanics of CSF flow through the SAS was investigated in chapter 9. This step was accomplished through analytical and numerical

studies and a unit cell model of a single trabecula. The trabecular buckling, due to velocity boundary condition, was studied and was compared with the finite element study. In addition, Darcy's law was used to estimate the permeability of the SAS when it is considered as a porous media. The results of this study confirmed the validity of the proposed structural unit cell model and the results of the analytical solutions. The results also indicate that Darcy's permeability is an appropriate model for the SAS. This study can be used as a basis to further investigate the transduction of mechanical and hydrodynamic forces through the SAS.

To further investigate the mechanotransduction of the external load to the brain, in chapter 10, two basic local models, that is, one with a tree-shaped and the other with an inverted tree-shaped of a single trabecula connecting the pia mater to the arachnoid were created and analyzed. The results of the analyses of the models revealed that the brain's strain, displacement and stress fields with the tree-shaped trabecula is less than that of the inverted one. The results of this study will lead to accurately modeling of the SAS and thereby determining the strain in the brain.

In chapter 11 the third aim of this study, which was to create a 3D head model, is presented. In this chapter, specifically, a three-dimensional (3D) model of the head-neck, using the magnetic resonance imaging (MRI) and Abaqus/CAE Sketch modules, was created. As the first objective of this aim, the 3D head model was validated against the experimental study of Feng et al. (2010). The validation indicates that the proposed Young's modulus (E) of 1000 Pa is a reliable and appropriate value for the SAS. The proposed value of E also suggests that the SAS material is soft and absorbs the brain

movement with respect to the skull. This confirms our hypothesis on the functionality of the SAS which act as a damper and a shock absorber of the brain. As the second objectives of this aim, in chapter 11, the effect of the different type of material properties of SAS on transferring the load to brain was studied. The results of these analyses provide the best material property for each types of the material modeling of SAS. As the third objectives of this aim reflected in chapter 11, strains in the brain as a function of applied velocity impacts was determined. The impact analyses reveals that the velocity speed on the frontal head is proportional to the maximum strain in the brain leading to different types of TBI. It has been concluded when the applied impact velocity to the head varies from 2.5 MPH to 27 MPH, the maximum strain in the brain increase from 2% to 20%.

For the safety reasons, human and animal experimental studies are restricted to a mild impact or a low acceleration. Therefore validated computer models are valuable tools for investigators to quantify the strain in the brain leading to TBI. The analysis of the impact velocities revealed that, for the velocity impacts of 17-25 MPH, the stain in the brain varied in the range of 12-17%. This strain is less than the %20 strain threshold of the brain injury (TBI) addressed in the literature, Meany et al. (1995) and Bayly et al. (2003). This thesis reveals that the material properties of the meningeal layer is a significant factor in determining the strain in the brain and therefore understanding different types of the brain/ head injuries as it is briefly describe in chapter 12. In Chapter 13, the future experimental and finite element studies are presented.

CHAPTER 2 Anatomy

2 ANATOMY

The brain is the most important part of the human body. Head represent only 2% of the total body weight and it dominates 25% of the volume of the body. In anatomy, the head of an animal is the rostral part that usually comprises the brain, eyes, ears, nose and mouth.

Brain controls everything from our blood pressure to the release of molecules affecting our mood. This structure has developed a complex vascularization as well as an efficient protective system to preserve integrity and functioning of the whole body as much as possible. We can describe the head as consisting four different parts: Scalp, Skull, Meninges and the Brain, (Moore, 1999), Figure 2.1.

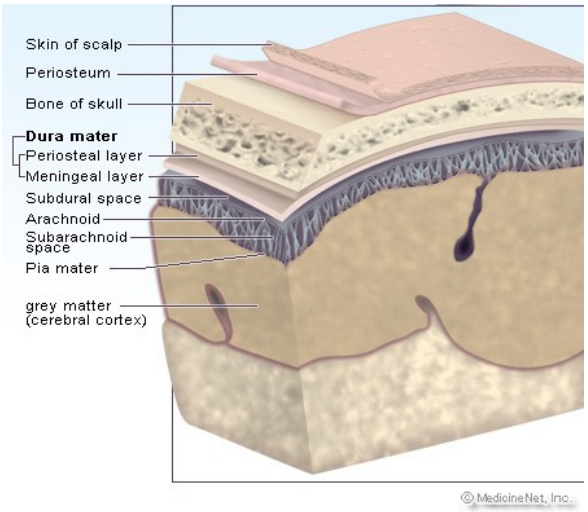

Figure 2.1 Different layers of the human head.

2.1 Scalp

Scalp is the most outer layer of the head and it is bordered by the face and the neck . The scalp extends from the external occipital protuberance and superior nuchal lines to the supraorbital margins. It is consists of 5 layers: the skin, connective tissue, epicranial aponeurosis, loose areolar tissue, and pericraniu, Figure 2.2. The first 3 layers are bound together as a single unit which can move along the loose areolar tissue over the pericranium and adherent to the calvaria.

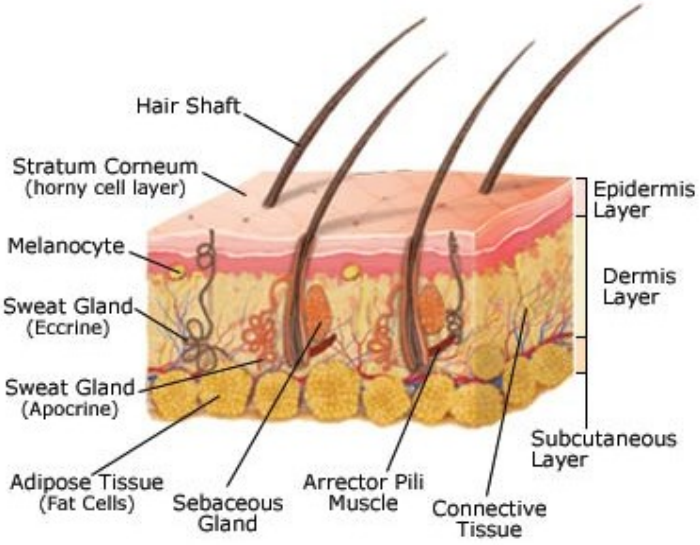

Figure 2.2 Scalp anatomy. (tree.com)

2.2 Skull

Skull is the bony structure of the head which include cranial and facial bones and it protects the brain from injury. In humans, the skull normally includes 22 bones. Except for the mandible, all of the bones of the skull are joined together by sutures, rigid

articulations allowing very little movement. There are eight bones, including one frontal, two parietals, one occipital bone, one sphenoid, two temporals and one ethmoid to protect the brain. Fourteen bones form thesplanchnocranium, the bones supporting the face. The skull contains the sinus cavities. The exact functions of the sinuses are unclear; they may contribute to decreasing the weight of the skull with a minimal decrease in strength, or they may be important in improving the resonance of the voice. Figure 2.3 shows skull anatomy.

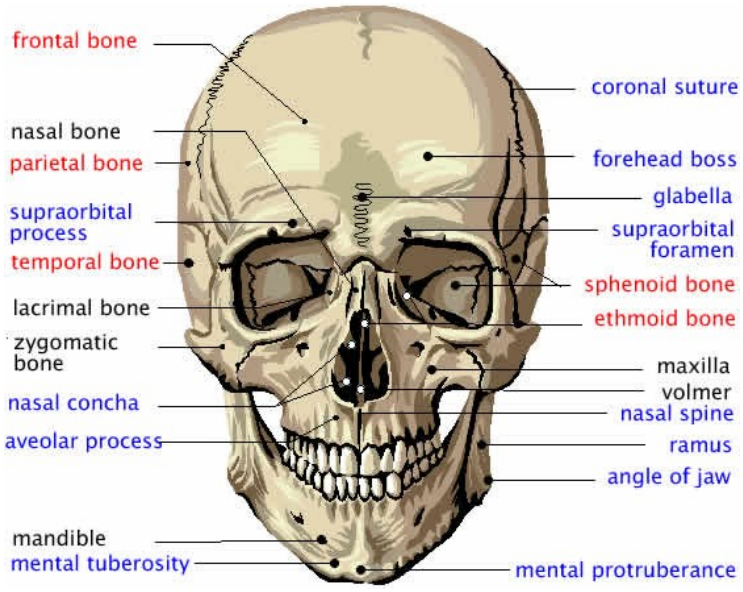

Figure 2.3 Skull anatomy. (face-and-emotion.com)

2.3 The Meninges

The Meninges is the second protecting layer for the brain. The meninges layer consists of three layers, the dura, the arachnoid and the pia mater. Figure 2.4 shows sagittal and lateral view of meninges layer. Each of these layers has a different

architecture and function. The primary function of the meninges and the cerebrospinal fluid (CSF) is to protect the central nervous system.

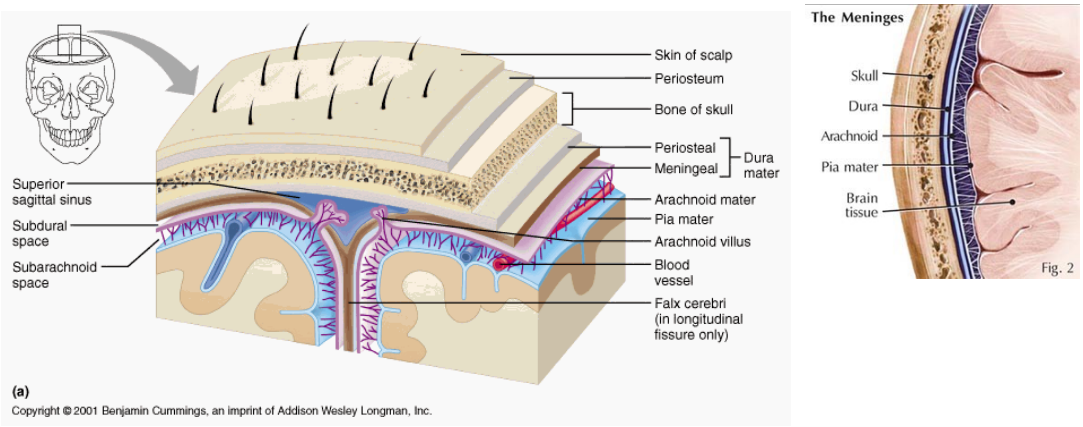

Figure 2.4 Sagittal and lateral view of meninges layer.

2.3.1 The Dura mater

The Dura mater is a thick, durable membrane, closest to the skull. It consists of two layers, the periosteal layer which lies closest to the calvaria, and the inner meningeal layer which lies closer to the brain above the subarachnoid space. Figure 2.5 shows the dura mater in spinal cord. Larger blood vessels in dura mater split into the capillaries in the pia mater. It is composed of dense fibrous tissue, and its inner surface has the same type of cell as the pia mater and the arachnoid. It also has several vein-like sinuses that help carry oxygen-rich blood back to the heart after it has traveled to the brain. While these veins have no valves, they allow for drainage of normal blood flow. In excessive bleeding an anomalous amount of blood will gather between the dura mater and the arachnoid, this state is known as subdural hematoma and it is usually the result of head injury from a trauma. Similarly, a collection of blood between the dura mater and the

inner skull is called an epidermal hematoma and is typically the result of arterial bleeding.

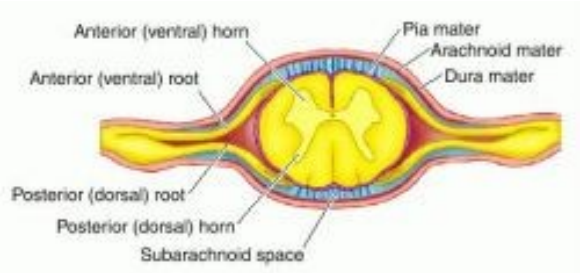

Figure 2.5 The dura mater in spinal cord. (medical-dictionary.thefreedictionary.com)

2.3.2 The Arachnoid mater

The Arachnoid mater is a delicate layer which is attached to the inside of the dura and environs the brain and spinal cord but does not line into brain's folds (sulci). It is one of the three meninges layer the membranes that cover the brain and spinal cord. The arachnoid mater provides a cushioning effect for the central nervous system. It is a thin, transparent membrane and composed of fibrous tissue like the pia mater, and is covered by flat cells also thought to be impermeable to fluid. Since it does not follow the convolutions of the surface of the brain the layer looks like a loosely fitting sac. Figure 2.6 shows the arachnoid mater around the brain.

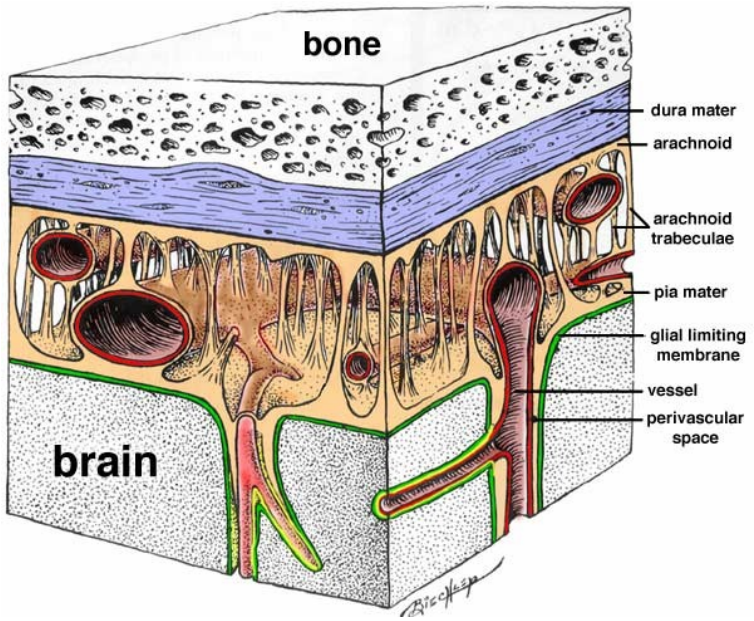

Figure 2.6 The arachnoid mater. (vanat.cvm.umn.edu)

The space bellow the arachnoid mater called subarachnoid space (SAS) and serebrospinal fluid (CSF) under this membrane in the subarachnoid space, which is full of the delicate fibers of the arachnoid extending down to attach to the pia mater (called trabeculae). The portions covering the brain and spinal cord are called arachnoidea encephali and arachnoidea spinalis, respectively. The arachnoid and pia mater are sometimes considered as a single structure, the leptomeninx, or the plural version, leptomeninges, (Lepto- from the root meaning thin in Greek). Similarly, the dura in this situation is called the pachymeninx.

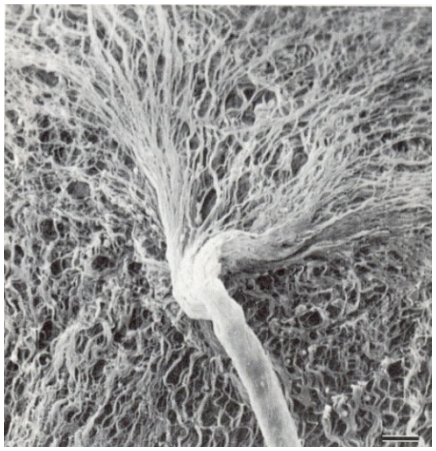

Figure 2.7 Scanning Electron Microscopes (μ 240) of an arachnoid trabeculae (Alcolado et al. 1988).

2.3.3 The Trabecula

The trabecula is a very thin and microscopic tissue level, it can be found in the form of a beam, plate, strut or rod, providing mechanical support for some soft solid region. It is mostly composed of dense collagenous tissue. Trabecula are tension elements supporting and suspending the brain from a sudden trauma or an impact, and along with CSF fluid, they can be found around the brain, optic nerve and spinal cord. Figure 2.7 is the SEM view of an arachnoid trabeculae (Alcolado et al. 1988). And Figure 2.8 shows the trabeculae tissue on the patient with Alzheimer.

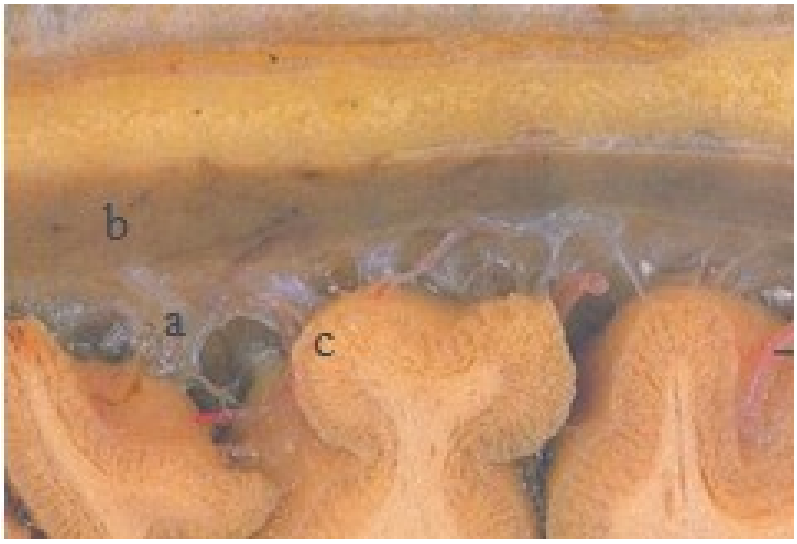

Figure 2.8 Cross section of the skull and the brain. **a**: trabeculae tissue between arachnoid and pia mater, **b**: dura mater, **c**:the gray mater, Ruan et al. 1993.

2.3.4 The cerebral spinal fluid (CSF)

The cerebral spinal fluid (CSF) is produced from arterial blood in the choroid plexuses of the lateral and fourth ventricles with combined process of diffusion and active transfer. A small amount is also produced by ependymal cells. CSF and trabecula acts as a shock absorber which protects the brain from impacts and supports the venous sinuses. CSF also has a great roll in homeostasis and metabolism of the central nervous system (CNS). The choroid plexus (CSF Generation) consists of bunches of capillaries with thin fenestrated endothelial cells. The total volume of CSF in the adult is about 140 ml. The volume of the ventricles is about 25 ml. CSF is produced at a rate of 0.2 - 0.7 ml per minute or 600-700 ml per day. The circulation of CSF is obtained with the pulsations of the choroid plexus and by the motion of the cilia of ependymal cells. CSF is absorbed across the arachnoid villi into the venous circulation. The arachnoid villi act as one-way

valves between the subarachnoid space and the dural sinuses. In the study of Gupta et al. (2011), the morphology of the SAS with its complex trabecula structures was modeled as a porous media with anisotropic permeability. Finite-volume was used to solve the governing equations. They observed a total pressure variation from -42 Pa to 40 Pa within one cardiac cycle in the investigated domain. Their study revealed that the maximum CSF velocities of 15 cms occurred in the inferior section of the aqueduct, 14 cms in the left foramen of Luschka, and 9 cms in the foramen of Magendie. Flow velocities is varied in different region of the brain. The observed transient flow patterns indicate a compliant behavior of the cranial subarachnoid space.

There are some abnormities about CSF; 1) Blood may be spilled into the CSF by accidental puncture of a leptomeningeal vein during entry of the LP needle. This blood may stain the fluid that is drawn initially and clears gradually. If it does not clear, blood indicates subarachnoid hemorrhage. Erythrocytes from subarachnoid hemorrhage are cleared in 3 to 7 days. A few neutrophils and mononuclear cells may also be present as a result of meningeal irritation. Xanthochromia (blonde color) of the CSF following subarachnoid hemorrhage is due to oxyhemoglobin which appears in 4 to 6 hours and bilirubin which appears in two days. Xanthochromia may also be seen with hemorrhagic infarcts, brain tumors, and jaundice". 2) Increased inflammatory cells (pleocytosis) may be caused by infectious and noninfectious processes. Polymorphonuclear pleocytosis indicates acute suppurativ meningitis. Mononuclear cells are seen in viral infections (meningoencephalitis, aseptic meningitis), syphilis, neuroborreliosis, tuberculous meningitis, multiple sclerosis, brain abscess and brain tumors.

Generally they are four primary functions for CSF:

Buoyancy: The actual mass of the human brain is about 1400 grams, but the net weight of the brain suspended in the CSF is equivalent to a mass of 25 grams, Noback et al. (2005), The brain therefore exists in neutral buoyancy, which allows the brain to maintain its density without being damaged by its own weight, which would cut off blood supply and kill neurons in the lower sections without CSF, Saladin et al. (2007).

Protection: CSF protects the brain tissue from injury in impacts. In certain situations such as auto accidents or sports injuries, the CSF cannot protect the brain from severe contact with the skull it then can causing hemorrhaging, brain damage, and sometimes death, Saladin et al. (2007).

Chemical stability: CSF flows throughout the inner ventricular system in the brain and is absorbed back into the bloodstream, rinsing the metabolic waste from the central nervous system through the blood-brain barrier. This allows for homeostatic regulation of the distribution of neuroendocrine factors, to which slight changes can cause problems or damage to the nervous system.

Prevention of brain ischemia: The prevention of brain ischemia is made by decreasing the amount of CSF in the limited space inside the skull. This decreases total intracranial pressure and facilitates blood perfusion.

2.3.5 The Pia mater

The Pia mater is the delicate innermost layer of the meninges. It is membrane-like that surrounds the brain and the spinal cord. The thin, mesh-like pia mater closely

envelops the entire surface of the brain, running down into the fissures of the cortex. It is the lowest layer of the meninges and supplies blood to the superficial areas of the cortex. It also supports and covers larger blood vessels passing over the surface of the brain. The pia mater is anchored to the brain by the processes of astrocytes. It joins with the ependyma which lines the cerebral ventricles to form choroid plexuses that produce cerebrospinal fluid. In the spinal cord, the pia mater attaches to the dura mater by denticulate ligaments which pass through the arachnoid mater. Figure 2.9 shows the pia mater, arachnoid and the SAS in human head

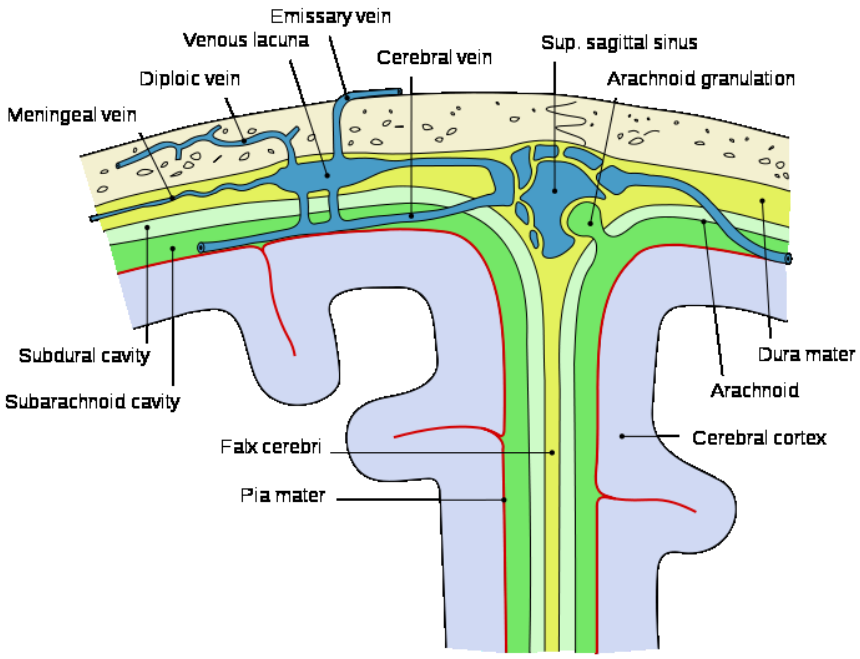

Figure 2.9 The pia mater, arachnoid mater and the SAS in human head.

(en.wikipedia.org)

2.4 The Brain

The brain is the center of the human nervous system and is a very complex organ. It is encased in the cranium. Human brain weights almost three times more than brain in same body size mammals because of its function in humans. Most of the extra weight comes from the cerebral cortex, a convoluted layer of neural tissue that covers the surface of the forebrain. Especially expanded are the frontal lobes, which controls executive functions such as self-control, planning, reasoning, and abstract thought and the portion of the brain which controls the vision is also greatly enlarged in human beings, Figure 2.10 shows the anatomy of the brain.

The brain monitors and regulates the body's actions and reactions. It continuously receives sensory information, and rapidly analyzes this data and then responds, controlling bodily actions and functions. The brainstem controls breathing, heart rate, and other autonomic processes that are independent of conscious brain functions are controlled with the brain stem. The neocortex is the center of higher-order thinking, learning, and memory. The cerebellumis is responsible for the body's balance, posture, and the coordination of movement.

The brain is protected by the thick bones of the skull and is suspended in cerebrospinal fluid. It is isolated from the bloodstream by the blood-brain barrier. The delicate nature of the human brain makes it susceptible to many types of damage and disease. Closed head injuries are one of the most common brain injuries. Others injuries may be summarized as blow to the head, a stroke, or poisoning by a wide variety of

chemicals that can act as neurotoxins. Because of the barriers that protect the brain usually there is no infection of the brain, but is very serious when it occurs. The human brain is also susceptible to degenerative disorders, such as Parkinson's disease, multiple sclerosis, and Alzheimer's disease. A number of psychiatric conditions, such as schizophrenia and depression, are widely thought to be caused, at least partially, by brain dysfunctions, although the nature of such brain anomalies is not well understood.

The adult human brain weighs about 3 lb with a volume of around 1130 cm^3 in women and 1260 cm^3 in men. Men with the same body height and body surface area as women have on average 100g heavier brains. The brain is very soft, like very soft gelatin or firm tofu. The brain consists of two parts: gray mater and white mater. The white mater is pinkish color in the interior part of the brain and the gray mater is live cortex and darker than white mater. At the age of 20, a man has around 176,000 km and a woman, about 149,000 km of myelinated axons in their brains.

The cerebral cortex is nearly symmetrical, with left and right hemispheres. Anatomists predictably divide each hemisphere into four "lobes", the frontal lobe, parietal lobe, occipital lobe, and temporal lobe.

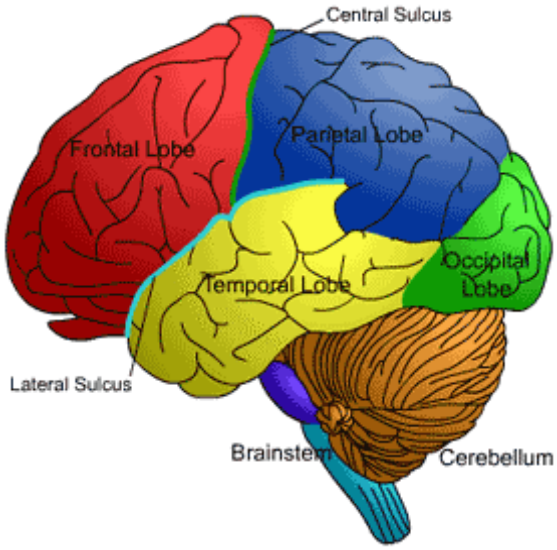

Figure 2.10 The human brain anatomy.

Brain pathology: Clinically, death is defined as an absence of brain activity as measured by Electroencephalography (EEG). Injuries to the brain tend to affect large areas of the organ, sometimes causing major deficits in intelligence, memory, personality, and movement. Head trauma may be caused by vehicular or industrial accidents and it is a leading cause of death in youth and middle age. In many cases by fall, contact sport, vehicular or industrial accidents and it is a leading cause of death in youth and middle age. In many cases, more damage is caused by resultant edema than by the impact itself. Stroke, caused by the blockage or rupturing of blood vessels in the brain, is another major cause of death from brain damage.

Other problems in the brain can be more accurately classified as diseases than as injuries. Neurodegenerative diseases, such as Alzheimer's disease, Parkinson's disease, motor neurone disease, and Huntington's disease are caused by the gradual death

of individual neurons. Some infectious diseases affecting the brain are caused by viruses and bacteria. Infection of the meninges, the membrane that covers the brain, can lead to meningitis. Bovine spongiform encephalopathy (also known as "mad cow disease") is deadly in cattle and humans and is linked to prions. ‘Kuru is a similar prion-borne degenerative brain disease affecting humans. Both are linked to the ingestion of neural tissue, and may explain the tendency in human and some non-human species to avoid cannibalism. Viral or bacterial causes have been reported in multiple sclerosis and Parkinson's disease, and are established causes of encephalopathy, and encephalomyelitis.’

The brain metabolism normally is completely dependent upon blood glucose as an energy source. During times of low glucose (such as fasting), the brain will primarily use ketone bodies for fuel with a smaller requirement for glucose. The brain does not store any glucose in the form of glycogen. Each part of brain will controls individual work in human as shown in Figure 2.11.

Frontal lobe: Movement, intelligence, behavior and memory.

Temporal lobe: Speech, behavior, memory, hearing and vision.

Parietal lobe: intelligence, language, sensation and reading.

Occipital lobe: Vision,

Cerebellum: balance and coordination and the brain stem is responsible for breathing, blood pressure, heartbeat, swallowing and consciousness

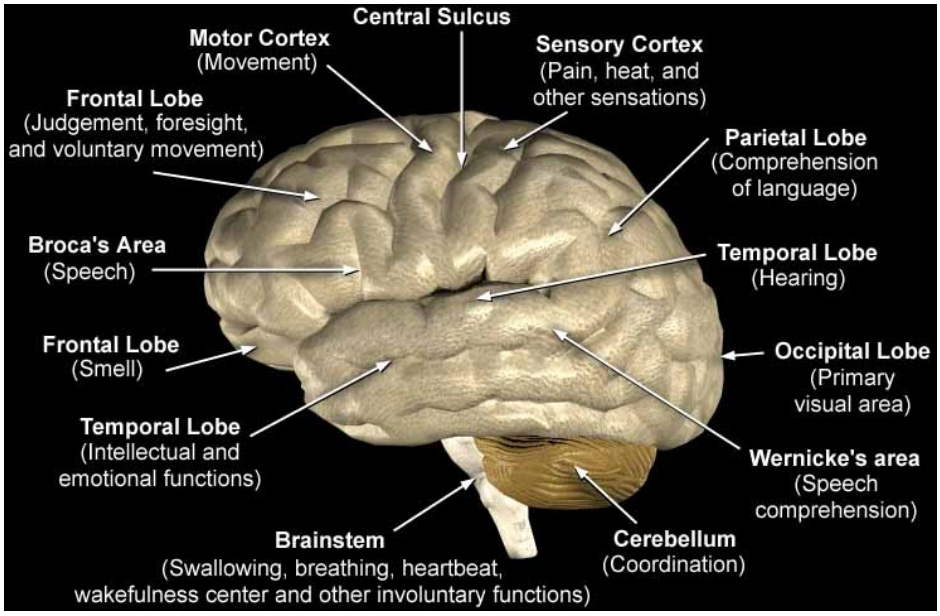

Figure 2.11 Functionality of the brain. (drrobertamoran.com)

2.5 The neuron

The neuron or nerve cell is an electrically excitable cell that processes and transmits information by electrical and chemical signaling. Chemical signaling occurs via synapses, specialized connections with other cells. Neurons connect to each other to form networks. Neurons are the core components of the nervous system, which includes the brain, spinal cord, and peripheral ganglia. A number of specialized types of neurons exist: sensory neurons respond to touch, sound, light and numerous other stimuli affecting cells of the sensory organs that then send signals to the spinal cord and brain. Motor neurons receive signals from the brain and spinal cord, cause muscle contractions, and affect glands. Interneurons connect neurons to other neurons within the same region of the brain or spinal cord. Figure 2.12 shows the typical structure of the nerve cell.

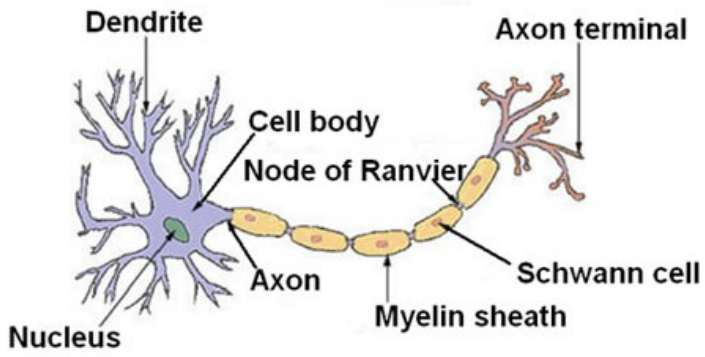

Figure 2.12 Structure of a typical neuron. (wikieducator.org)

CHAPTER 3 Traumatic Brain Injury

3 TRAUMATIC BRAIN INJURY

Traumatic brain injury (TBI) is a major public health problem, especially among males young people, adults ages 15 to 24, and elderly people of 75 years and older. Children aged 5 and younger are also at high risk for TBI. TBI is a complex from of brain injury that is generally caused by automobile accidents, falls, shaking a child, contact sport injuries or any type of accident or medical procedures. In recent years, it has been reported that exposure to a blast from and improvised explosive device (IED) can cause TBI. Each year about 1.7 million people experience a TBI in USA and approximately 52,000 people are dying from head injury accidents.

During an impact the brain moves in an oscillatory motion with respect to the skull which causes a shear wave through the brain. TBI can be classified based on the severity of accident. In severe head trauma, an intracranial hemorrhage occurs, where there is bleeding inside the skull. That is when a blood vessel in the skull is ruptured. This could be due to a physical trauma such as head injury or nontraumatic causes such as inhemorrhagic stroke like aneurysm. Figure 3.1 shows different type of the cranial hemorrhage.

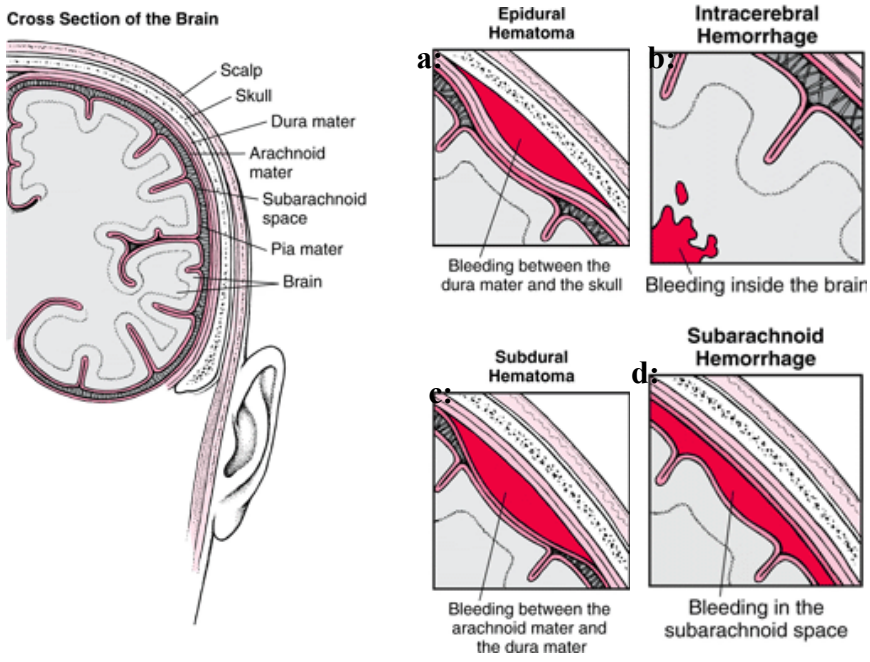

Figure 3.1 Example of the different cranial hemorrhage. **a:** Epidural hematoma, **b:** Intracerebral hemorrhage, **c:** Subdural hematoma and **d:** Subarachnoid hemorrhage

3.1 Different type of the TBI:

3.1.1 Concussion

Concussion is the most common type of head injury and may be defined as the loss of consciousness immediately following a trauma. Concussion is also included in the broad category of "Closed Head Injury" (CHI). A major defining characteristic of concussion, which helps to distinguish it from other types of TBI, is the absence of a post-trauma "waiting period'. In general, the severity of a concussion is characterized by the duration of loss of consciousness (LOC). Concussions and other brain injuries are fairly common. About every 21 seconds, someone in the United States has a serious brain

injury. One of the most common reasons people sustain concussions is through sports injuries such as football, boxing, and hockey even with the use of protective headgear.

3.1.1.1 Different Grades of Concussion

The severity of concussion is determined after all of the symptoms have been resolved, i.e. the neurologic examination is normal, and brain function has returned to normal. There are different types of concussion:

a) Simple concussion happens when symptoms of the concussion is resolved in 7-10 days.

b) Complex concussion happens when symptoms last longer than 7-10 days. It also considers complex concussion if a) person loses consciousness (passes out) for more than 1 minute or has a seizure at the time of the injury. b) If patient has had a concussion before, no matter how long ago.

Symptoms of concussion can range from mild to severe. They could show as headache, altered level of consciousness (drowsiness, hard to arouse, or similar changes), loss of consciousness, memory loss (amnesia) of events surrounding the injury. Head injuries which result in concussion often are associated with injury to the neck and spine. If the symptoms are severe (such as seizures or a long period of unconsciousness) or the person seems to be getting worse, that's an indication of a serious head injury.

3.1.2 Contusion

Contusion refers to a bruising of part of the brain, frequently on the cortex (outer layer). It may result from either head contact, or head acceleration without contact, and a secondary contusion may result from brain movement within the skull due to a trauma. Contusions occur primarily in the cortical tissue, especially under the site of impact. The brain may be contused when it collides with bony protuberances on the inside surface of the skull. Because contusion involves structural brain damage, they are more serious than concussions.

Contusions can be very minor with few symptoms and little or no damage to the brain, or they can be quite severe. More severe contusions lead to swelling in the brain, which can cause additional brain damage i.e. memory loss, attention problems, emotional disturbances, loss of ability to understand or express speech could be some symptoms of brain contusions.

The prognosis for contusion depends upon the severity of the injury. Mild contusions are able to heal on their own with no medical intervention, while extremely severe contusions can cause herniation of the brain, and eventually coma.

3.1.3 Coma

Coma is a state of unconsciousness that can last for more than 6 hours when a person cannot be awakened and fails to respond normally to painful stimuli, light or sound and does not initiate voluntary actions. In order for a patient to maintain

consciousness, two important neurological components, the cerebral cortex which is the gray mater covering the outer layer of the brain and reticular activating system (RAS or ARAS) located in the brainstem, must function perfectly.

Injury to either or both of these components is sufficient to cause a patient to experience a coma. It is very important to prevent infections and maintain physical health when patient is in coma. The outcome for coma depends on the cause, severity, and site of neurological damage. Some may emerge from coma with a combination of physical, intellectual, and psychological difficulties that need special attention. Recovery usually occurs gradually, some individuals never progress beyond very basic responses, but many recover full awareness. Duration of coma usually last between 2 to 4 weeks. The most common cause of death for someone in coma is infection, such as pneumonia.

3.1.4 Coup- Countercoup Injury

Coup- Countercoup Injury A contusion may occur at the point of impact (Coup) or at the opposite from the site of initial impact (or injury), in which case is referred to as "Countercoup." This kind of trauma occurs when the force impacting the head is not only great enough to cause a contusion at the site of impact, but also is able to rebound the brain and cause it to slam into the opposite side of the skull, which causes the additional contusion.

A cerebral contusion is different than cerebral hemorrhage as it combines vascular and tissue damages. It occurs directly beneath the site of the impact at the coup site but it also occurs on the contralateral site of the impact, the countercoup site. The energy

dissipated at the site of impact is important to determine whether the damage is going to be of the coup or countercoup type. A small area of impact will dissipate the energy there, whereas a bigger area of impact will dissipate the energy of impact either at the beginning or end of the head motion, leading to countercoup injury.

CHAPTER 4 Literature Review

4 LITERATURE REVIEW

Experimental, analytical and numerical methods and in particular finite element (FE) methods have been employed by investigators to explain the likely injury process of the brain and to quantify the response of the human head to blunt impacts (Al-Bsharat et al. (1999), Kleiven et al. (2002), Ruan et al. (1993), Zhang et al, (2001b,c), and Zhang at al. (2002))) The complicated geometry of the SAS and trabeculae makes it impossible to model all the details of the region. Thus, in these studies and other similar studies, the meningeal layers and the subarachnoid region have been simplified as a soft elastic material or in some cases as water i.e. soft solid having bulk modulus of water and very low shear modulus, e.g., (Kleiven et al. (2002), Zhang et al, (2001b and 2002). The short coming of these approaches is that the hydraulic damping, i.e. the fluid solid interaction, and the mechanical role of the fibrous trabeculae and the cerebrospinal fluid (CSF) in the subarachnoid space (SAS) were ignored. In addition to the simplified models, the mechanical properties of SAS are not well established in the literature. There have been a wide range of young modules for Pia Arachnoid complex (PAC), form $21.5x10^6$ Pa (Zhang et al. (2002)) to $11.18x10^3$ Pa (Jin X et al. (2006)), up to three orders of magnitudes. In the study of Zoghi and Sadegh (2010), the damping characteristics of SAS region were determined using the experimental study of Hardy et al. (1997). This was done by determining the damping coefficient of the brain/skull system and relating it to the hydraulic resistance of the CSF in the SAS region.

4.1 Experiment study

4.1.1 Alcolodo et al (1986)

In the experimental study of Alcolodo et al. calacification in the human choroid plexeus, meningiomas and pineal gland, 20 postmortem brains and one biopsy was studied using light microscopy, transmission and scanning electron microscopy. The result of their study was compared with clacification in psammoma bodies in normal arachnoid. They have been concluded that psammoma bodies in the choroid plexus form by a process of dystrophic calcification associated with arachnoid cells and collagen fibers. Also, scanning electron microscope (SEM) of the tree-shaped trabecula connecting the pia mater to arachnoid mater was observed.

4.1.2 Frederickson (1991)

The electron microscopy was used to study the subdural region within the cranial meninges in guinea pigs. They specially look at the fine structure of the arachnoid membrane, dura mater, inner surface of the dura and outer surface of the arachnoid. Their study reveals that, the subdural space was not observed in the guinea pig. They have concluded that the reason a intermediate cells are located in the light cell layer, next to the dark arachnoid cells is because of a grater complement of rough endoplasmic reticulum.

4.1.3 Meaney et al. (1995)

In the experimental study by Meaney et al. (1995) Diffuse Axonal Injury (DAI) of brain injury was investigated. To explain the connection between initial loading and brain deformation a surrogate model was used. They used acceleration data obtained from pig skull models that induce significant damage within the brain and applied those accelerations to the pigs. A diffuse axonal injury was found to occur when the brain tissues are subjected to a strain of 20%. This threshold value is taken as a reference in most of the mechanical studies about TBI.

4.1.4 Ibrahim et al. (2010)

Ibrahim et al. (2010) used 5 days and 4 weeks old piglet heads to develop a method to measure deformations of the brain due to rapid rotations of the heads. The result of their study was useful to validate finite element models of the brain deformations. Unfortunately the experiment was only focused on the brain material properties; no investigation of the SAS was done.

4.1.5 Nahum et al. (1977)

In their experiment study, Nahum et al. (1977), applied initial velocity of the impact and measured intracranial pressures, duration of the applied load and the impactor's mass. They also measured the input force, changes in skull acceleration and in vivo intracranial pressure with time during the impact. Their study performed two series of experiments on cadavers. Series I consisted of 8 individual experiments and series II, 7

multiple sequential impacts on a single specimen. Pressure changes were measured with transducers placed at the frontal, parietal and occipital bones as well as the posterior fossa and carotid siphon. They found linear relationship between the peak pressure at the given locations and skull acceleration. All locations tested were found to be linear but they had different slopes. Frontal location indicate sharpest slope which suggest that the pressure in this region is most sensitive to head acceleration. This discovery simplifies the study of brain response during impact and provides data for model validations

4.1.6 Hardy et al. (2001-2006)

Hardy et al. in (2001) and Al-Bsharat et al. (1999) measured the relative motion of the brain with respect to skull in human cadaver heads using neutral density technology and high-speed biplanar X-ray. A blunt head impact was applied to human cadavers and X-ray snap shots of the specimen's heads were taken to develop the 3D trajectory of the brain relative to the skull. They observed that brain undergoes displacement relative to skull on the order if +/- 5 mm, when impacted with an angular speed of 17 to 22 rad/s. The result of their study can be used for computer simulation study and have a better understanding of TBI phenomena. Modified finite element simulation was also done by Al- Bsharat et al. (1999). Based on experimental study, to create the same contact between CSF and outer layer sliding elements was introduced. The result was in a good agreement with experimental study where it was also a validation for Finite element model.

In the study of Hong Zou et al. (2006) the brain motion was divided to the rigid body displacement and deformation in low impacts. They have concluded that increase of the brain motion is more due to deformation where the rigid body displacement is limited in the scale of 4-5mm and rotation of ±5º.

4.1.7 Miller's Group (1977-2002)

Miller's group from 1977 to 2002 performed a series of study in determining a constitutive model for the brain tissue as well as mechanical properties of brain tissue. Their study concludes the brain tissue respond differently under compression and tension. The material property that they suggest for the brain base on their study was hyper viscoelastic constitutive model. Although it was a good study but they did not count for blood vessel and CSF pressure. These study include Miller and Chinzei (1997), Miller (1999), Miller et al. (2000) and Miller and Chinzei (2002)

4.1.8 Jin X et al. (2006)

In the experiment study by Dr. Albert King's group at Wayne State University, the subarachnoid space has been studied. They considered pia, arachnoid and trabeculae as a complex (PAC) region. While their study was in vitro, they did not include the effect of the CSF fluid. They performed uniaxial quasi- static and dynamic loading at different strain rate (0.05, 0.5, 5 and 100 s-1) in tangential direction to gain knowledge of the material properties of pia, arachnoid complex (PAC). The samples were taken from different regions to also study the variety of PAC in different section. The result of their study reveals the mechanical property of the PAC to be much less than what it was

reported in the literature (about 3 orders of magnitude less) they also conclude the PAC is rate-dependent and is isotropic region that support the brain during an impact. For a strain-rate of 0.05 s-1, the modulus in the toe region was 0.94 MPa and for the high-strain linear region the modulus was 6.75 MPa. These results are about 40% lower than the results found by Aimedieu's et al. (2001) and Prange et al. (2002).

Two set of experimental work were performed, the large strain of the gray and white mater of adult porcine was measured in the shear test and validated in the compression test. The most an isotropy part of the brain was confirmed to be gray mater and corpus callosum. The brain tissue was regionally different. They also indicate that the fresh adult human brain properties were slightly stiffer than adults porcine and finally depends on the age, direction and region of the brain they will have slightly different material properties.

4.1.9 Killer at al. (2003)

The histology of the trabeculae in the optical nerves has been studied by Killer et al. (2003). Their study was based on 12 optic nerves harvested from nine subjects. To indicate the same functionality the sample were used 7 hours after death, following qualified consent for necropsy. TEM and SEM were used to study the anatomy and arrangement of trabeculae in optic nerve and to describe the pillars, septa and plate like structure for trabeculae in sub arachnoid space. The best conclusion from this study was that the human optic nerve is not a homogeneous media. It's a complex region and is filled with cerebrospinal fluid and it contains a complex system of arachnoid trabeculae

and septa that divide the subarachnoid space. The SAS is regionally different and as it gets morecloser to the canalicular portion the trabeculae are more oriented shape like pillar.

4.1.10 Mehdizadeh et al. (2008)

In the experimental study by Mehdizadeh et al. (2008), the material properties of gray and white mater were investigated using swine brain. The experiment was based on the necking phenomena of the gray and white mater of the brain. The tension test was set up and the curvature of the soft tissue was compared to the range of known material properties. The results of their study indicate the true Young modulus of 24.6 kpa for gray mater and true Young modulus of 19 kpa for white mater.

4.1.11 Sabet et al. (2007) and Bayly et al. (2005)

They have studied the brain deformation of adult volunteers subjected to a mild angular acceleration and a rapid deceleration. Images of the brain were obtained with the use of tagged MRI scans. Three human subjects (two males and one female) were tested. The strains were obtained when the subjects were under accelerations ranging from 250 to 300 rad/s^2. In comparison, the peak acceleration in the study by Meaney et al.(2005) was 105'000 rad/s^2. They conclude that, a large part of the axial planes were experiencing a strain of 2%, and some regions were subjected to a strain greater than 2%, typically between 2-5%

4.1.12 Rowson et al (2011)

Football players always have been subject to the blunt impact of the other players. Unlike automobile safety there are not enough analytical mechanisms to calculate the protective performance of football helmets. In the study of Rowson et al. (2011) a new set of equations was introduced to calculate helmet performance by integrating player head impact exposure and risk of concussion. Head acceleration data points of 62,974 incidents of players were used to study the effect of the impact to the head/helmet. Finally, they provided risk factors of concussion for each impact and they developed the new injury risk function based on 32 measured concussion and associated exposure data. New equation was given (STAR) to be used for football helmets performance.

4.1.13 Other experimental studies

Ommaya et al. (1967) used Rhesus monkeys to perform experiments on concussion-producing head rotations. The aim of their study was to develop a tolerance criterion for concussion in Rhesus monkeys. Ono et al. (1980) conducted three sets of experiments (translational acceleration, rotational acceleration and both at the same time) on live monkeys. They conclude the translation force alone cannot cause severe head injury. Rotational acceleration produced a higher rate of brain damage than translational because it will have more deformation of the skull and higher shear strains. Other experimental studies have been reported in the literature to explain likely the injury relations between the head impact severity and mild TBI i.e. Greenwald et al.(2008), Hardy et al.(2007), Guskiewicz et al. (2007) and Broglio et al. (2010).

4.2 Analytical and numerical studies

In every research analytical studies are required to simulate and develop the same model as experimental cases. The validity of mathematical modeling is related to kinetic and kinematics parameters of impacts and head injuries. These studies help investigators to obtain valuable information about some cases that are not achievable experimentally.

4.2.1 Engin et al. (1969)

In the study of Engin et al. (1969) the brain material properties was considered as viscoelastic to be applied in their numerical model. In this analysis the brain's material was used as an incomparable. This work was extension of the Anzelius et al. (1943) model who studied the viscoelastic response to head impacts. Their theoretical analysis was based on the results from experimental studies on Rhesus monkeys Fallenstein et al. (1969). Their study determined the shear modulus of the brain as a function of oscillation frequency.

4.2.2 Nahum et al. (1977)

Based on their own experiment study they constructed a three-dimensional linear FEM model of the human brain. Blunt head impact was applied to the model to study the respond of the brain. Different bulk module was used to report pressure responses of the brain. This parameter provides incompressibility and was varied to best fit the data. Incompressibility reduces the correlation between experiments and simulations. Their

results indicate 20% damping factor for the brain was found to significantly improve the correlation.

4.2.3 Wayne State University Brain Injury Model (WSUBIM)

The Wayne State University brain injury model (WSUBIM) has been developed and improved over the last several years, (Ruan et al. (1993), Zhou et al. (1995), Al-Bsharat et al. (1999), Zhang et al. (2001), Jin X et al. (2006) . The 3D FEM model of the human head has been validated by experimental data published by Nahum et al. (1977). In (2001), the model was improved to be used for direct and indirect impact combined with translational and rotational acceleration. The main advantages of this model are the simulations of bone fractures in the face and skull.

Soft solid element was used for the CSF and subarachnoid trabeculae modeling. The material properties for these solid elements were the bulk modulus of water and a very low shear modulus for better representation of the fluid nature of the area. An additional frictionless sliding interface between the outer arachnoid and inner dural membranes was incorporated to better mimic realistic anatomy. General contact was defined to eliminate the separation between the brain and dura mater. The advantage of defining that was tensile forces could be transmitted between the two contact surfaces. Due to these modifications, the model was better able to match intracranial pressure values obtained experimentally. The ventricles were modeled as solid elements with shear modulus lower than the CSF. They conclude fluid elements are the better option for

CSF and the SAS because solid modeling cannot simulate the mechanical and thermodynamic properties of CSF.

They indicate that to improve the model the pia mater should be included. Blood vessel walls were modeled as being directly connected to the brain tissue. This is because nothing is currently known about the mechanical interactions between vessel walls and brain tissue. This may have added greater stiffness to the model than what is physiologically relevant.

In the last model principal strain responses to rotational and linear loading were tested. The results showed an overall 37% reduction in the maximum principal strain with the introduction of blood vessels. Shear strain in the x-y plane was also tested for both rotational and linear loading. The results showed a 33% increase in shear strain due to the presence of blood vessels. Finally, it was terminated that intracranial pressure of the blood vessels does not affect intracranial pressure in linear loading but have a small decrease in rotational loading.

4.2.4 Darvish (2001 -2008)

Darvish group (2001-2009) studied the nonlinearity of viscoelastic effects in deformation of brain, they performed two nonlinear constitutive models to describe the dynamic viscoelastic behavior of brain tissue. The bovine brain tissue was tested in simple shear using forced vibrations (0.5 to 200 Hz) with finite amplitudes (up to 20% Lagrangian shear strain). Based on the experimental work quasilinear viscoelastic model and fully nonlinear viscoelastic model was proposed to describe the spatial and temporal

nonlinearities. They concluded that the linear complex modulus demonstrated non recoverable asymptotic strain conditioning behavior under finite strains.

4.2.5 Takhounts et al.2008 – SIMon model

National Highway Traffic Safety Administration (NHTSA) created a very sophisticated head model to be used for computer simulation study of TBI. Their new model consisted of several parts; cerebrum, cerebellum, falx, tentorium, pia arachnoid complex, CSF, ventricles, brainstem, and blood vessel. Dimensions and details for modeling were taken from CT scans of human head. The material properties for different section were base on previous study of Takhounts et al. (2003) study. However to define the brain material property they performed a simple cube test and applied shear force. The result then was compared with the experimental study. The brain material property was then state to be a simple linear viscoelastic. They also used the football player helmet example to indicate the real impact force to the head.

Their model was validated using neutral density targets (NDT) and respond data; the stability of the FEHM model was tested with the translational and rotational acceleration. The SIM model represents the best geometrical finite element model where it can helps investigator to have better understanding of TBI. They also conclude that the angular injury criteria better predicts traumatic brain injury.

4.2.6 Gupta et al. (2009)

In the study of Gupta et al. (2009) they used combination of a finite-volume computational fluid dynamics (CFD) approach and magnetic resonance imaging (MRI) experiments to investigating 3D subject-specific cerebrospinal fluid (CSF) dynamics in the inferior cranial space, the superior spinal subarachnoid space (SAS), and the fourth cerebral ventricle. Velocity boundary conditions were applied in the spinal subarachnoid space and Velocimetric MRI was used to measure the velocity field at the boundaries. To model SAS structure with trabecula they used porous media. This study reveals that the max velocity for the CSF is about 15 cms and it occurred in the inferior section of the aqueduct, 14 cms in the left foramen of Luschka, and 9 cms in the foramen of Magendie. They also suggested that this model can be used as a basic model for further FEM modeling.

4.2.7 Feng et al. (2010)

In their study, a human subject's head was dropped on its own gravity approximately 2 cm. The forehead of the subject came in contact with a rubber band, that is used as a stopper. Displacement data were then obtained from this mild frontal head angular acceleration of the head and the impact with the rubber band. Tagged magnetic resonance imaging method was used to measure in vivo relative displacement between the brain and the skull of three adult male human subjects. Their study provides an important set of displacement measurements in the human brain during the mild frontal skull impact. The result of Feng et.al (2010) shows that, at the four specific locations in

the brain, the rotation and the displacement of these points relative to the skull is approximately 2-3 mm.

4.2.8 Other Finite Element Models

Finite element head models have proved to be reliable tools for understanding the biomechanics of traumatic brain injury (TBI). Different FE models were created and enhanced over the years to investigated TBI. Some of these models are: Ruan et al. (1993), Bandak and Eppinger (1995), Bandak et al. (2001), Kleiven et al. (2002), Takhounts et al. (2003a), Levchakov et al. (2006) and kleiven et al. (2007), Moss et al. (2009).

CHAPTER 5 Experimental study

5 EXPERIMENT STUDY

The histology of the trabecular structures of the SAS is not well established in the literature. The trabeculae the SAS of the optic nerves, as reported by Killer et al. (2003), have veil- like and pillar structures. While the SAS of the optic nerve has the same functional as that of the brain, their architecture could be different. There are un answered questions about the architecture and histology of the SAS of the brain. The only recognized fact about the trabeculae is that they are made of collagen fibers surrounding by fibroblast cells.

The fibroblasts can be found in all connective tissues. They are surrounded by an extracellular matrix (ECM) having a thickness between 50 and 200 nm and composed of collagen fibers, proteoglycans, laminins, and fibronectins. Those molecules are connected together in a 3D network to provide a cell-to- cell interaction, a cell-substrate interaction or a mechanical support for the tissue.

In the SAS, the collagen fibers are arranged in bundles surrounded by the fibroblasts and the ECM. This complex forms the SAS trabeculae. The fibroblasts are also connected to the blood vessels circulating within the SAS, to the pia mater and to arachnoid mater via specific junctions.

In this study, through a series of in-vivo and in-vitro experiments the histology and the architecture of the brain trabeculae were investigated. Specifically, five different

experimental methods, namely; Micro CT Scan, Histology section using florescent and bright light, Two-photon laser scanning microscopy (TPM), Scanning Electron Microscopy (SEM), and Transmission Electron Microscopy (TEM) were used. The conclusions of each experimental work leads us to have better understanding of the tissue in this region.

5.1 Micro CT Scan

Computed tomography (CT) is a medical imaging method employing tomography created by computer processing. Digital geometry processing is used to generate a three-dimensional image of the inside of an object from a large series of two-dimensional X-ray images taken around a single axis of rotation. Figure 5.1 schematically shows the function of a Micro CT scan machine.

CT produces a volume of data which through a process known as "windowing", can be manipulated, in order to demonstrate various bodily structures based on their ability to block the X-ray beam.

Micro computed tomography or "Micro-CT" is a 3D x-ray imaging, it is using the same method as a large scale CT or CAT scans in hospitals. The only difference is its higher resolution in smaller scale and generating real 3D images. The Micro- CT is easy to use since there is no need for any sample preparation, staining or slicing. That is, the Micro- CT will image our samples completely and give us a 3D structure at high resolution, about 1 μm, after the reconstruction.

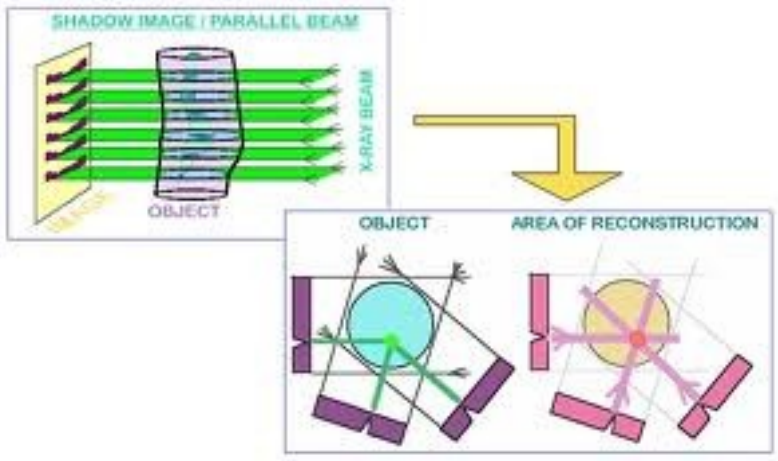

Figure 5.1 Diagram of Micro CT scan machine

A Micro-focus x-ray source illuminates the object and a planar x-ray detector collects magnified projection images. Based on hundreds of angular views acquired while the object rotates, a computer synthesizes a stack of virtual cross section slices through the object. Once the 3D images are generated, then we can look through the cross sections, interpolating sections along different planes, to inspect the internal structure.

5.1.1 Materials and methods

Since cadaveric human brain was already fixed by formaldehyde, the arachnoid had been collapsed on the pia mater and the CSF had been drained. Several techniques were employed to separate the arachnoid from the pia mater and to recreate the subarachnoid space, which is approximately 2 to 3 mm in human. The techniques involved several steps including confining the region and injection of Microfil (Silicone Rubber Injection Compounds) from flowtech, Inc, which solidifies quickly and keeps the two layers separated. To inject the Microfil solution into the SAS the region was confined

using clear tube with a key -way on its side for the insertion of a needle. It was a very dedicated job since we had to make sure the solution is injected exactly between pia mater and arachnoid mater. The viscosity of the fluid was also important because if the Microfil mixed with the solidifier was too thick we were not able to inject between two layers using a small needle and if it was diluted then it was just drained between cortexes and wouldn't open the SAS space. Several tissue samples from different regions of cadaver's brain were prepared, Figures 5.2, 5.3 and 5.4 show the human brain fixed in formaldehyde and Micofil solution injected between pia and arachnoid mater to separated and rebuild the SAS. Once the specimen was solidified it was taken to the SkyScan 1172 Micro-CT System, having 2μ resolution. Then 2D structure of the trabeculae was taken from SkyScan machine where we were able to reconstruct the 3D structure of the tissue. Because the trabeculae are so thin and their dimension is about 2-7 micron we had to increase the resolution of the machine which made of result file too big (2020 files where each file was almost .5 MB). The reconstruction process was successful and we obtained our 2D images ready to import them to Mimic software where we could get the 3D structure of the trabeculae and then save these files as .STL to be imported to any FE program. At this step the size of the files was a problem and our processor and software didn't support the big size of the file. We had to crop the files in order to import them partially to the Mimic software.

Figure 5.2 Cadaveric human brain fixed in formalin

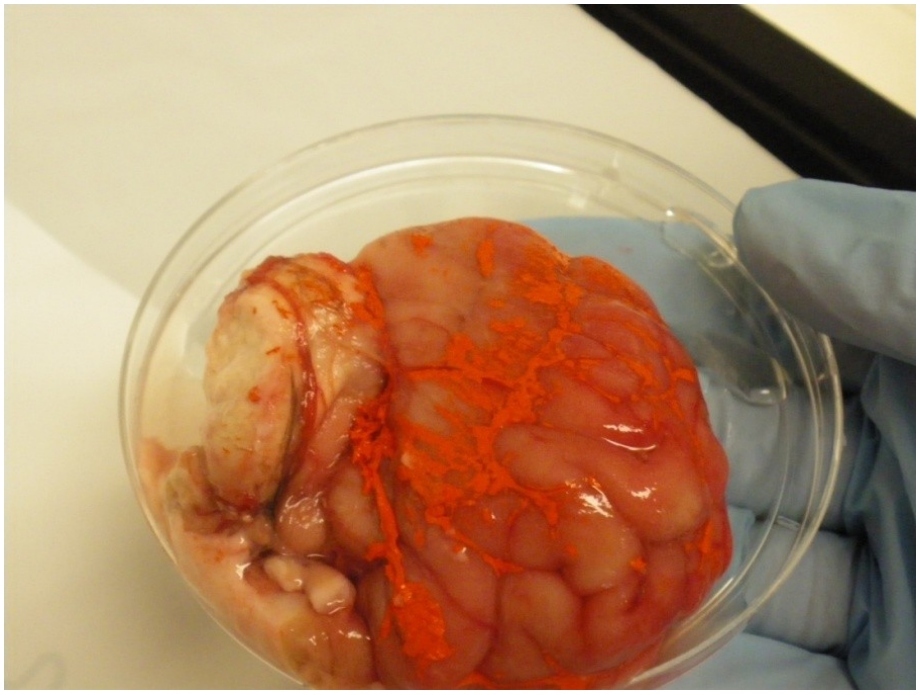

Figure 5.3 Brain tissue with Microfil (orange solution)

Figure 5.4 The brain tissue with Microfil fixed in formalin

5.1.2 Results

We were unable to obtain very good results using the Micro CT- Scan machine, as shown in Figure 5.5. One reason was because of the trabecular structure and its material property. Since the trabeculae are collagen based and are transparent the CT-Scan machine is not the best mechanism to capture the trabeculae structure, i.e., the X-ray was not absorbed by the tissue to predict the 2D images. The other problem was the size of these tissues, which made our 3D construction very hard. To avoid the first problem we might need to use some contrast agent for the trabeculae tissue to make them more sensitive to X-ray machine.

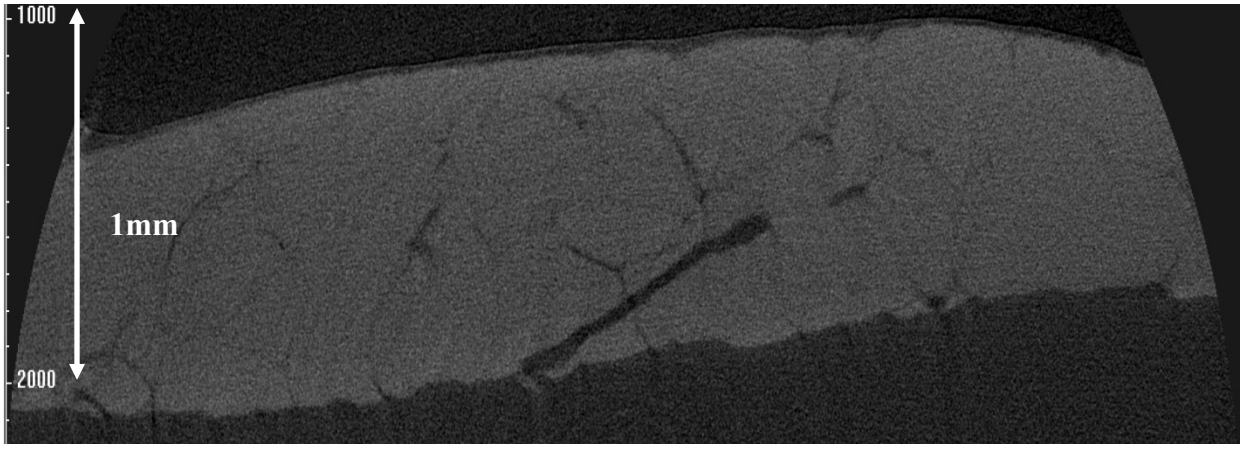

Figure 5.5 2D projection of trabeculae after reconstruction procedure by the 3D Micro-CT Scanning system.

5.2 Histology section using fluorescent and bright light

The knowledge of the histology of the SAS is important for the material modeling and understanding of the damping mechanism of the brain, and therefore the effect of the external impact on the brain . CT- Scan machine didn't provide good imaging of the trabeculae tissue also we were not able to reconstruct the entire file for the 3D structure. Another possibility to investigate the trabeculae architect was to observe the images under the florescent and bright lights. The light microscope employs visible light to detect small objects; it is the most well-known and well-used research tool in biology. A fluorescence microscope is much the same as a conventional light microscope with added features to enhance its capabilities. Figure 5.6 is the diagram of Fluorescent Microscopy. The same sample was also observed under florescent light. Fluorescent microscopy is often used to study images of specific features of small specimens such as microbes. It is also used to visually enhance 3-D features at small scales. When the reflected light and

background fluorescence is filtered in this type of microscopy the targeted parts of a given sample can be imaged. This gives an investigator the ability to visualize desired organelles or unique surface features of a sample of interest.

Confocal fluorescent microscopy is most often used to accentuate observe the 3-D nature of samples. This is achieved by using powerful light sources, such as lasers, that can be focused to a pinpoint. This focusing is done repeatedly throughout one level of a specimen after another. Most often an image reconstruction program pieces the multi level image data together into a 3-D reconstruction of the targeted sample.

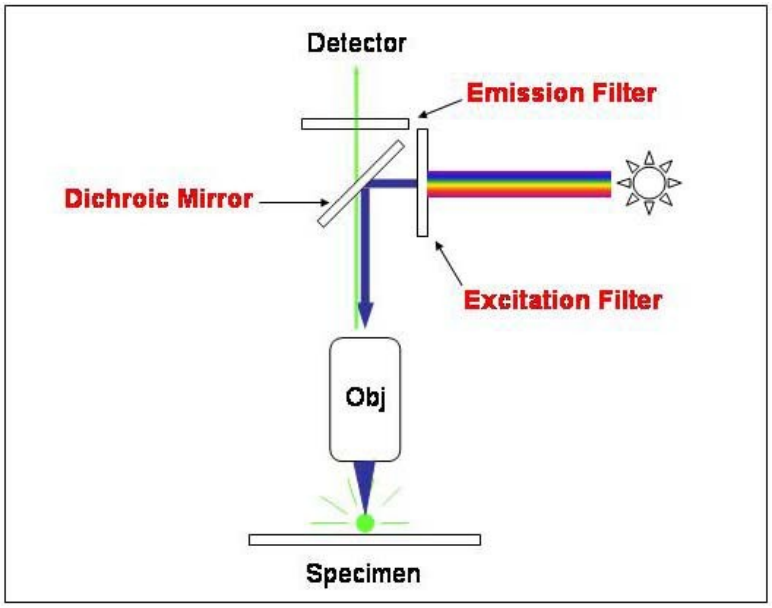

Figure 5.6 Fluorescent Microscopy.

5.2.1 Materials and methods

Similar process used in preparation of the tissue for the Micro -CT scan were employed and several tissues from human cadaverwere prepared using Microfil solution.

The samples then were stained using Hematoxylin-Eosin staining protocol and sliced using vibrotom machine. Note that since the tissue was already fixed in the formaldehyde the micro fill did not survived the staining procedure and it was wash out during the sample preparation, method. However we were able to see the trabeculae structure and make a distinguish between pia and arachnoid mater. Light microscopy of the subarachnoid space are shown in Figures 5.7 and 5.8. As shown in the Figures 5.7 and 5.8, it was determined that the trabeculae are collagen base tissue.

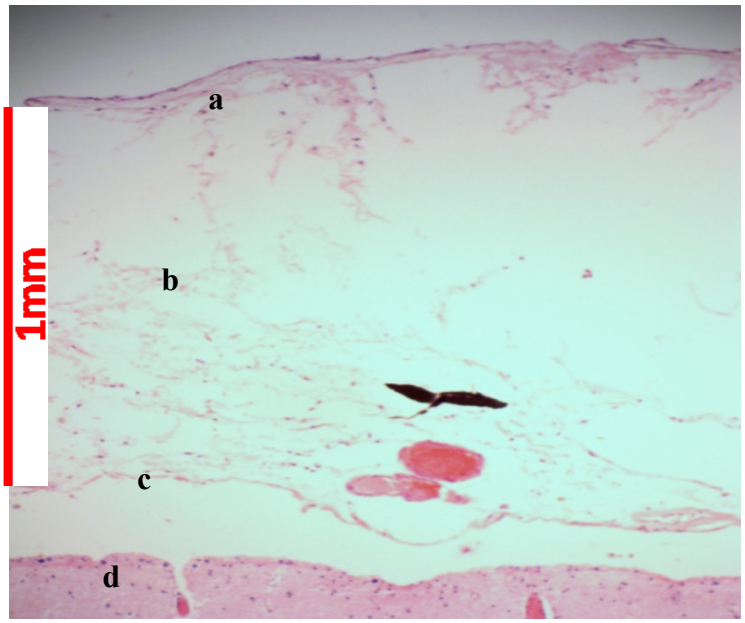

Figure 5.7 Light Microscopic view of subarachnoid, a: the arachnoid mater, b: SAS, c: the pia mater and d: the brain- resolution 10X

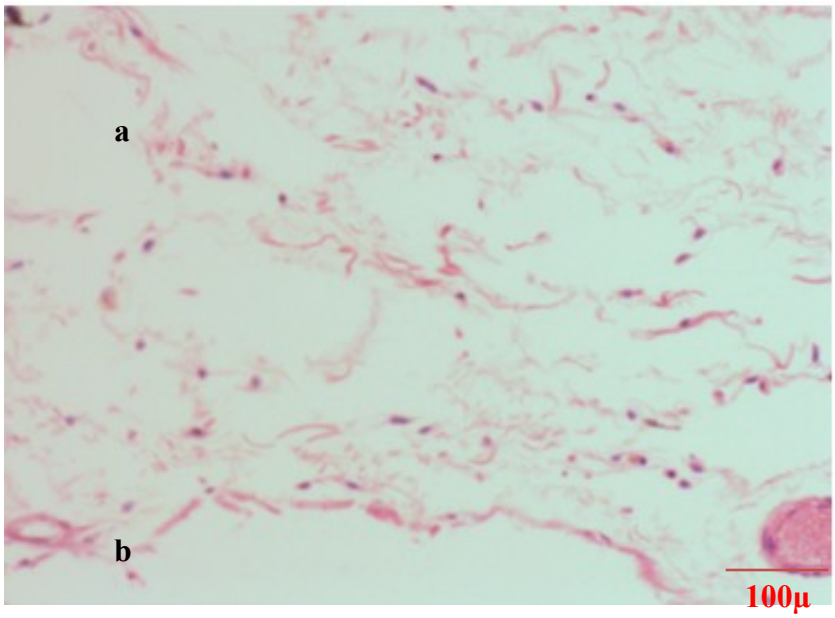

Figure 5.8 Light Microscopic view of subarachnoid, a: the trabeculae and b: the pia resolution 20X

The samples were also observed with florescent light miscopy. Figure 5.9 and 5.10 indicated the trabecula tissue under the florescent light where we can clearly see the structure of the trabeculae. The result from this experiment was used to estimated permeability and porosity of the SAS to be modeled as a porous and Darcy's analytical and numerical models, see chapter 9.

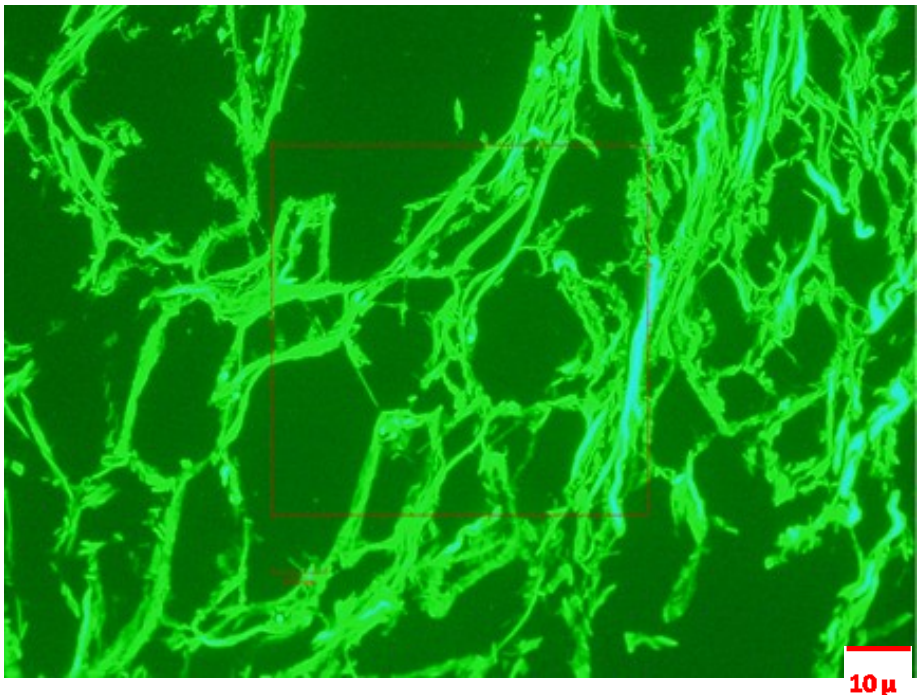

Figure 5.9 Trabeculae of cadaveric brain tissue under the fluorescent light - magnification 10x.

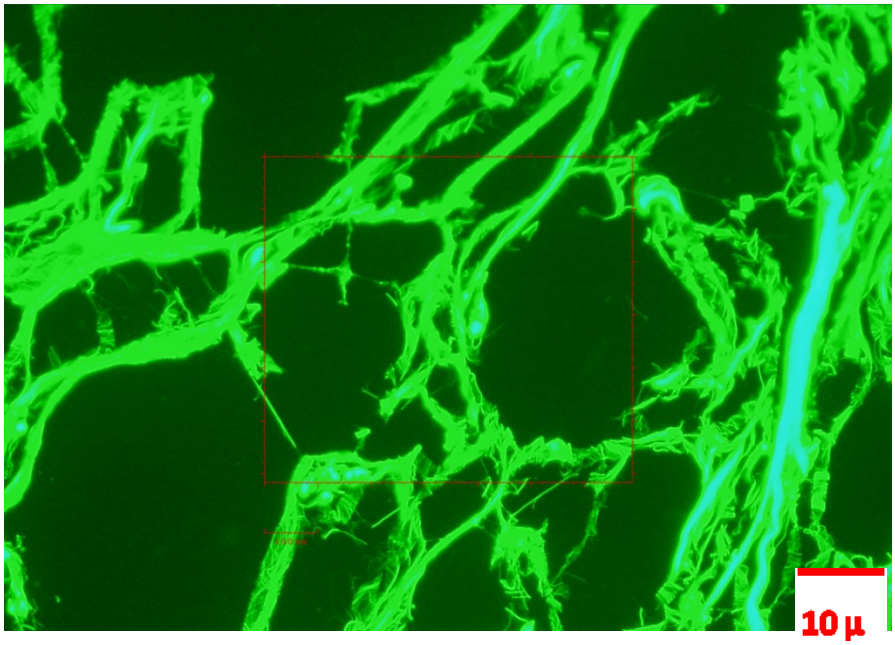

Figure 5.10 Trabeculae of cadaveric brain tissue under the fluorescent light - magnification 40x.

5.2.2 Animal Experiments: Histological sections- Staining for collagen

The objective of this animal study was to observe the SAS and the trabecular architecture of the brain of a Sprague-Dawley SD rat in vivo. It is known that as soon as the animal dies the CSF is desorbed and the SAS collapses. To preserve the space between the arachnid and the pia mater, and to prevent the absorption of the CSF and the collapsing of the SAS in the rat brain when the animal dies, perfusion-fixation method was used, Figure 5.11. Perfusion-fixation is thought to be a method of fixation that is quick enough to maintain the SAS open by stabilize the trabecula, pia mater and arachnoid mater before the CSF has completely absorb by the blood.

Figure 5.11 Anesthesied and restrained an SD rat with pentobarbital sodium.

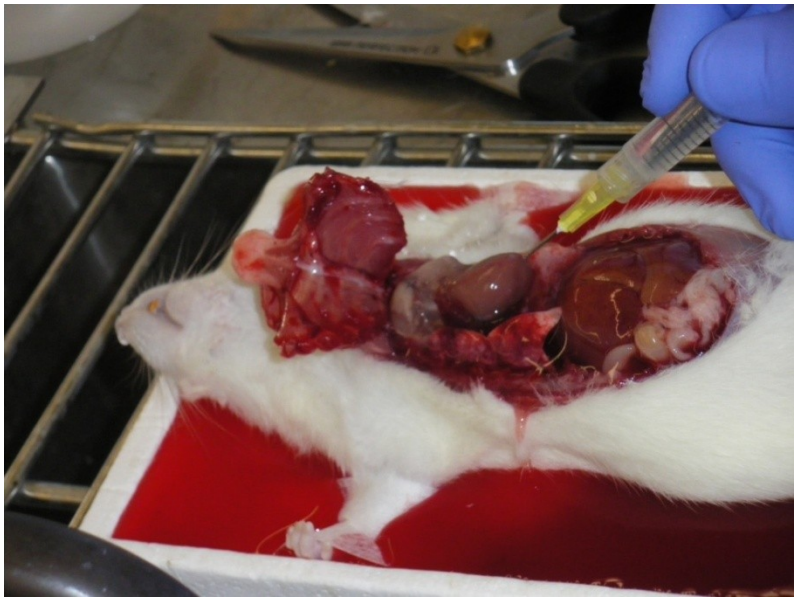

Figure 5.12 Perfusion-fixation of the SD rat.

The rats were anesthetized with pentobarbital sodium given subcutaneously (80-100 mg/kg body weight for initial anesthetization and 30 mg/kg body weight for maintenance as needed) and kept warm on a heating pad. As the pentobarbital sodium was at physiological pH the heart kept beating. After 2-3 minutes the pump was switched and started injecting the pre-fixative solution, a mix of 2.5% glutaraldehyde and 2% formaldehyde. Glutaraldehyde and formaldehyde are two common organic compounds that strengthen the tissues by having crosslinkings with the biological proteins. They also prevent the degradation and the damage of the tissues by disabling the proteolytic enzymes. After 3-5 minutes the pump was turned off, the head of the animal was chopped off; the skull was dissected and placed in paraformaldehyde 4% with sucrose to continue the fixation, Figure 5.12. After the perfusion, the brain of the rat was exposed by cutting the skin and the bone in the middle of the top head and pulling them apart. This step had

to be performed carefully in order to preserve the dura mater attached on the brain. The brain was taken out by using a small spatula to detach it from the cranial cavity. This was one way to extract the brain. Another technique that has less damage to the dura and the SAS was to remove the skull piece by piece by alternating cutting and harvesting pieces of bone with a tweezers. This technique required more time and precision but preserved the dura better.

Once all the samples were fixed, they had to be sectioned prior to be stained. Every sample was sectioned with a microtome. Before the sectioning, the pieces had to be strengthened to prevent them from falling apart while slicing them. To get sections from the rat brain we used the frozen section technique. The rat brain was fixed in paraformaldehyde 4% with sucrose for 36 hours and then placed on the microtome stage where it was frozen as shown in figure 5.13. The frozen sections are supposed to have fewer damages within the tissues compared to the samples embedded in paraffin. The sucrose added in the paraformaldehyde 4% solution also helped to minimize the formation of water crystals within the tissues. The rat brain was cut in 20μm-thick sections that were placed in a phosphate buffered (PB) solution before to be mount on the glass slides.

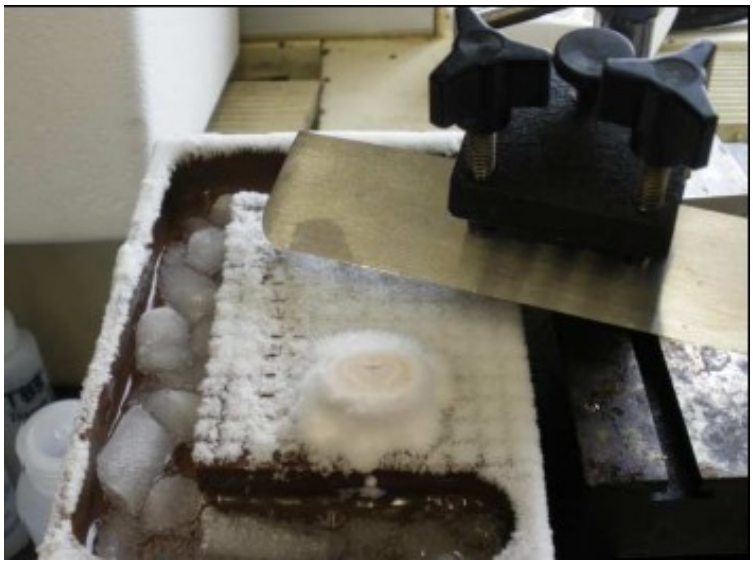

Figure 5.13 Frozen rat brain on the microtome stage.

After the sectioning, the samples of each species were stained. The first set of samples (cadaver human brain and rat brain) were stained according to the Hematoxylin-Eosin staining protocol (Appendix 1), whereas the other samples were stained according to the Gomori's trichrome staining protocol (Appendix 3). The Hematoxylin-Eosin staining was used to stain the nucleus and the cytoplasm of the cells. In the Gomori's trichrome protocol different dyes were used to differentiate the structures of the samples. The nucleus and cytoplasm of the cells were stained with hematoxylin and eosin (Sigma Aldrich), respectively. The collagen fibers were stained in green with a fast green FCF (Sigma Aldrich). After the staining steps the slices were fixed on slides with a coverslip mounted with permount. The slides were dried in oven for an hour before to be observed under the microscope.

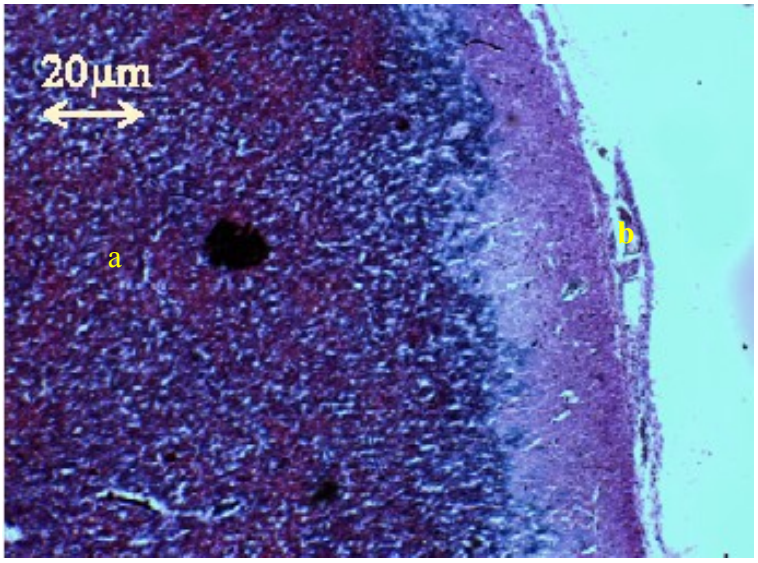

Figure 5.14 Histological sections of a rat brain stained following the Gomori's trichrome staining protocol, a: the brain and b: the SAS

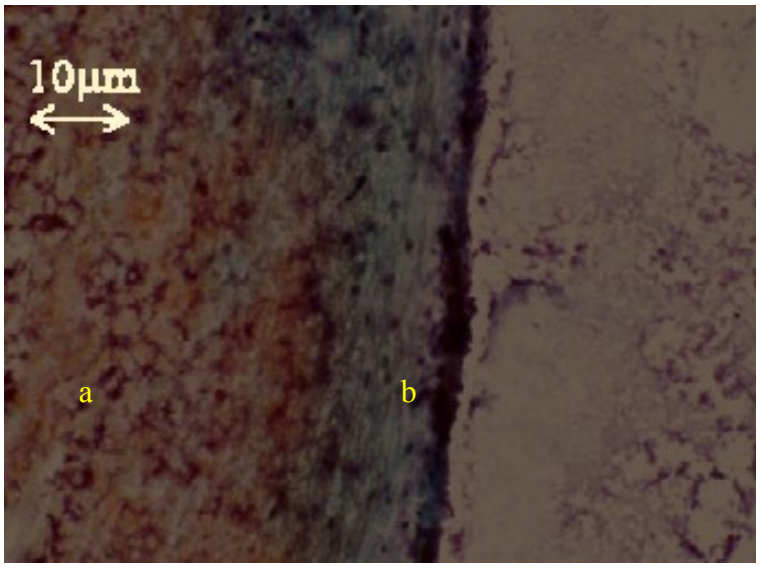

Figure 5.15 Histological sections of a rat brain stained following the Gomori's trichrome staining protocol, a: the brain and b: the SAS

The rat brain samples, exhibited different colors as the staining protocol was different as shown in Figure 5.14. The collagen fibers where supposed to be green but it appears that some superficial brain tissues also appeared green, which makes it difficult to identify specifically the collagenous structures. The staining was very inhomogeneous therefore the results were varying a lot among the different sections. The identification of the different structures was not as easy as expected, even with this specific staining as shown in figure 5.14 and 5.15. The rat brain is on the left side and the pia mater is the purple layer lining the brain. We were unable to get the good result from the human cadaver samples.

5.2.3 Conclusion

The histological sections were expected to give us valuable facts of the SAS in the rat and human sample. Only the results from the human samples provided a first insight of the SAS. We were able to observe the collagen fibers. As the fibers seemed to be ruptured, it was difficult to understand their connections and insertions within the arachnoid and pia layer. For the rat samples, the staining appeared to be inhomogeneous and unfortunately the SAS was not preserved. For the future work, the samples need to be prepared differently to avoid damages to the SAS. The vibratome could be used instead of the microtome to get slices of the sample. Regarding the staining procedure, staining time could be adjusted as the staining protocol was initially written for muscular tissues. Thus the cerebral tissues could be reacting differently with the reagents and they might need different times of exposure to the reagents. The histological sections should also be investigated in parallel with a mapping of the brain. Samples should be removed at

different locations on the brain to analyze whether there are differences in the SAS given the anatomical location. General results should also be compared with different species.

5.3 Two-photon laser scanning microscopy (TPM)

The SAS is a delicate region of the head/brain which make it very hard for any in vivo or in vitro experimental study. It could be ruptured or collapsed depending on the type of the preparation method. When an animal dies the CSF will be absorbed by the blood vessels and therefore there is no pressure to hold the SAS and the trabeculae. Therefore it is obvious not to see the SAS on cadaver or any in vitro experimental study when the animal is dead. One way to obtain images and learn the structure of these layers is by using Two-Photon Microscopy (TPM) as the animal is still alive. The Two-Photon Microscopy (TPM) is a technique that is suitable for in-vivo studies and provides a proper resolution for the structures under study in the SAS. It is a fluorescent imaging technique that works on the same basic concept as the Confocal Laser Scanning Microscopy (CLSM), but is an alternative to the CLSM. The main advantages of the TPM over the CLSM are its greater imaging depth and its reduction of phototoxicity which enables noninvasive intra-vital imaging of cells or subcellular systems.

5.3.1 The basic concept of Two-Photon Microscopy

The phenomenon of fluorescence has first been described more than 150 years ago but the first fluorescent microscope was only built up 60 years ago. Fluorescence is defined as the luminescence of a substance excited by radiation. It soon became a useful tool for the biologist as it allows applications such as in-vivo identification of cells or

molecules, screening of molecules, cell sorting, DNA assays, etc. The technique has been considerably improved since its beginning in the past 60 years. Fluorescent microscopy relies on the principle of energy transfer from light to molecules and vice versa. Energy levels of a fluorescent dye are composed of vibrational energy levels and electronic energy levels. Figure 5.16 shows the diagram of a two-photon excitation microscope. When fluorophore absorbs two infrared photons simultaneously, it will absorb enough energy to be raised into the excited state. The fluorophore will then emit a single photon with a wavelength that depends on the type of fluorophore used. Because two photons are absorbed during the excitation of the fluorophore, the probability for fluorescent emission from the fluorophore increases quadratically with the excitation intensity. Therefore, much more two-photon fluorescence is generated where the laser beam is tightly focused than where it is more diffuse. Effectively, excitation is limited to the tiny focal volume (~1 femtoliter), resulting in a high degree of rejection of out-of-focus objects. This localization of excitation is the key advantage compared to single-photon excitation microscopes, which need to employ additional elements such as pinholes to reject out-of-focus fluorescence. The fluorescence from the sample is then collected by a high-sensitivity detector, such as a photomultiplier tube. This observed light intensity becomes one pixel in the eventual image; the focal point is scanned throughout a desired region of the sample to form all the pixels of the image.

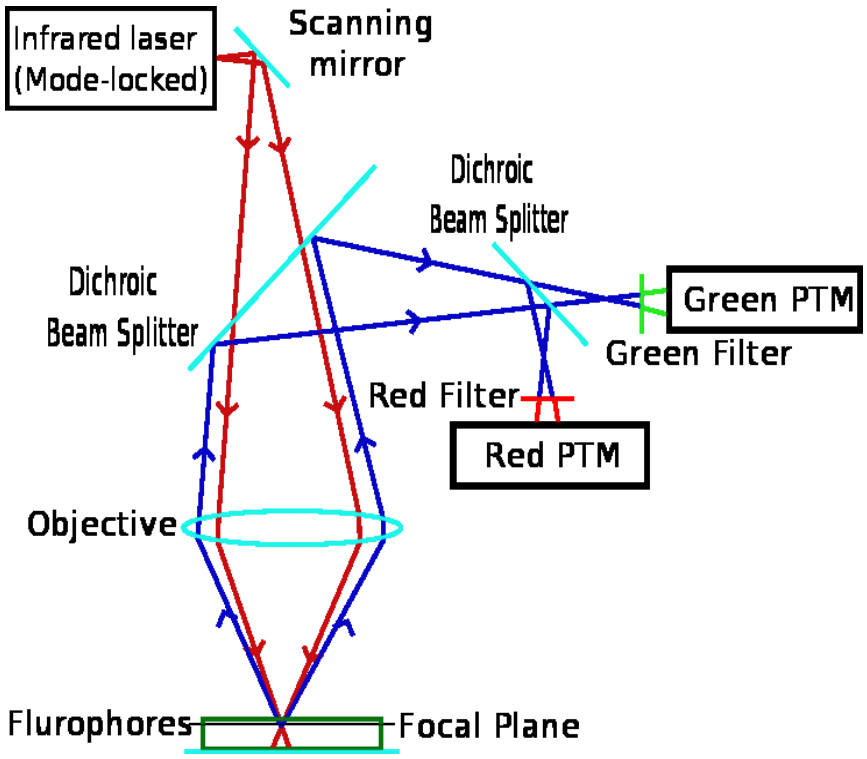

Figure 5.16 Diagram of a two-photon excitation microscope.

The emitted photon doesn't carry the same amount of energy as the excitation photon as some energy has already been lost during the Internal Conversion (IC). The whole process of excitation-emission is cyclical, so unless the molecule is destroyed while it is in the excited state (photobleaching), a photon can be detected many times from a molecule.

The TPM has been a helpful tool for numerous biological researches. The requirements for high resolution in-vivo imaging techniques in many biological studies made the TPM a real success. The TPM is particularly used in the neuroscience field to get insights in the electrical activity in some neuronal regions.

5.3.2 Materials and methods

The TPM was used to obtain images of the SAS in a live Sprague-Dawley rat. The animal was anesthetized with pentobarbital sodium injected subcutaneously. To get better images a quantity of fluorescein, a fluorescent dye, was also injected into the blood stream. The animal body temperature was kept close to 37 °C as the rat was easily flat to hypothermia. In order to get images of the SAS, we first needed to perform a craniotomy on the animal. This provides better precision to get images of the SAS. For the craniotomy the top of the head was shaved and scissors were used to cut the skin and the muscles surrounding the cranial bones. These muscles were cut to avoid the animal head of moving too much as the animal was breathing and to provide a better stability of the head for the TPM and achieving better accuracy when analyzing the images. Once the skull was bare, the bone was rubbed with a 2 mm diameter flat head drill. An area of about 2 -3mm in diameter was created on top of the skull next to the sagittal suture. While performing the craniotomy, the area rubbed down was cooled several times with a saline solution to prevent the tissues to be warmed too much by the rotating head. After the blood vessels of the SAS were getting apparent and the skull was getting softer, the head of the drill was switched to a smaller round head to pierce the thin layer of bone that was remaining. Particular attention was given at this step as we had to take care not to rupture the dura mater. Once the craniotomy was done, the animal was prepared for the TPM. Under a light microscope the craniotomy was examined and the area was cleared out of remaining hairs or bone fragments. To prevent the head of the animal moving while breathing, a fixture was set up. First, the exposed skull was dried and a curved nail

was fixed to the frontal part of the animal head with super glue. After the glue was dry the nail fixation was reinforced with dental cement (Jet Denture Repair) applied all around the nail. While waiting for the cement to be dry a transparent polymer was applied all around the craniotomy to create a small fountain onto the craniotomy. This fountain was used to contain a few droplets of water where the objective of the microscope would be applied later on. Once the cement was dry, the nail was fixed to a metal holder immobilized by magnets. This system was then moved with the rat under the Two-Photon Microscope. The hole was located on the head of the animal and the microscope was applied on top of it by touching the water in the fountain. At this stage it was really important that the head of the animal didn't move too much to not blur the images. If any movements were seen with the microscope then adjustments could be done on the fixation system. Images were taken with the Ultima IV two-photon microscope (Prairie Technologies) and the Prairie View software was used to visualize them. The resolution used was 512X512 pixels. The fluorescence provided by the dye was used to detect the blood vessels and to ascertain that we were imaging the SAS and not the skull. Unfortunately it appeared that the fluorescent dye was simply leaking out of the vessels throughout the whole SAS, making it impossible to visualize the vessels. Nevertheless everything was fluorescent but the bone of the skull which helped to localize the SAS.

5.3.3 Result

Photograph of the SAS of the live rat were taken at different positions on the z-axis, as shown in Figure 5.17. Prior to taking photo the SAS was first examined in depth to determine a "top" and a "bottom". Then the program could take images at an interval

of 10μm between those two boundaries. The head of the animal was still moving a little bit despite the fixation system. This was not helping to have the structures of interest at the same position on the x-y plan, making it difficult to track the trabeculae structures.

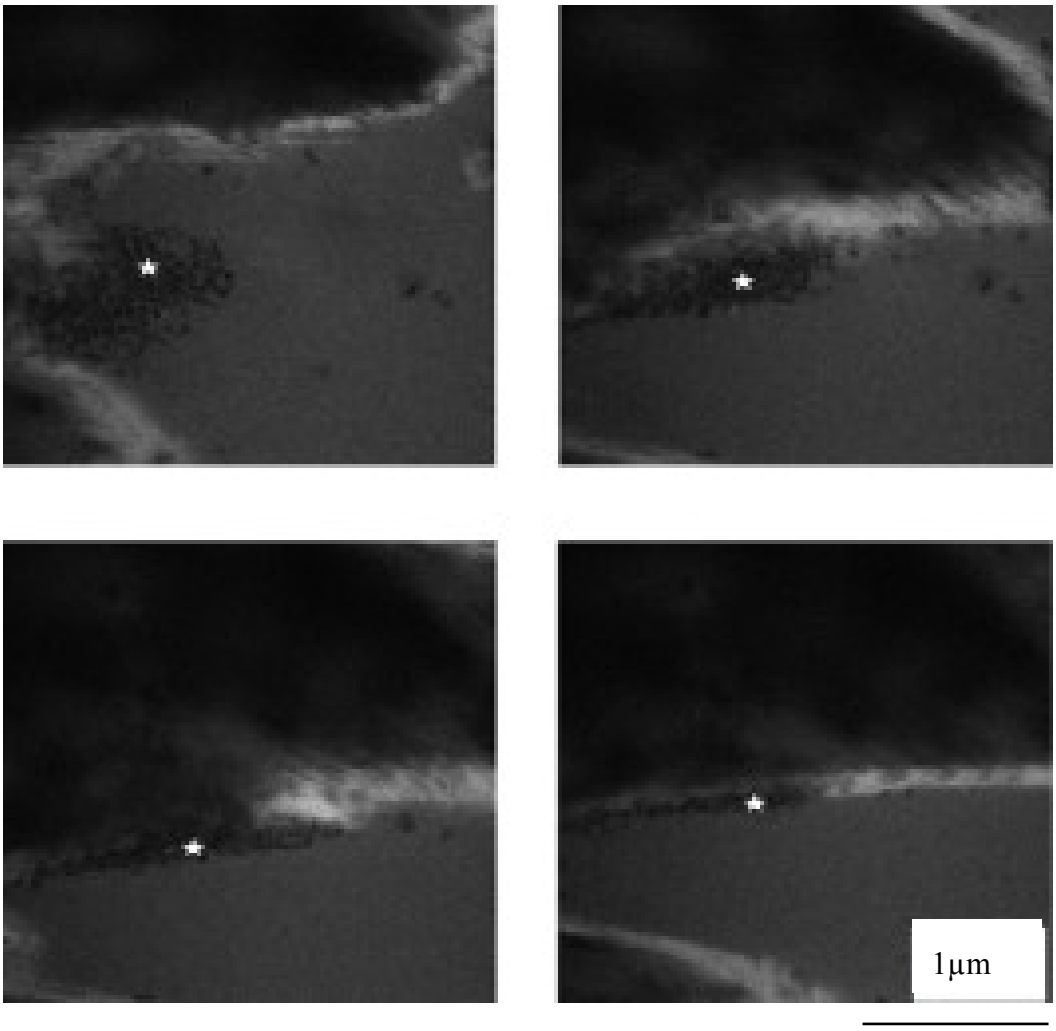

Figure 5.17 Two-photon micrographs of SAS in the live rat. Star indicate the cross section of one trabeculae.

5.3.4 Conclusion

The results obtained with the two-photon microscopy represent a good start for the animal experimental study of the SAS. The fluorescent stain allowed locating the SAS with respect to the bone. The skull appeared as a dark space on the photos as shown in Figure 5.17, where the SAS was fluorescent. The boundaries between these two structures could be easily pointed out, and surprisingly some interesting features were observed in this space. Indeed at various locations next to the skull an agglomeration of dark spots were found. Given the scale bar these structures seemed to have a diameter of between 100nm and 200nm. They always appeared grouped close to the skull.

It was not easy to understand and interpret those results. The little dots could be either the trabeculae or they could be some parts of the skull as they seemed related to it. With the fluorescent staining we were sure that the images are taken in the SAS.

Nevertheless it was impossible to know whether the dark spots were belonging to the SAS or to the skull. There was a possibility that we destroyed some of the trabeculae which can explain why there was just a group of the trabeculae structure close to the skull. On the other hand, if the dots were parts of the skull an explanation for that could be that at those locations the skull had been ground and those features were the internal structures of the bone. At that point there was no means to understand those structures and to know to which part of the head they belonged to and what functions they had.

The two-photon microscopy was a very interesting technique for this experimental study. But there were numerous difficulties to set up the experiment. The

craniotomy had to be performed precisely to prevent the rupture of the SAS, the head of the rat had to be fixed tightly under the microscope to avoid any movement and to possibly get a set of pictures allowing a 3D reconstruction, and eventually the objective of the microscope had to be placed exactly on top of the craniotomy. All these steps were not easy to follow and a lot of experiments ended with no results. A lot of practice and improvements were needed.

There was a great expectation from the two-photon microscopy as this experiment was performed in vivo. We were hoping to visualize the entire SAS with the depth of focus of this technique. Unfortunately the results were not as accurate as we were expecting. The dark spots found in the craniotomy couldn't be explained as there was a lack of reference to be related to those structures. We couldn't state any conclusion about the results but later on the experimental study these results were used as a comparison and reference with the results obtained with the SEM and TEM.

5.4 Scanning Electron Microscopy (SEM)

3D imaging provides additional information in any anatomical study where we cannot find this information from 2D study. Scanning electron microscopy (SEM) is one of the important tools for understanding the shape and structure of trabeculae and also it can help us to have better understanding of the density and trabeculae network.

In addition to a 3D representation of the samples, the SEM also provides a much higher resolution than the light microscope, which allows obtaining details of the ultra structure of the SAS. The SEM study was done with the rat brain only because it was

easier to manage the sample preparation compared to the human and bovine brain. Indeed the human brain cadaver was already fixed in formalin but the SEM required a glutaraldehyde fixation. The bovine brain was fresh but the SAS was already collapsed therefore it didn't represent a good candidate for the SEM. The SD rat was the best option for the SEM. The SAS was fixed during a perfusion-fixation and then permanent in the adequate fixative. The results obtained with the SEM went past our expectations and gave us new perspectives about the SAS.

5.4.1 Basic concepts in SEM

An electron microscope is a type of microscope that produces an electronically-magnified image of a specimen for detailed observation. The electron microscope (EM) uses a particle beam of electrons to illuminate the specimen and create a magnified image of the particle. The microscope has a greater resolving power than a light-powered optical microscope, because it uses electrons that have wavelengths about 100,000 times shorter than visible light (photons), and can achieve magnifications of up to 2,000,000x, whereas light microscopes are limited to 2000x magnification. The Scanning Electron Microscopy (SEM) is a type of microscopy based on electrons to get images of samples. Compared to the light microscopy, the SEM provides a much higher magnification and a field of view that goes deeper into the probes which gives a three dimensional appearance to the image. as shown in Figure 5.18.

Figure 5.18 Scanning electron microscopy machine.

In addition to topology and morphometry information, this kind of microscopy furnishes data about the composition and the crystallography of the sample. SEM works by projecting electrons on a sample and collecting the signals coming out of the probe. A beam of electrons is accelerated by the positive electrical potential between the electrodes. The energy carried by the electrons goes from 100eV to 30keV but all the electrons in the beam always carry the same amount of energy (monochromatic beam). Eventually the scans coils deflect the beam and position it onto the surface of the sample. Figure 5.19 depicts SEM set up.

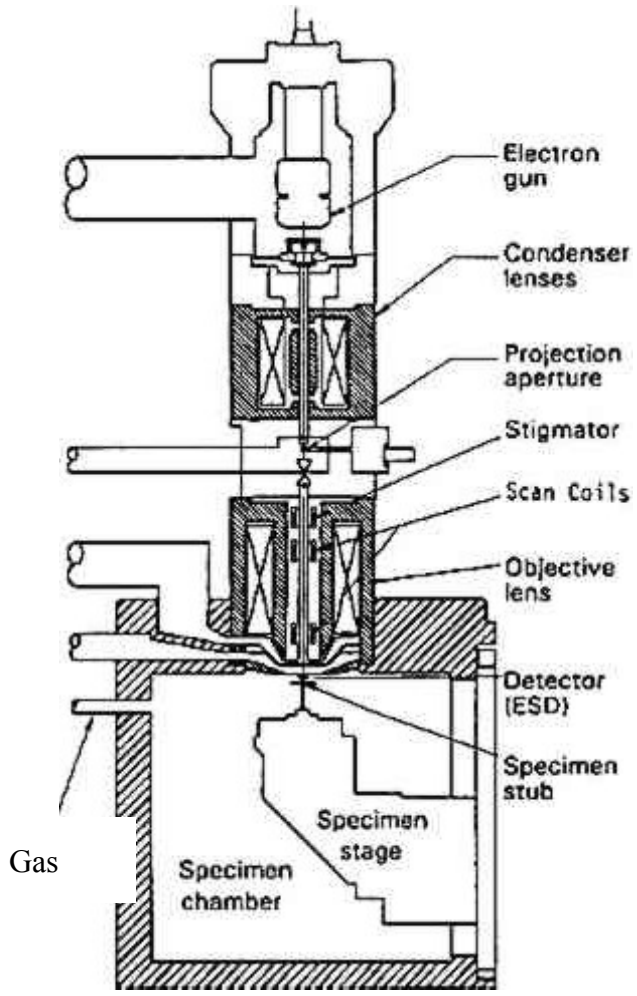

Figure 5.19 Setup of a scanning electron microscope.

5.4.2 Materials and Methods

For the first experiment using SEM the rat was perfuse-fixed following the same procedure as the perfusion-fixation for the histological sections. It appeared the injection of the fixative after the injection of PBS was not sufficient enough to keep the SAS open. Therefore we decided to directly perfuse the rat with a solution of glutaraldehyde 5%. Glutaraldehyde is a stronger fixative than the paraformaldehyde, so we expected it to better fix the structures in the SAS. In addition to that we expected that the direct

injection of fixative would be fast enough to fix the SAS before it has opportunity to collapse. The rat was perfused and fixed for about 5 minutes with glutaraldehyde 5%. Then the head was cut, the skull was carefully dissected and the brain was extracted with the dura mater. The sample was kept in the glutaraldehyde 5% solution for a night therefore the brain was completely fixed. In order to observe it with the Scanning Electron Microscope we needed to do some preparation. We followed the regular protocol of biological sample preparation (Appendix 2) with some adaptations for the type of sample we had. The first step in the preparation was to cut the brain to get smaller samples. Cerebral sections were obtained by cutting along a sagittal plane. The sections were then cleared from the glutaraldehyde 5%. This was done by taking the sample under the hood, selecting the samples we wanted to visualize under the SEM and washing them in distilled water (ddH2O). Care was given to keep the samples constantly wet. After 5 minutes the samples were rinsed with fresh ddH2O. In total, the samples were washed 5 times with ddH2O, each time for 5 minutes. In the end of this step, no glutaraldehyde 5% remained in the samples. The samples were then placed in a basket to perform the next steps. The ddH2O was washed out from the samples by the use of alcohol at different concentrations.

The basket was placed in a tube and 30ml of alcohol at 25%, 50%, 70%, 80%, 90%, and 100% were added consecutively in the tube for 5-10 minutes each time. The tube was shaken from time to time to get a better penetration of the alcohol within the tissues. Next the samples had to be dried. Drying them by air would lead to produce intolerable drying artifacts. Therefore the Critical Point Drying technique was used. The

samples were immersed in a chamber in liquid CO_2 and rinsed 7 times for 5-10 minutes. After the alcohol was washed out, the samples could be dried. The temperature of the chamber was raised to 40°C, letting the CO2 change from liquid phase to dry gas phase. This step was achieved without the effects of surface tension that produce artifacts in air drying. CO2 is the best solution for drying delicate probes such as biological samples. As it is not miscible with water, the samples have to be stored in another liquid before the liquid CO2 is added. This is why the alcohol is used in the previous step.

Eventually the dry samples were mounted on the SEM pins, where a double-face tape had been taped beforehand. If specimens are not coated immediately after the drying, they have to be kept in the oven at 60°C to avoid moisture to be trapped by the samples. Eventually the samples were coated with gold particles just prior to observe them with the SEM. The coating enhances the conductivity of the electrons and prevents an accumulation of charge in a certain area that could lead to artifacts.

5.4.3 Results

The results obtained with the first trial of SEM were interesting but didn't really show the trabecula and their network. Most of the SAS and the blood vessels had collapsed and only a few trabeculae were kept intact see Figure 5.20. The structure of the pia mater and the arachnoid was exposed and it appeared that they were made of bundles of fiber highly oriented and tightly packed together.

The second trial with the SEM technique provide us really good results. The SAS was almost fully open and the blood vessels as well as the red blood cells were extremely

preserved, (Figure 5.21 to 5.30). Those results allowed to clearly observing the different layers of the meninges, the SAS Figure 5.21, the trabecula ,Figure 5.22, and their fine structure as shown in Figure 5.23. The high resolution of the SEM uncovered the constitution of the trabecula down to the molecular level. A new dimension of the SAS was exposed.

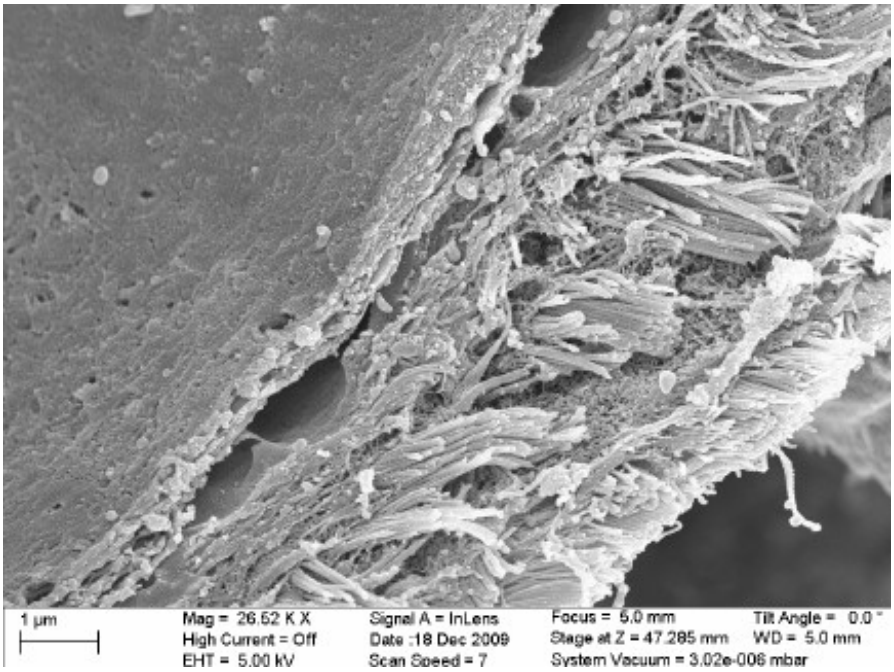

Figure 5.20 SEM micrograph of the dura and arachnoid layer in the rat brain.

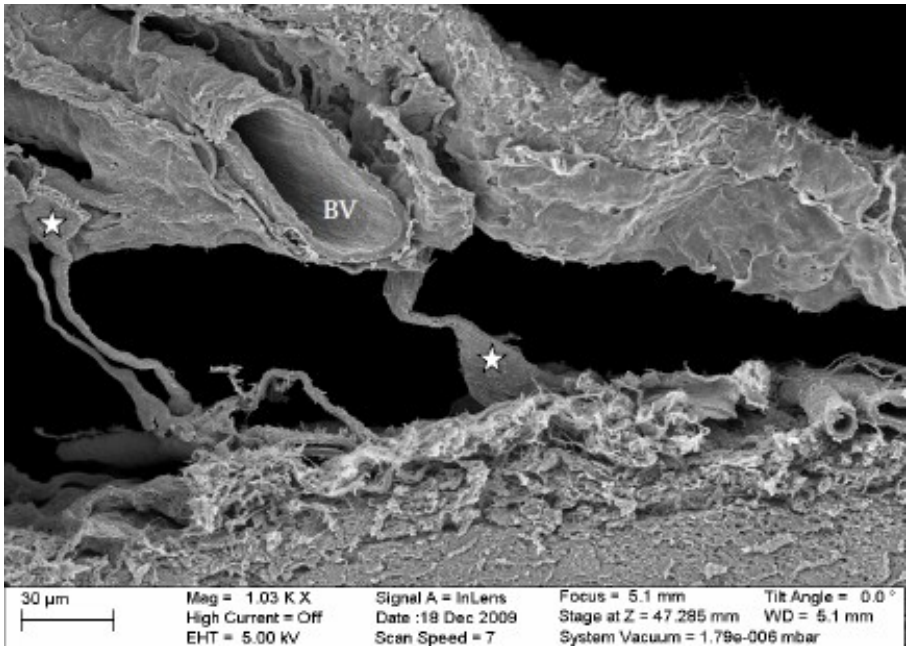

Figure 5.21 SEM image of the SAS in the rat with some trabecula (star) surrounding a blood vessel (BV).

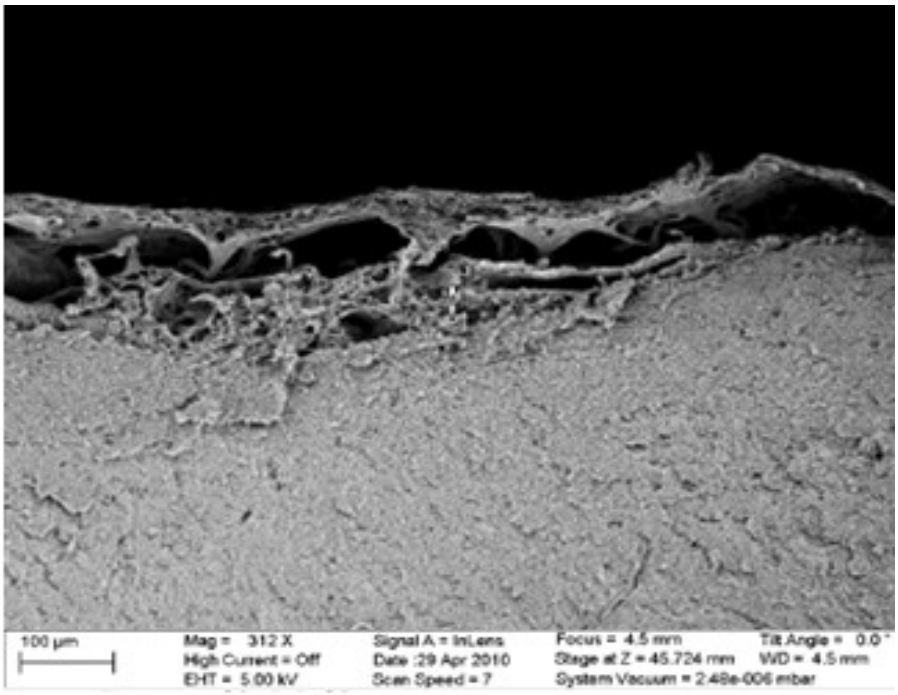

Figure 5.22 SEM image of the SAS of the rat.

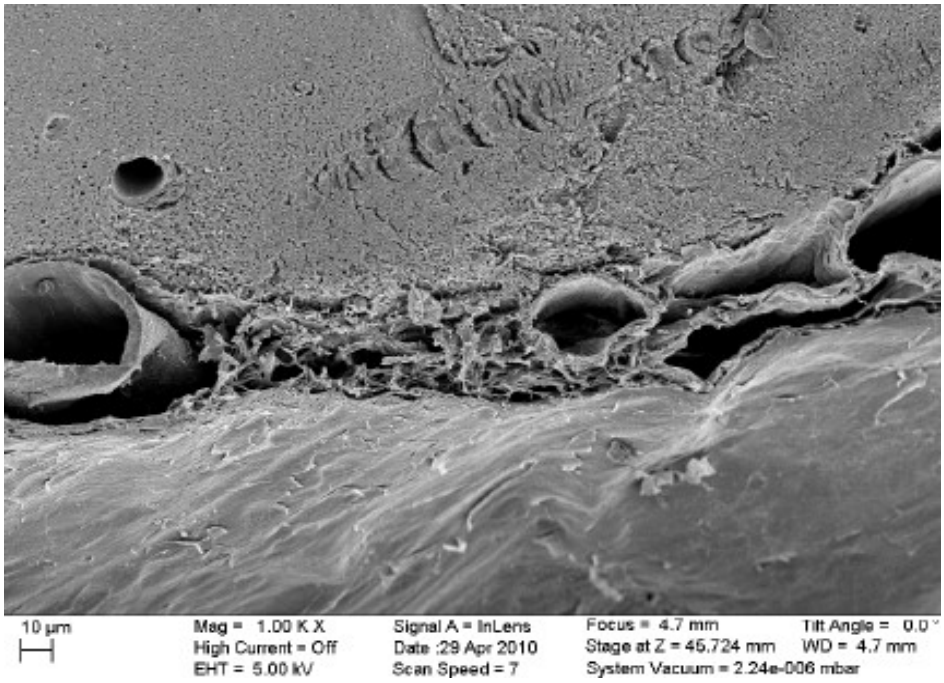

Figure 5.23 The SEM image of the brain of the rat.

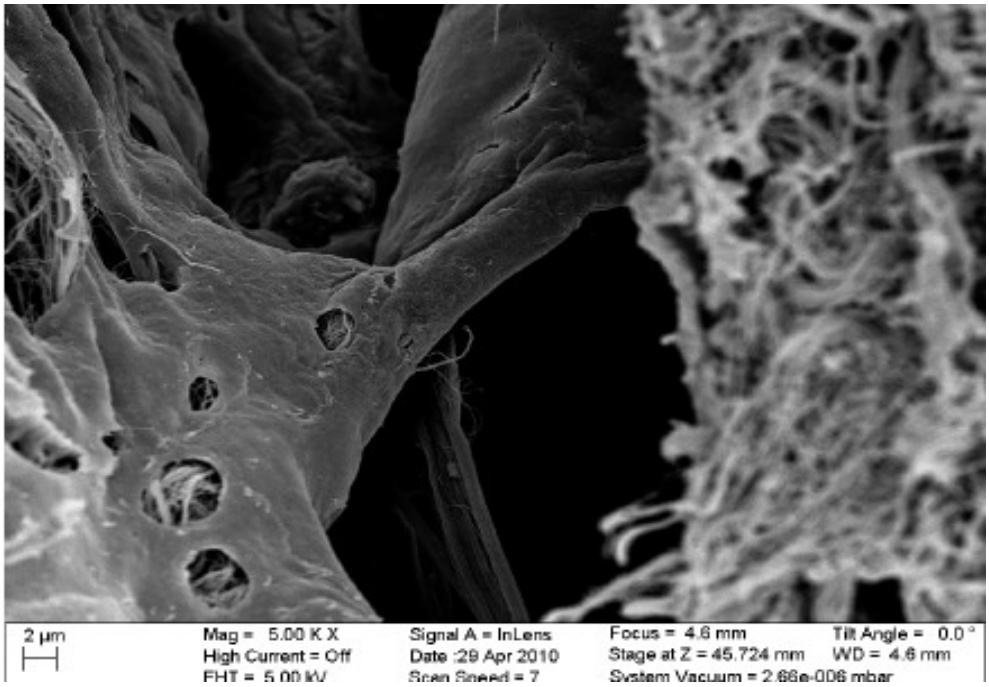

Figure 5.24 SEM image of plate appearance of a trabecula.

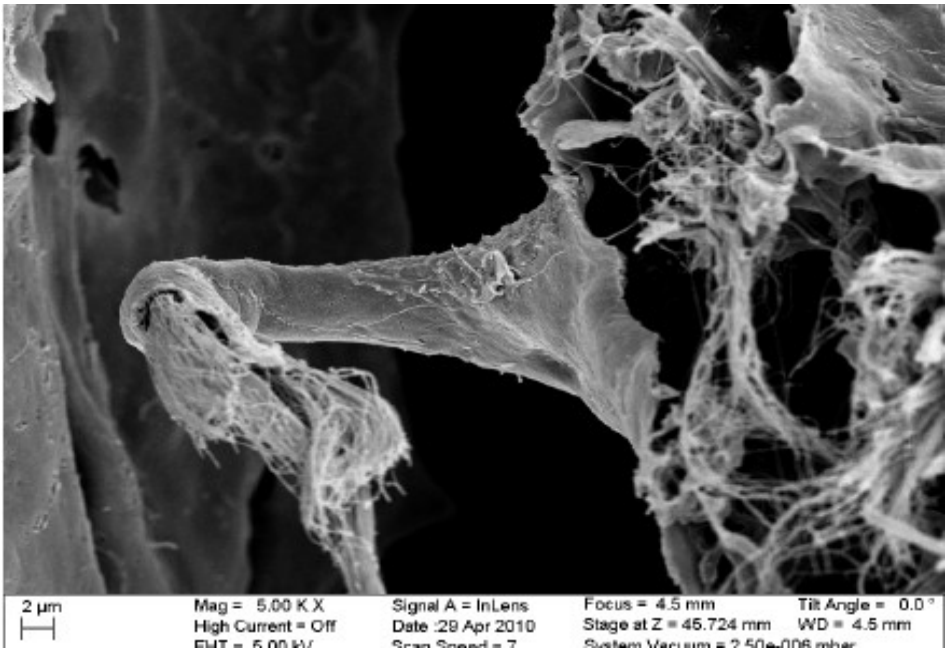

Figure 5.25 Internal structure of a trabecula.

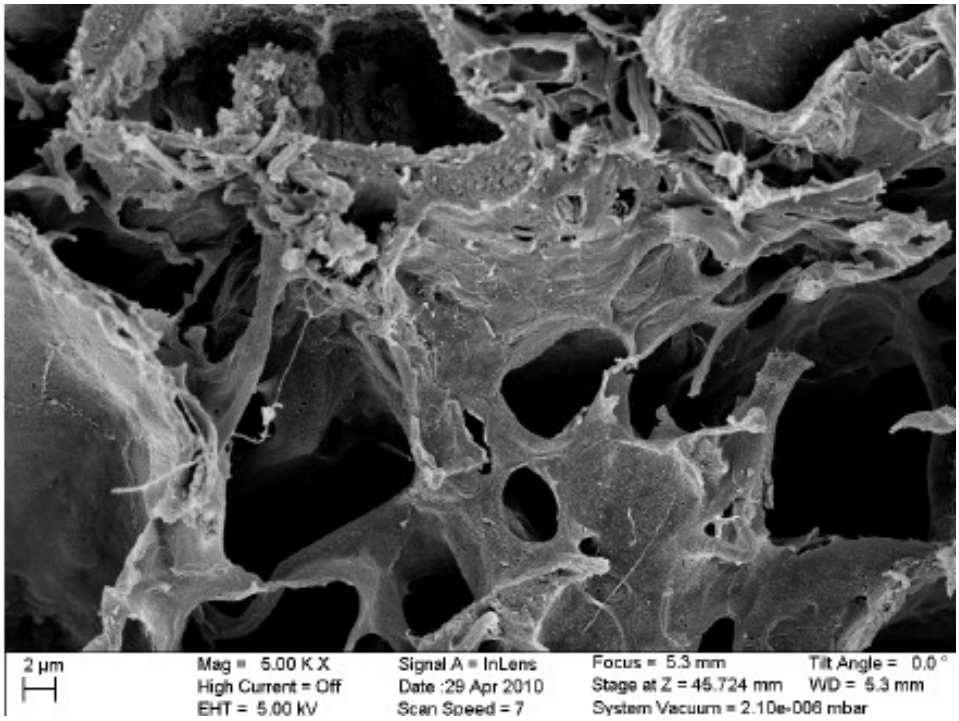

Figure 5.26 A trabeculae network.

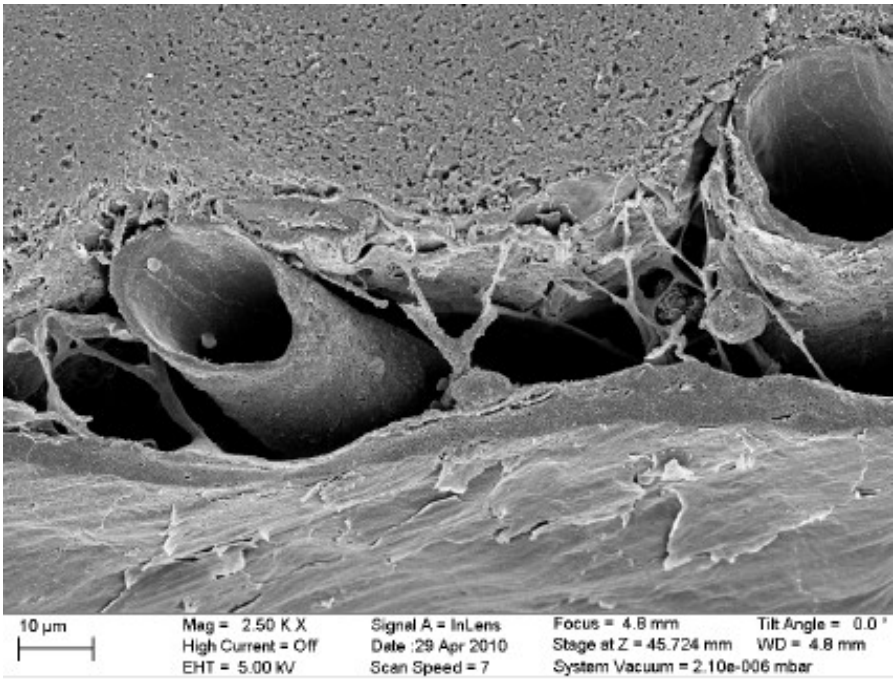

Figure 5.27 Branched trabecula within the SAS.

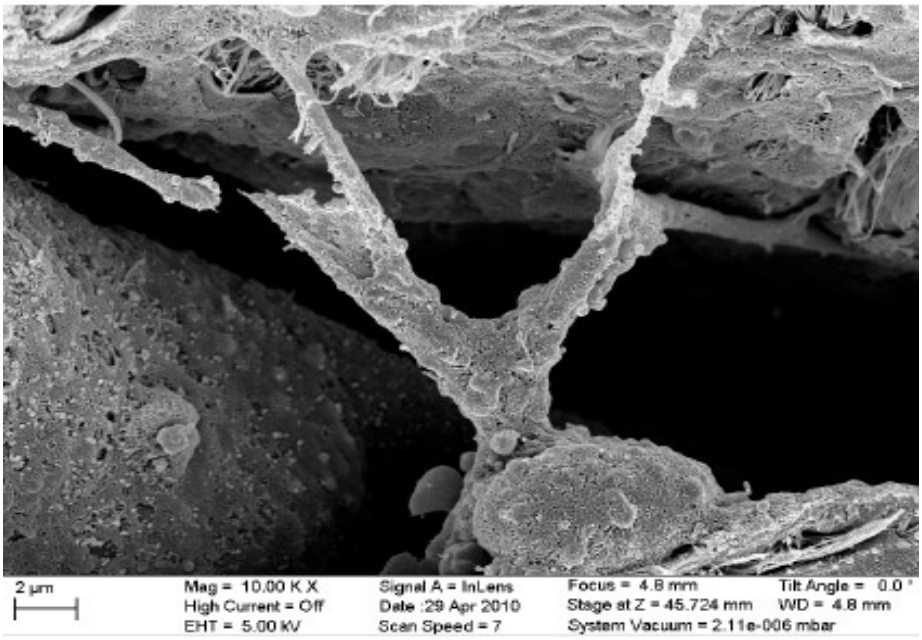

Figure 5.28 Branched trabeculae in the SAS.

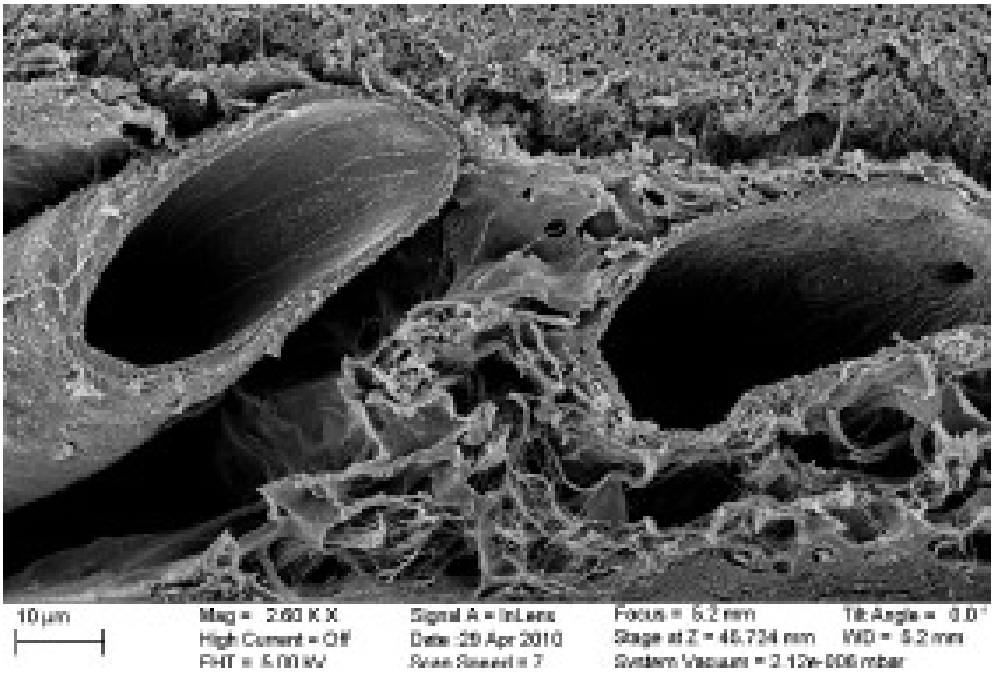

Figure 5.29 Veil-like networks within the SAS.

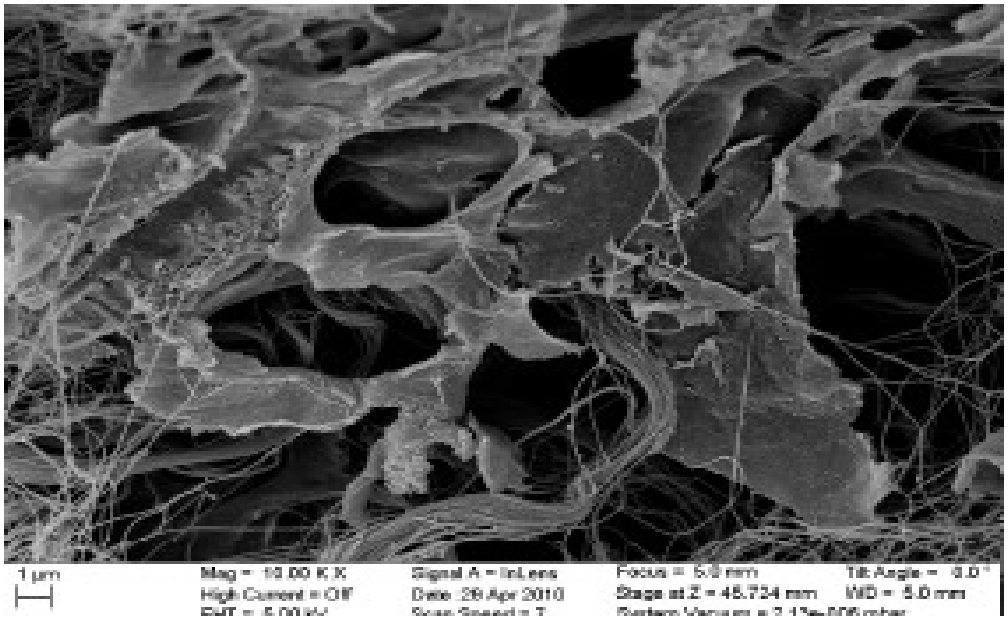

Figure 5.30 Veil-like networks.

5.4.4 Conclusion

The results presented by the SEM were more encouraging than the results found with the two-photon microscopy or with the histological sections. The SAS appeared completely different than what was mostly sketched or explained in the anatomy books. Instead of being simply rods connecting the pia and arachnoid layer, the trabecula displayed various shapes and organizations. They were taking the form of simple or branched rods, tree-shaped, pillars, plates, or complex networks. The basic building blocks for the components of the SAS were the collagen fibrils. Those fibrils were found everywhere in the SAS and were providing the tissues with structural and impermeable characteristics. The SEM photographs taken by Killer et al, 2003 in the SAS of the human optic nerve confirmed our results. Both SAS were exhibiting the same kind of shape for the trabecula. It was also extremely important to be able to compare those results as they were coming from two different species.

5.5 Transmission electron microscopy (TEM)

The TEM provides 2D images in histological sections. The advantage of this technique is that the resolution is very high, in nanometer scale. This allows clearing the cellular structure as well as the structure of the organelles within the cells. TEM represents a complement to the SEM study but not a good result for architecture of the SAS. It also helps understanding the connections between the cells in the meninges or between the trabecula and the blood vessels.

5.5.1 The basic concepts of TEM

TEM works the same way as a light microscope, except that the light is replaced by electrons. In this technique electrons are produced, accelerated and focused in the same way as in SEM. The difference with SEM happens at the sample level. In TEM, the thickness of the sample is about 100nm which allows the electrons to travel through the specimen and to end up hitting a fluorescent screen. Some electron may disappear or be deflected, but in that case it doesn't provide any information in comparison with the secondary electrons in the SEM. If there is dark spot in images it means a smaller number of electrons passed through that section. The structures and gradients of the sample are produced by the varying amount of electrons passing through the specimen.

5.5.2 Materials and methods

The samples for the TEM were obtained from the same brain used for the SEM. In this technique the specimens need to be at most 1 or 2 mm in size, therefore we had to choose the location of the brain to be cut. We decided to extract the area surrounding the superior sagittal sinus by cutting the brain along a sagittal plane on both sides of the sinus. The section was then shortened to be about 1mm high from the top of the brain and chopped into approximately 1mm-size pieces. The samples were prepared following the regular protocol for biological samples preparation with some modifications for the kind of tissue we had (Appendix 2).

Brain tissues are very soft, therefore we used acrolein (a chemical used as tear-gas during World War I) to help the fixative to penetrate the tissues. A better fixation of the

tissues decreases the number of damages that can occur in the next steps of the sample preparation.

After one hour in acrolein the specimens had turned black. They were immersed in the secondary fixative, osmium tetroxid 2%. Osmium tetroxide 2% and acrolein are two extremely toxic chemicals, therefore these steps were performed under the hood. The samples stayed 30 minutes in osmium tetroxide 2% and were then washed with ddH2O three times for 5 minutes. Once washed, the samples were dehydrated in alcohol with grading concentrations (20%, 30%, 40%, 50%, 60%, 70%, 80%, 90%, 100%) and then rinsed twice in propylene oxide for 5 minutes. The specimens had to be embedded in resin. This step was done by infiltrating the samples with increasing concentration of resin (30%, 70%, 90%, 100%). For each concentration the jar containing the resin and the samples was placed on a shaker for three hours. Eventually each piece was transferred to the bottom of a triangle-shaped beam capsule with the pipette and then each capsule was filled ¾ of the way with resin at 100%. The capsules were place in the oven at 60 °C to allow the resin to solidify.

After one day, the resin was solidified and the samples were ready to be cut. The specimens were released from the capsules and among them one was chosen to be sliced. The sample chosen has to be the one that best exposed the surface of interest. This step was a little bit tricky as the samples were all dark by that time. Therefore it was extremely difficult to find the orientation of the samples. Once a block had been picked up the sample was exposed by trimming the extra resin at the tip of the block. The block

was given a pyramid shape by cutting it with a razor blade. This pyramid had to be 0.5mm on each side.

The block was transferred to the microtome and its position was adjusted with respect to the diamond knife. The thickness of the sections was set to 100nm. This dimension was assessed by looking at the color of the sections under the microscope. Given the thickness and the homogeneity of the sections those exhibited different colors. According to the color-thickness scale, gold is the color corresponding to a thickness of about 100nm. Once we had enough sections, we used a moist eyelash to group them by 6-7, and then we transferred them on the shiny side of the small round grids. The grids with the sections facing up were dried on a lens paper.

The sample were stained with uranyl acetate and lead citrate. Uranyl acetate is always the first stain to use. The samples were stained one by one by placing them in a droplet of uranyl acetate for a time varying between 30 minutes and 2 hours. For the first TEM experiment we stained only one grid for 15 minutes and then brought it under the TEM to check whether we sectioned it in an appropriate orientation or not. If this was the case, the other grids were stained for 2 hours in uranyl acetate, and then 15 minutes in lead citrate. Lead citrate does not really stain the sections, it enhances the contrast and helps distinguishing the different structures within the samples.

The preparation of samples for a TEM study is a long process. As it requires more steps than SEM it is more likely to either damage the samples or to dirty them during the preparation. Therefore the solutions used in the different steps have to be freshly

prepared, the tools used to carry the specimens or the grids have to be clean and the samples have to be handled with an extreme care.

Although the section from our first experiment had SAS and we were able to observe the cellular structure of SAS but because of the quality of the diamond blade that was used for sectioning our images were not good enough to be used for publication. To prevent the problem with the sectioning new set of the samples were obtained using the same procedure and this time we used a new bald for sectioning and followed by using uranyl acetate and lead citrate. The sections were stained in Uranyl acetate (2% in 50% ethyl alcohol) for 40 minutes followed by Reynolds lead citrate (0.06 grams lead citrate in 20 cc distilled water and 0.2 cc 10N sodium hydroxide) for 4-5 minutes. Staining times was varied with the sample contents. Stained grids are studied using Philips CM-12 transmission electron microscopy at 80kv accelerating voltage.

5.5.3 Results

With the TEM images we were are able to observe the cellular and subcellular structure of the SAS. Comparing the result with SEM the different layers of cells could be clearly identified. The separation between the brain and the SAS was not as clear as the SEM, therefore the myelin sheet of the neurons were taken as reference to locate the brain. The contrast between the different components of the tissue sections was varying because not every sample had been stained with lead citrate, and for the samples stained with lead citrate, they were not all stained during the same amount of time. The sections stained with lead citrate provided a better contrast and made the recognition of the different

components easier. Figure 5.31 to 5.41 show different orientation for SAS in rat brain. Figure 5.41 shows the longitudinal and cross section of Collagen fibers in the SAS. The thickness of individual fibers and general appearance of the bundles confirm that they are type I collagen, Kierszenbaum (2007). However the periodicity is better seen in samples fixed with the addition of 1% phosphotungstic acid to the glutaraldehyde fixative.

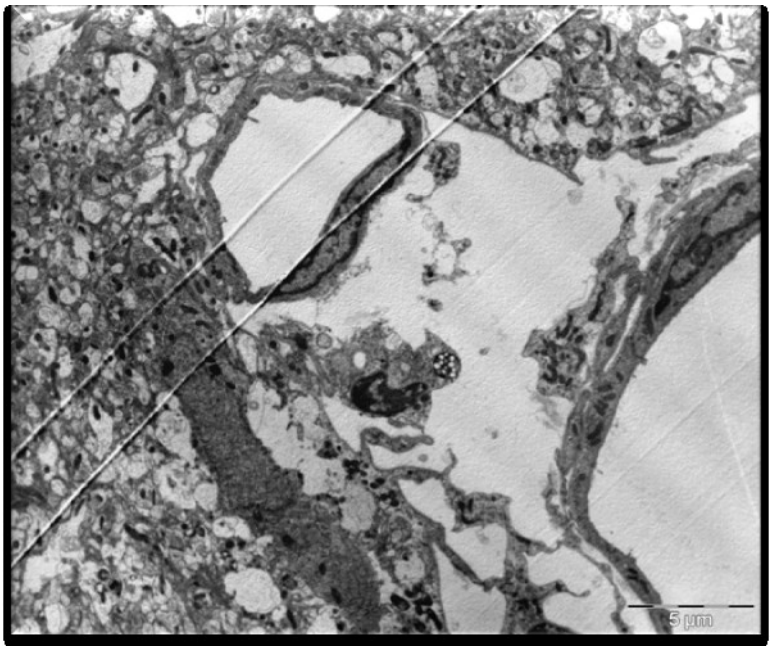

Figure 5.31 TEM section of the SAS in the rat brain.

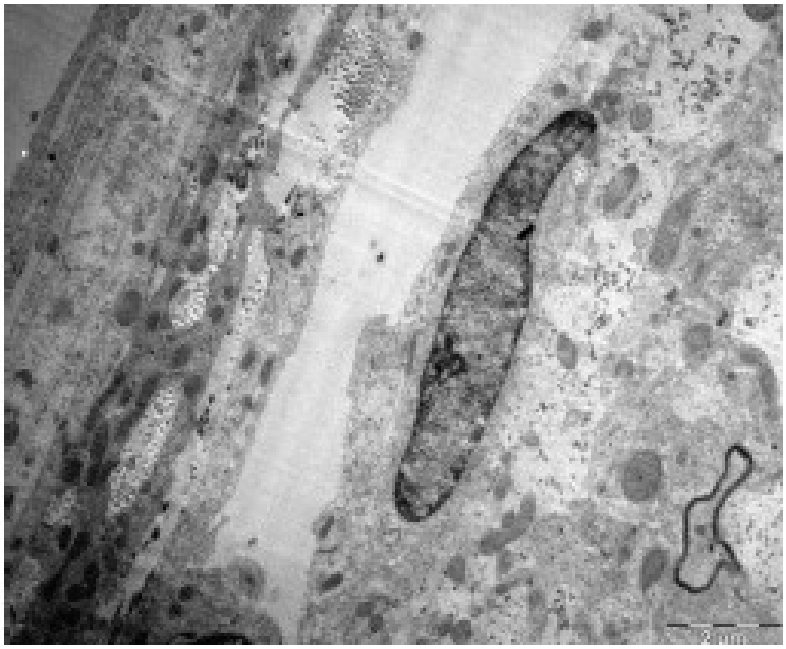

Figure 5.32 TEM section of the SAS in the rat brain.

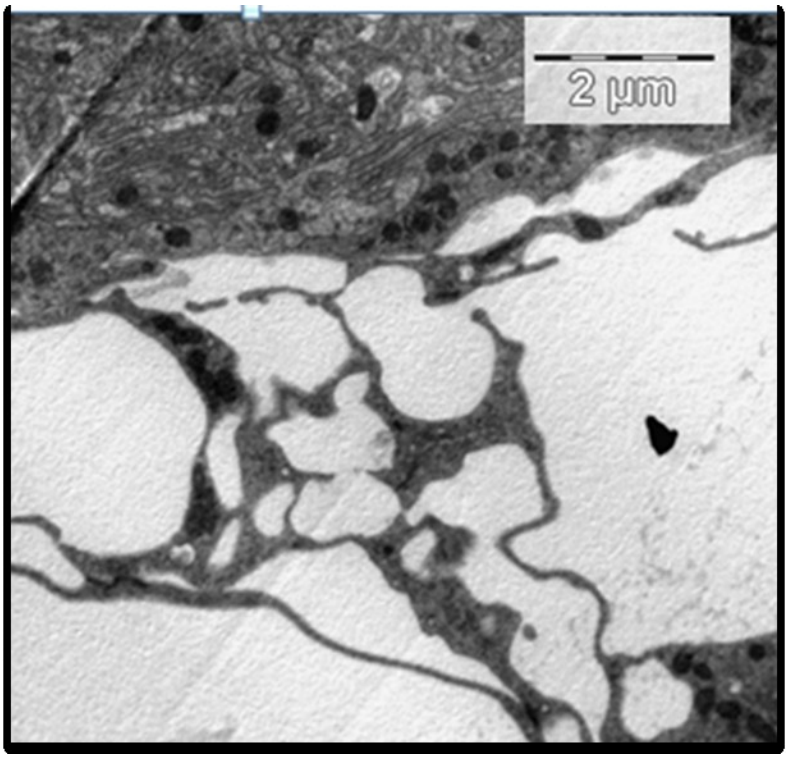

Figure 5.33 TEM section of the SAS structure in the rat.

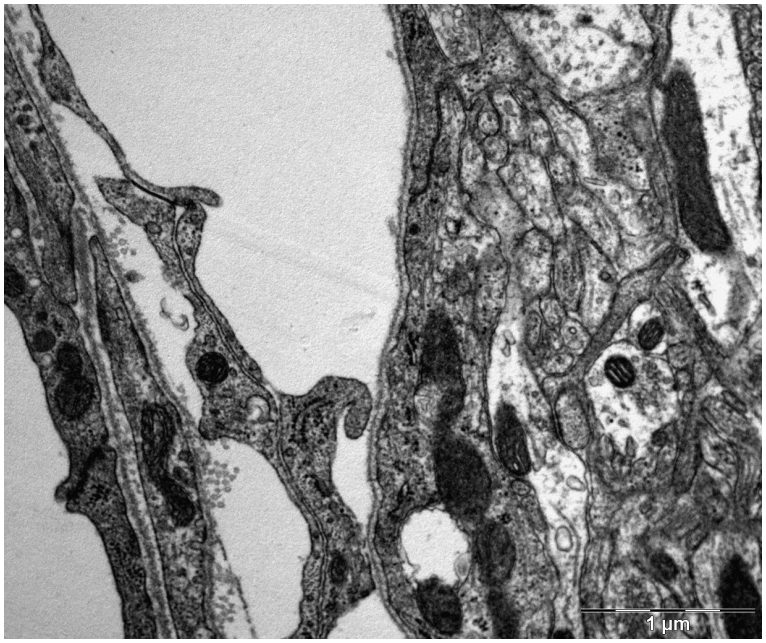

Figure 5.34 TEM section of the SAS in the rat.

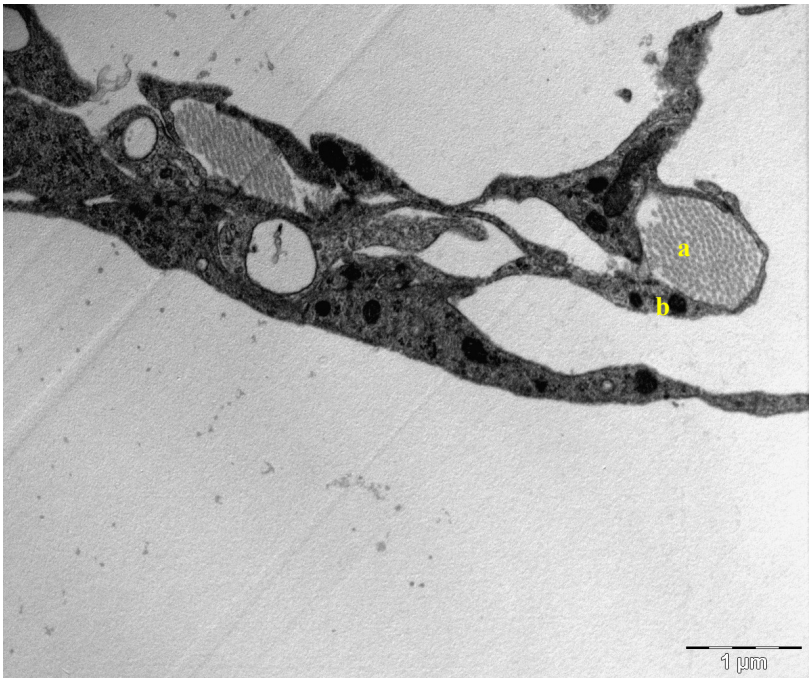

Figure 5.35 Bundle of collagen fibrils (a) surrounded with fibroblasts (b).

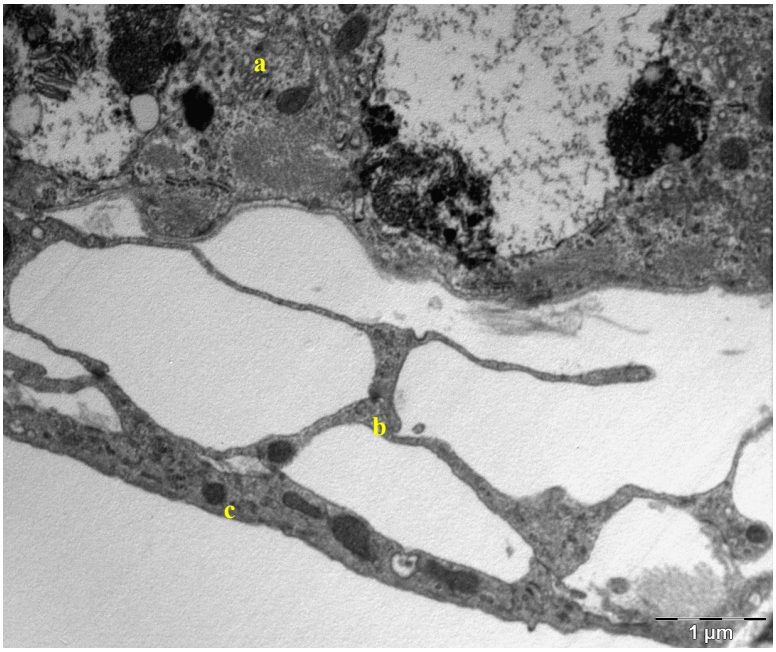

Figure 5.36 TEM section of the SAS structure in the rat, a: the brain, b: the SAS structure and c: the arachnoid mater.

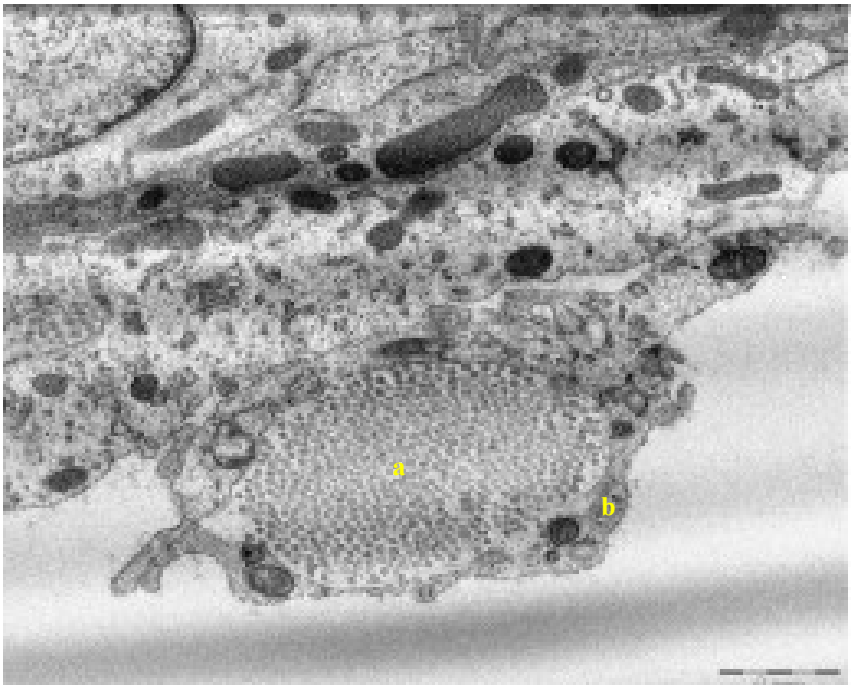

Figure 5.37 Bundle of collagen fibrils (a) surrounded with fibroblasts cells (b).

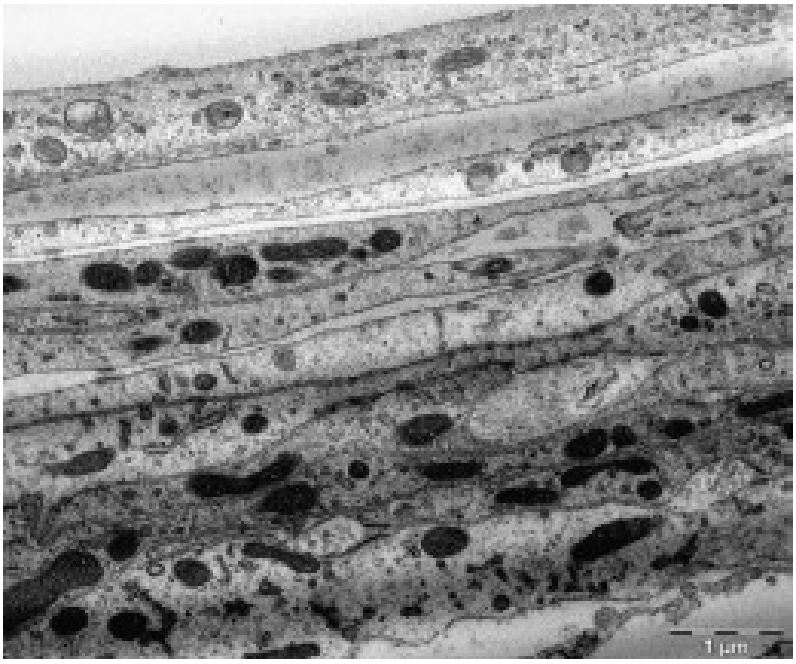

Figure 5.38 Layers of fibroblast cells in the arachnoid.

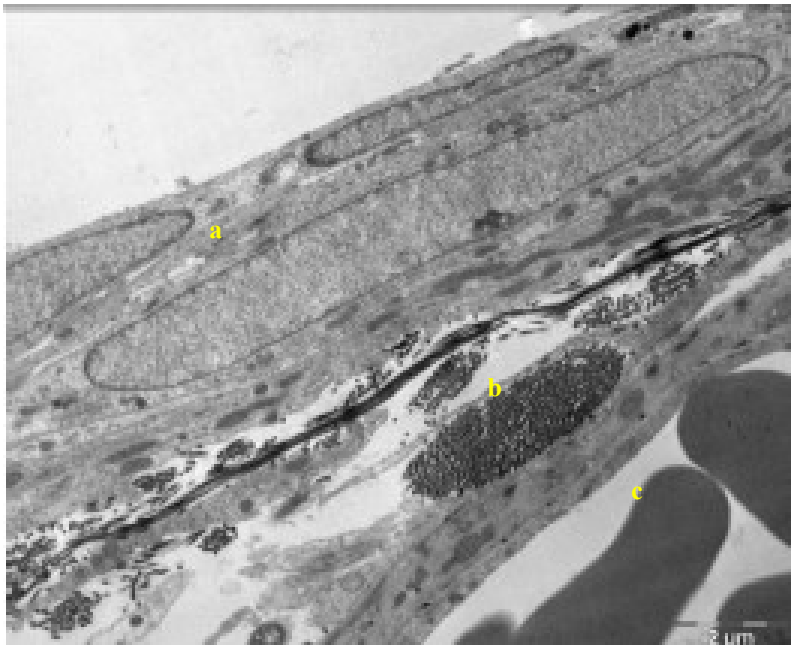

Figure 5.39 Arachnoid mater, a: the arachnoid mater, b: Bundle of collagen fibrils and c: the blood vessels inside the SAS.

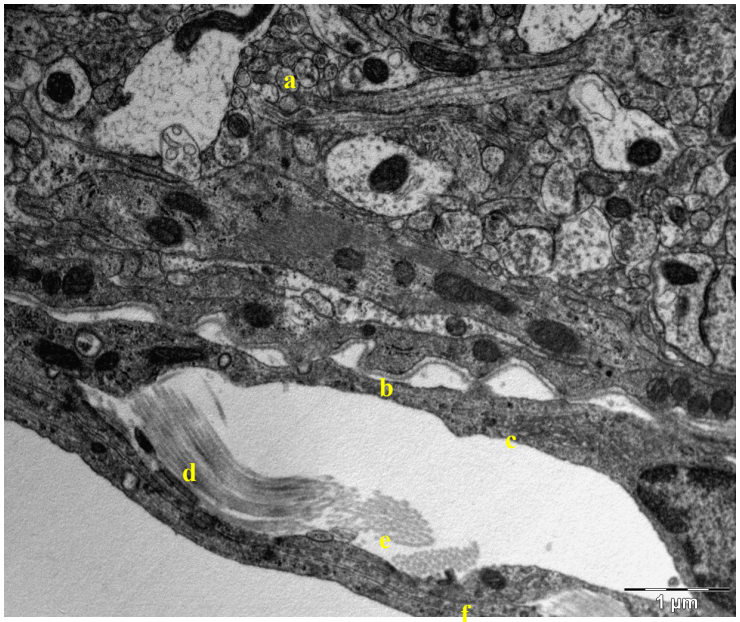

Figure 5.40 longitudinal and cross section of Collagen fibers in the Arachnoid side of the SAS, a: the brain, b: the basal lamina, c: the pia mater, d: longitudinal section of Collagen fibers, e: cross section of Collagen fibers and f: the arachnoid mater.

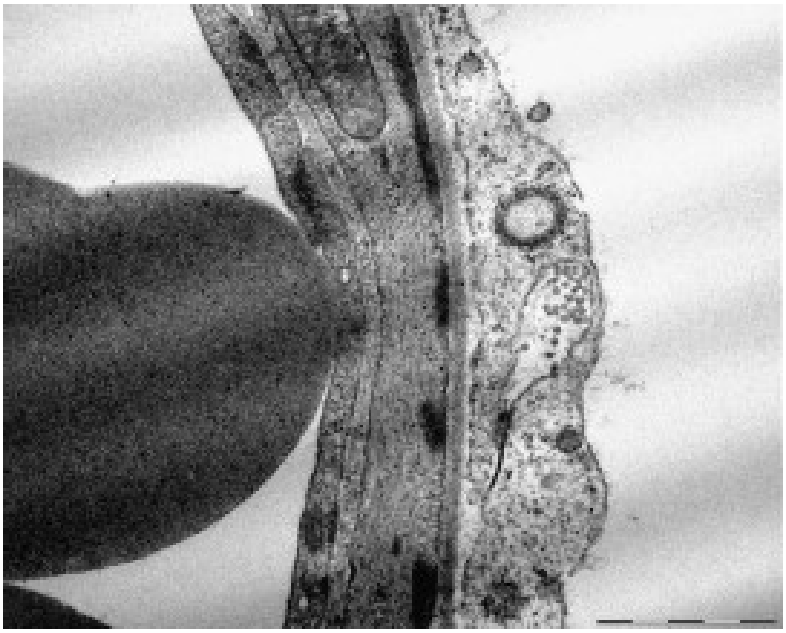

Figure 5.41 Small bundle of collagen fibrils on the external wall of a blood vessel.

5.5.4 Conclusion

The results from the TEM were obtained from a specific region of the rat brain: the super sagittal sinus. From the images obtained, one can identify that the sections could be either in a coronal plane or in a sagittal plane given the orientation of the layers of cells. No other detail helped to define an orientation or a location within the super sagittal sinus. The results provided good information about the cellular content of the SAS, In these figures the SAS side, the arachnoid layer and the brain could be easily distinguished from each other.

The flat cells on the arachnoid side were well defined and arranged in layers as shown in Figure 5.38. Whereas in the brain it was difficult to define the contour of some cells except for the axons of the neurons that were surrounded by a dark layer: the myelin sheet Figure 5.32. The blood vessels also helped to locate the SAS. The vessels were not collapsed, and the gap surrounding them indicated that the SAS was not collapsed either. The collagen fibrils were arranged in groups surrounded by fibroblastic cells. These bundles were located at different place. They were lining the fibroblasts of the arachnoid layer, inserted within the arachnoid layer or linked to the blood vessels via a fibroblast. The collagen fibrils in the arachnoid layer confirmed the results found with the SEM. The fibrils had two orientations: transverse Figure 5.37and lateral Figure 5.40. The transverse orientation was seen when the fibrils appeared as dots and the lateral was seen when the fibrils were forming long thin and dark straps. Those bands, when looking at them with a high magnification, were composed of an alternation of a light and dark strip. It was known that the periodicity of the strips is a characteristic of the type of collagen that is

forming the fibrils. In our case the quality of the images and of the samples was not good enough to be able to see those features and to measure them. The bundles of fibrils also appeared to have different compositions. Some bundles were full of fibrils tightly packed whereas other bundles were half or less full of fibrils. The reason for the inhomogeneous bundles was that the arachnoid didn't need to be as hard as some other structures containing collagen in the body. The collagen fibrils had a role of structure more than a role of support.

On the SEM results, the dura mater or the arachnoid mater seemed to possess very packed structures; therefore we thought that those layers would be impermeable. On the TEM results we noticed that some liquid was located between the cells on deep down the arachnoid layer. Thus this layer is permeable and some fluid was allowed to flow between the fibroblasts at some positions.

The TEM represented a much longer process than the SEM. The preparation of samples had more steps, and many of those steps were critical for the cleanliness of the sections. Nevertheless we were able to obtain good results to confirm or correct the guesses we made with the SEM results. The TEM images provided the information about the cellular content of the SAS that were lacking in the SEM. The arachnoid layer was made of fibroblasts, not only of collagen fibrils and those cells were forming a permeable layer. The pia mater was represented by a single layer of fibroblast cells covering the brain. The collagen fibrils were arranged in bundles and scattered in the SAS at the border and within the arachnoid layer, and also around the endothelial sheet of the blood vessels.

The second set of the samples was obtained for TEM study, where the glutaraldehyde was directly injected to the heart to perfuse the rat. The reason for injecting the glutaraldehyde as a first fixative was the sensitivity of the trabecula to collapse in the absent of CSF pressure.

CHAPTER 6 Material Properties

6 MATERIAL PROPERTIES

Material properties of the SAS are an important factor in modeling and finite element analyses of the SAS, when its histology and functionality is known. The second significant factor in the modeling is to accurate identify the type of tissue and the material for each segment of the SAS as it transfers the load to the brain. A wide range of material properties for the SAS region has been addressed in literature. In this chapter we briefly explain the material properties that are used for each part of the head/brain analyses.

Brain: The brain material properties are relatively established in the literature. While a wide range of material properties are reported in the literature, depending on the type of the study, different material properties can be used. Holbourn et al. (1943), Koeneman et al. (1966), Galford and McElhancy (1969), Fallenstien et al. (1969) a-b, used simple linear elastic material properties for their constitutive brain tissue. Arbogast et al. 1995, Miller and Chinzei (1997), Estes et al. (1970) and Bilston et al. (1998) used Linear and quasi- linear viscoelastic. Darvish et al. (2001) and Takhounts et al. (2003b) applied fully non linear Green- Rivlin for their model. Nicolle et al. (2004) used Ogden Rubber with linear viscoelastic and Takhounts et al. (2008) used linear viscoelastic model. Atomic Force Microscope Indentation (AFM) was used to measure the mechanical property of the brain and more specifically in the hippocampus of the rat, Elkin et al. (2007).

The extensive variety of the brain material properties reported in the literature make the decision rather complicated. Takhounts et al. (2008) performed simple shear displacement test on the 1x1x1 cube and study the effect of different material properties, the strain filed was compared with the existing experimental study e.g. Hardy et al. (2001). They conclude that the linear viscoelastic model will be fitted in most of the analyses and it's a suitable model for brain/ head impact analysis. Summary of different material properties were used for simple shear displacement are given on Table 6.1. Zhang et al. (2001and 2002) also used linear viscoelastic material properties for the brain tissue, Table 6.2 is a summary of the brain shear modulus and bulk modules that is used for this study.

Kelvin- Maxwell Viscoelastic (Takhounts et al., 2003b)		Quasi- Linear Viscoelastic (Takhounts et al., 2003b)		Linear Viscoelastic (Takhounts et al., 2003b)		Ogden Rubber (Nicolle et al., 2004)		Ogden Rubber (Kelvin, 2007)	
G_0 (pa)	1662	G_1(Mpa)	0.4	G_1(Mpa)	9.276e-04	μ_1(Mpa)	0.06	μ_1(Mpa)	5.38e-5
G_1 (pa)	928	G_2(Mpa)	0.41	G_2(Mpa)	7.352e-04	μ_2(Mpa)	0.00056	μ_2(Mpa)	-1.204e-04
β	16.95	G_3(Mpa)	0.19	G_3(Mpa)	3.876e-04	μ_3(Mpa)	0.00000125	μ_3(Mpa)	0.0
		β_1	0	β_1	0.0	α_1	0.0451	α_1	10.1
		β_2	17.08	β_2	16.95	α_2	-3.9	α_2	-12.9
		β_3	1.05	β_3	1.17	α_3	16.3	α_3	0.0
		C_1(Mpa)	.000985			G_0(Mpa)	0.32	G_0(Mpa)	0.32
		C_2(Mpa)	0			G_1(Mpa)	0.078	G_1(Mpa)	0.078
		C_3(Mpa)	0.03958			G_2(Mpa)	0.0062	G_2(Mpa)	0.0062
						G_3(Mpa)	0.008	G_3(Mpa)	0.008
						G_4(Mpa)	1e-4	G_4(Mpa)	1e-4
						G_5(Mpa)	0.003	G_5(Mpa)	0.0003

Table 6.1 Different models and material properties of the brain for constitutive models.

Brain tissue	
Shear modulus at t=0 (G_0) (Pa)	$10.0*10^3$
Shear modulus at t=∞ (G_∞) (Pa)	$2.0*10^3$
Bulk modulus at t=0 (K_0) (Pa)	$5.0*10^7$
Bulk modulus at t= ∞(K_∞) (Pa)	$5.0*10^7$
Relaxation time (λ) (s-1)	16
Density (ρ) (kg/m3)	$1.04*10^3$

Table 6.2 Tissue material properties of the brain as a linear viscoelastic model, used in this study.

The Subarachnoid Space: The histology, architecture and material properties of the subarachnoid space trabeculae have not been fully addressed in the literature. However, Killer and Groscurth (2003) studied the structure of the trabeculae in human optic nerve. They found that the structure of the trabeculae varies along the optic nerve. That is, the architecture and histology of the trabeculae gradually changes as the nerve approaches the brain. They conclude that the subarachnoid space of the human optic nerve is not a homogeneous region and it contains a complex system of arachnoid trabeculae and septa that divide the subarachnoid space. The variation of the trabeculae, septa, and pillars along the optical nerve and the cerebrospinal fluid play important roles in protecting the optical nerves.

While the function of the trabeculae of the brain's subarachnoid space is the same as the trabecula of the optic nerves their architectural structure, and possibly their histology, appear to be different. It has been observed that the SAS trabeculae are very thin transparent membrane like structures with tension only characteristics. That is, the brain's CSF creates sufficient pressure in the space between the arachnoid and pia which erects the trabecular structure and presents the trabeculae from collapsing. Space that is created by the CSF pressure plays an important role in protecting and damping the brains impacts. In fact, in cadavers, since the CSF is drained and the pressure is zero the arachnoid layer collapses on top of the pia mater, i.e. the trabeculae completely buckle and collapse.

The trabeculae are collagen based and their material properties are not explicitly reported in the literature. However, it has been reported that the trabecula is a soft connective tissue containing 50% collagen and 50% water, Alcolodo et al. (1988). Because of the softness and elastic membrane characteristics of the trabeculae, the combination of the CSF and the trabeculae absorbs head impacts and protects the brain. The abundance of the trabeculae in the SAS region and the fact that its material properties are still not known. Therefore, for the modeling and FE analysis of head/brain biomechanics investigators substitute and approximate the dura mater and the meninges including the CSF by a soft elastic material. We believe that this approximation compromises the mechanism and magnitude of the external load transfer to the brain. Nevertheless, in the recent article by Jin X et al. (2006), they experimentally measured some mechanical properties of pia-arachnoid complex (PAC) as 59.81×10^3 Pa where it

was stretched in the tangential direction (with respect the head) and not in the radial direction. Previously, Zhang et al. (2001) reported the mechanical properties for arachnoid trabeculae (as 11.5x 10^6 Pa), see Table 6.3. As one can compare the two reported properties, they are three orders of magnitude different.

Dura mater, skull and skin: The dura mater, the skull, and the scalp material properties are fully addressed in the literature and it consider to be soft elastic marterial, skull also modeled as a rigid region with young modulus of 12.2x10^9 (Pa), Takhounts et al. (2003), as shown in Table 6.3.

Muscles and cervical spine: the study of de Jager, et al. (1994) was used for the neck and the muscles material properties. They considered the approximated material properties for the neck consist of vertebra cervical and the disks. Table 6.4 show the summary of the material properties for neck vertebra cervical, the discs and an average young modulus for the neck model.

One of the goal of this study was to investigate the mechanotransduction effect of external loads or impacts to the brain using computer simulation. Therefore the material properties and method are playing an important role to obtain accurate results from the finite element analysis as they can compared and validated with experimental studies. The material property of the head/ brain was widely reported in literature except the SAS where any data about structure or its material property was not available. In the next section we describe several experimental works where we investigate the structure and

density of the SAS layer. Also different FEM models were created to investigate the material property of the SAS region.

Skin	Young's modulus (E) (Pa)	5.67*103
	Poisson's ratio (υ)	0.48
	Density (ρ) (kg/m3)	1.06*103
Skull	Young's modulus (E) (Pa)	12.2*109
	Poisson's ratio (υ)	0.22
	Density (ρ) (kg/m3)	2.12*103
Dura mater	Young's modulus (E) (Pa)	31.5*106
	Poisson's ratio (υ)	0.45
	Density (ρ) (kg/m3)	1.13*103
SAS	Young's modulus (E) (Pa)	1.15*103
	Poisson's ratio (υ)	0.48
	Density (ρ) (kg/m3)	1.13*103
Muscles	Young's modulus (E) (Pa)	1.0*107
	Poisson's ratio (υ)	0.38
	Density (ρ) (kg/m3)	1.01*103
Neck	Young's modulus (E) (Pa)	6.04*109
	Poisson's ratio (υ)	0.38
	Density (ρ) (kg/m3)	1.18*103

Table 6.3 Material properties of the head/brain model, Takhounts et al. (2003).

Disk	Young's modulus (E) (Pa)	$90*10^{6}$
	Poisson's ratio (υ)	0.4
	Density (ρ) (kg/m3)	$1.06*10^{3}$
Vertebral	Young's modulus (E) (Pa)	$12.*10^{9}$
	Poisson's ratio (υ)	0.2
	Density (ρ) (kg/m3)	$2.12*10^{3}$
Neck	Young's modulus (E) (Pa)	$6.045*10^{6}$
	Poisson's ratio (υ)	0.38
	Density (ρ) (kg/m3)	$1.8*10^{3}$

Table 6.4 Material Properties used for the neck, de Jager, et al. (1994).

CHAPTER 7 Finite Element Modeling

7 FINITE ELEMENT MODELING

One of the motivations of the SAS experimental study was to create more accurate models for computer simulation. The highly inhomogeneous and dense SAS, that was found during our experimental study made it impossible to create true global model for the SAS. Several 2D and 3D model were created using our experimental studies. Functionality of the SAS was one of main reason to investigate the SAS material properties using FE analysis.

7.1 2D cortex model

The histology and architecture of SAS trabeculae has not been fully addressed in the literature. Only, Killer et al. (2003) studied the structure of trabeculae in human optic nerve and they found that the structure of the trabeculae depends on the location within the different portions of the optic nerve. They also concluded that the SAS of human optic nerve is not a homogeneous media and it contains a complex system of arachnoid trabeculae, septa and pillars.

To investigate the effect of the SAS material properties on transferring an impact load to the brain, first a 2D model containing a cortex and two trabeculae in the form of rods was created. The dimensions were approximated by Zoghi et al. (2003-2010) and our Micro-CT Scan results. The trabeculae thickness was considered about 2 to 7 micron (W. Schachenmayr and R. L. Friede 1978). The material properties of the model for

brain (gray and white mater) – skull and dura were taken from Takhount et al, (2003), Table 6.3.

The SAS trabeculae are collagen based and their material properties is not fully investigated. It has been observed that in the absent of CSF the trabeculae, being a very soft tissue, collapses, i.e., trabeculae buckles under compressive load.

A model that resembles the anatomical region of Figure 7.1, consists of the skull, dura mater, two trabeculae and a cortex including the gray and white mater of the brain, as shown in Figure 7.2. The bottom layer of the cortex was fixed and the top layer (the skull) was subjected to a velocity impact corresponding to 5 miles per hour (displacement of 3 mm-that is the thickness of the SAS). The material properties used are shown in Table 6.3 .

Figure 7.1 Anatomical view of SAS

Figure 7.2 2D FE model of trabeculae and cortex.

Abaqus/CAE 6.9-2 was used for pre and post processing analyses. The model was subjected to a dynamic blunt impact corresponding to 5 miles per hour.

Several analyses were performed. First, the modulus of elasticity of 59.81×10^3 Pa, reported by Jin X et al. (2006), for Pia-Arachnoid Complex (PAC), was used. It was observed that the trabeculae did not buckle under the compressive load and the load was directly transferred to the brain tissue as shown in Figure 7.3. This indicates that the material property reported by Jin X et al. is too stiff and unrealistic. That is, the load or impact will directly transmit to the brain because the brain material property is softer than that of the trabeculae.

(a) 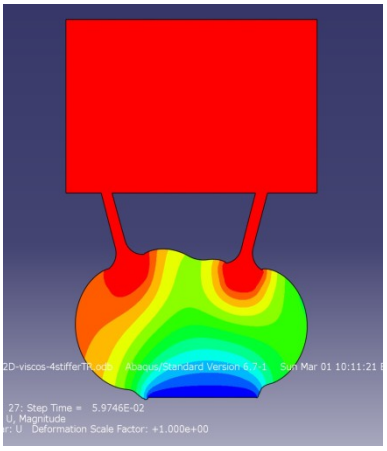 (b) 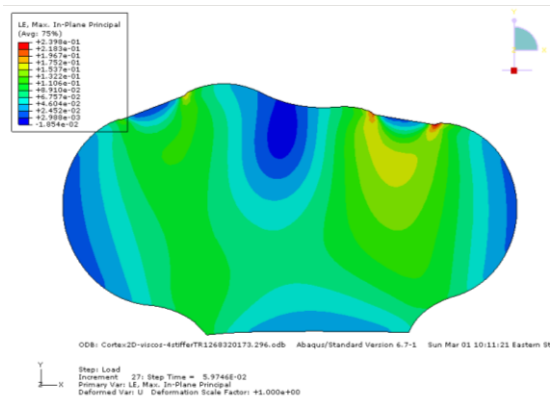

Figure 7.3 (a) Deformation of the brain due to the stiff material property of the trabeculae. (b) Brain deformation

The functionality of the SAS reveals that, this layer has to act as a damper and shock absorber to protect the brain form an impact. That is, the SAS must be very soft but the question is how much? Several analyses were set up to estimate the SAS material properties and see at which point trabeculae will collapse under the given load. The upper value case was based on the Xin et al. (2008) reported results. Our analyses revealed that the Young modulus of the SAS must be approximately 1000 Pa, otherwise the trabeculae do not buckle and the whole SAS region acts as a stiff section and will transfer the external load directly to the brain. In the next analysis the young modules of the trabeculae of 1000 Pa is used and was validated by Sabet et al. (2007). The results of this analysis, indicated that the trabeculae buckled, i.e., the impact load was absorbed by the collapse of trabeculae, and it is confirmed the functionality of SAS to act as a shock absorber, as shown in Figure 7.4.

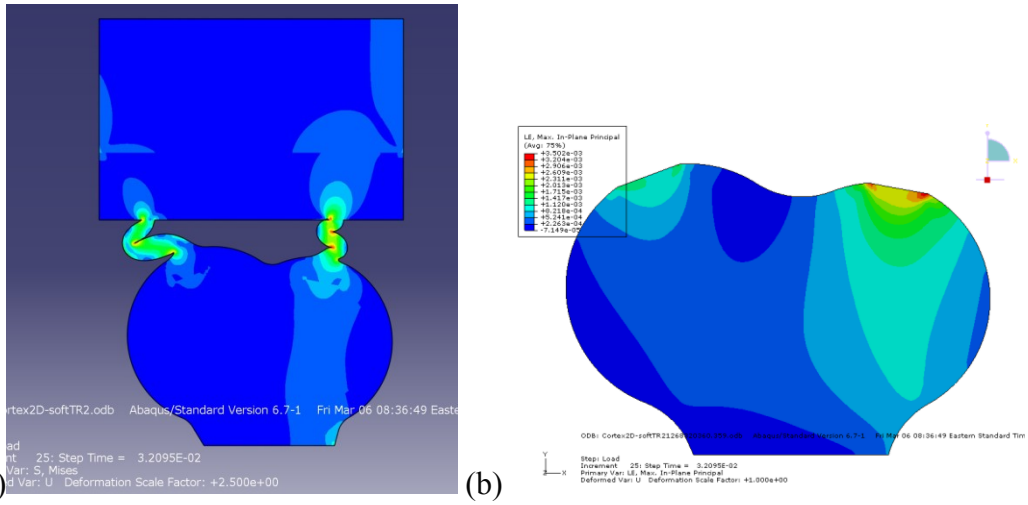

Figure 7.4 (a) Buckling of trabeculae due to softer material properties (b) Less deformation of the brain due to softer material property of the trabeculae

7.2 2D and 3D Local model using pressure instead of CSF fluid

For the next model we used the study of trabeculae in optical nerve by Killer et al. (2002). The histology study illustrates the connective tissues of the trabeculae are tree-shaped rod, pillar, septa or plate. To demonstrate the effect of the CSF fluid on the trabeculae soft tissue, local 2D and 3D models were created. Pressure boundary conditions were used in all the trabeculae surfaces to simulating the CSF pressure. The local models consist of the brain, SAS, dura mater, skull and skin are shown in Figure 7.5. Abaqus pre processor was used for pre and post analyses. The models were subjected to displacement boundary condition on skull and the bottom layer of the brain was fixed. It took about 25 minutes to solve the 2D model and about 68 minutes to solve the 3D model with 3.4 GHz processor.

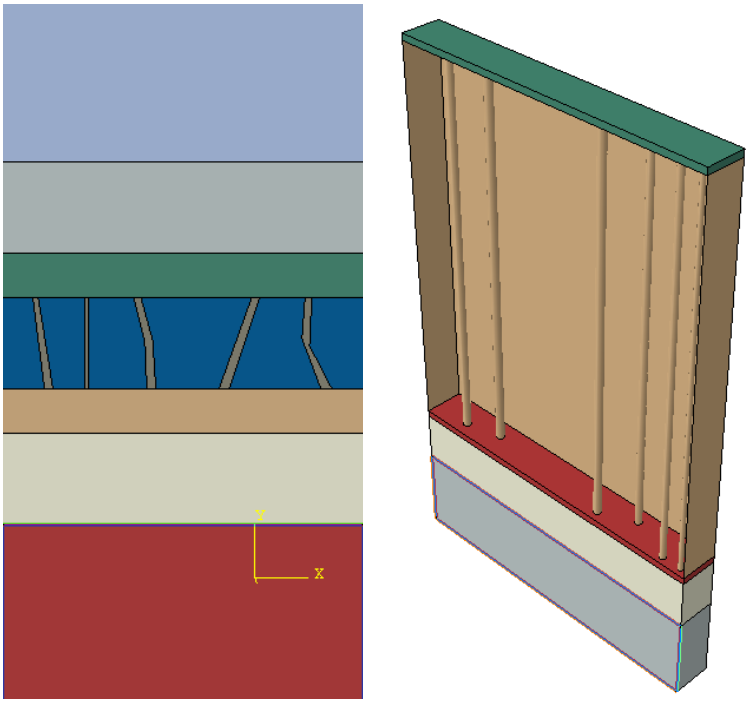

Figure 7.5 2D &3D local models

The same material properties, as shown in Table 6.3, were used for the models. The percentage of the strain in the brain then was studied, Figure 7.6.

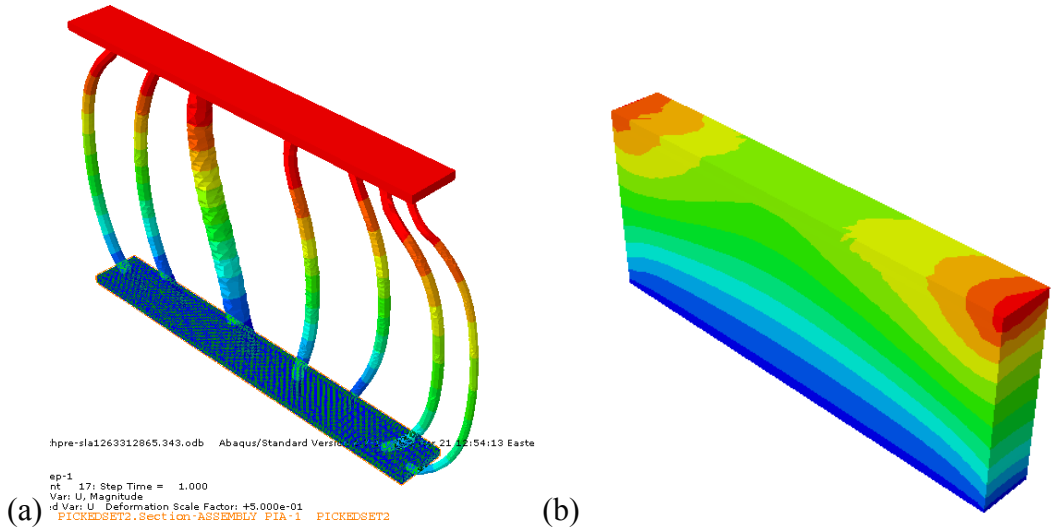

Figure 7.6 Results of the 3D local model (a) Trabeculae are collapsed due to displacement BC, (b) Displacement in white mater.

7.3 3D local models with Fluid elements

To further validate the material properties of the SAS trabeculae, two local three dimensional (3D) models of the SAS were created, one as a local model and the other one with the cortex, as shown in Figure 7.7 and Figure 7.8. The same material properties and the same boundary conditions as the previous models were used. Fluid elements were used for the space between the trabeculae representing the CSF. The same load as previous models (velocity equivalent to 5 mile per hours) was applied and the models were solved using Abaqus. It was determined that the selected material properties were appropriate i.e. the trabeculae of both models buckled as expected, Figure 7.9 and Figure 7.10. This proves the validity of the material properties of trabeculae.

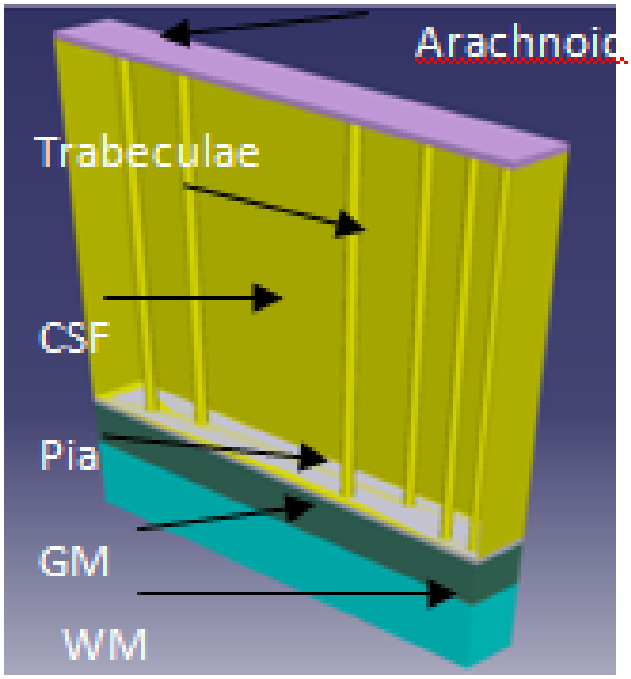

Figure 7.7 The 3D sliced model of the SAS with fluid element.

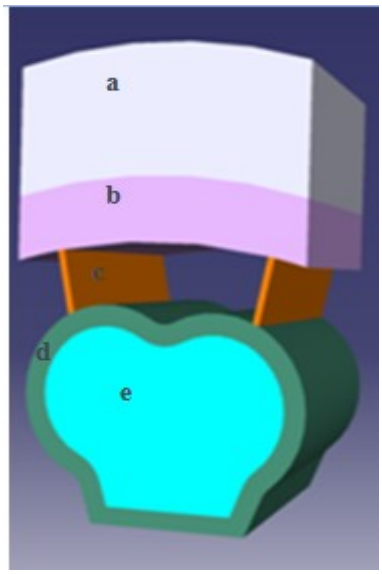

Figure 7.8 3D cortex model: a- Skull, b- Dura mater, c- Trabeculae, d-gray mater, e-white mater

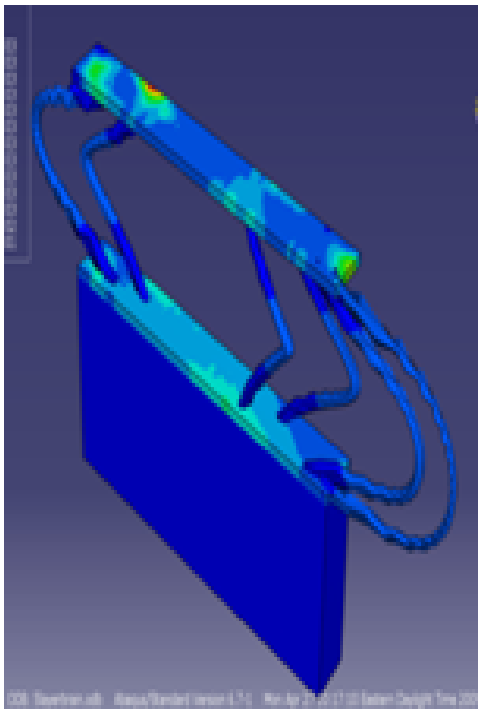

Figure 7.9 Result of the 3D sliced Fluid model showing the buckling of the trabeculae

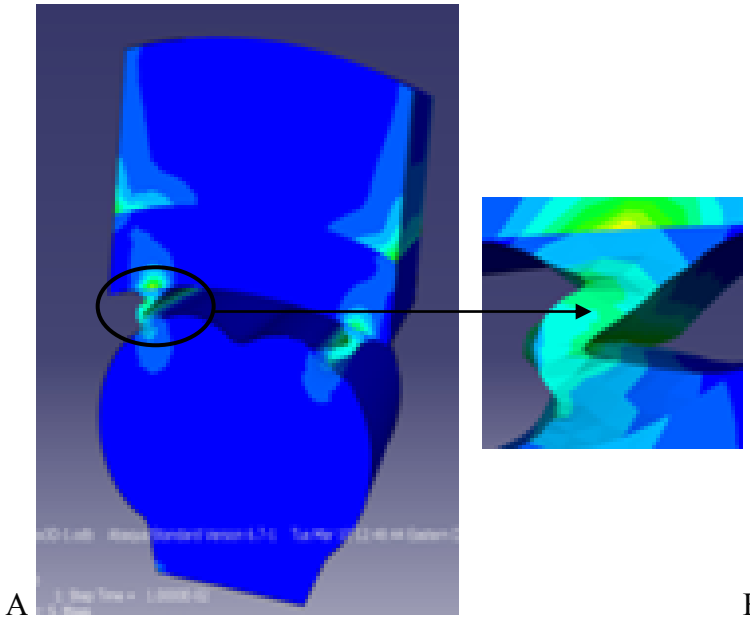

A B

Figure 7.10 Results of the 3-D model of the SAS with a cortex : A: Buckled trabeculae in and B: close up of the buckling.

7.4 Global model of the head

To simulate the function of trabeculae and the motion of the brain with respect to the skull, a 3D model of the brain, skull having four trabeculae were created, see Figure 7.11. The same dynamic load as in 2D model (velocity impact of 5 miles per hour) was applied to the skull and the motion of the brain with respect to the skull was investigated. The base of the neck, i.e. the region of the C7 was fixed. The simulation revealed that the brain initially rotates as shown in Figure 7.11 and then move to a coup and counter coup positions causing the trabeculae to be pulled (tension) and then buckled, Figure 7.12, Figure 7.13 and Figure 7.14.

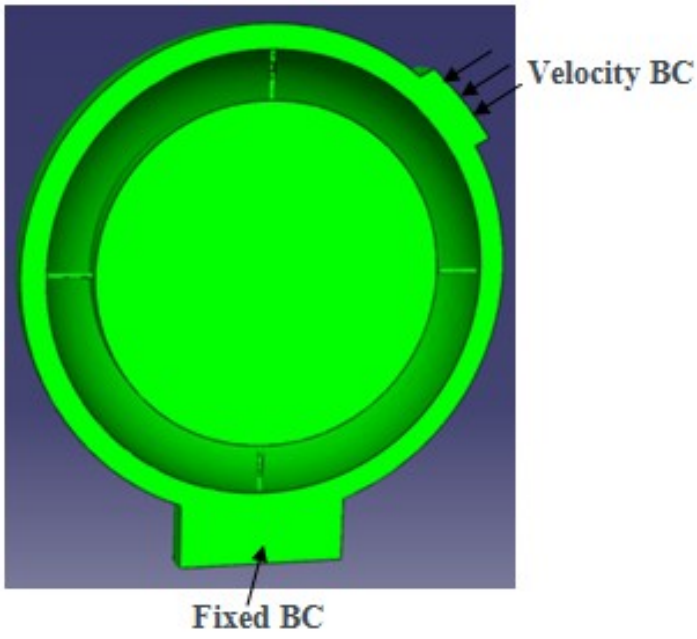

Figure 7.11 The global head model with four trabeculae and the BC.

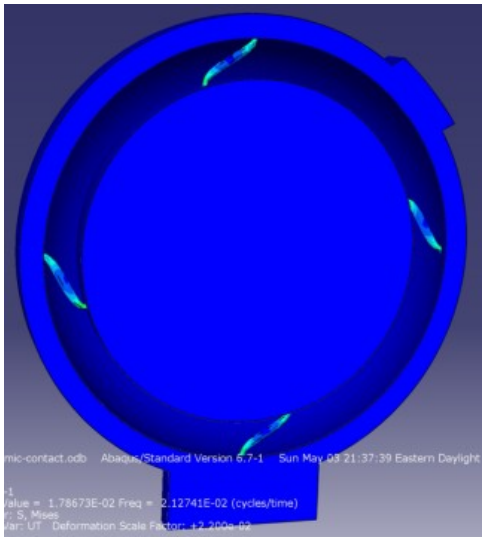

Figure 7.12 Stress field of the model: Rotation of the brain due to velocity BC.

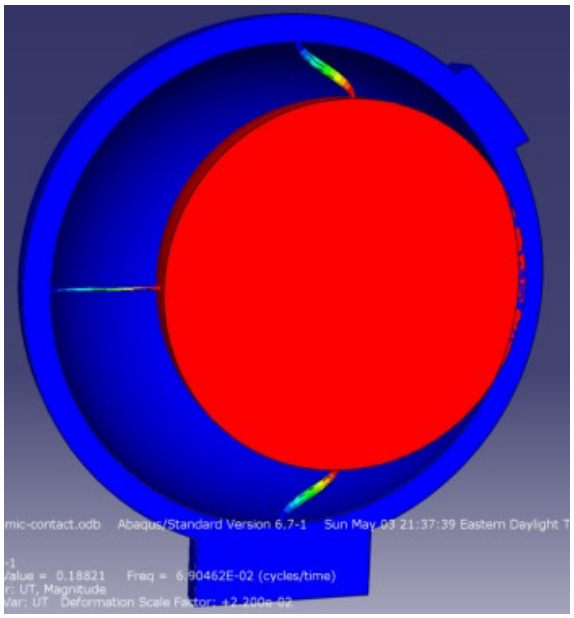

Figure 7.13 Further movement of the brain due to velocity BC.

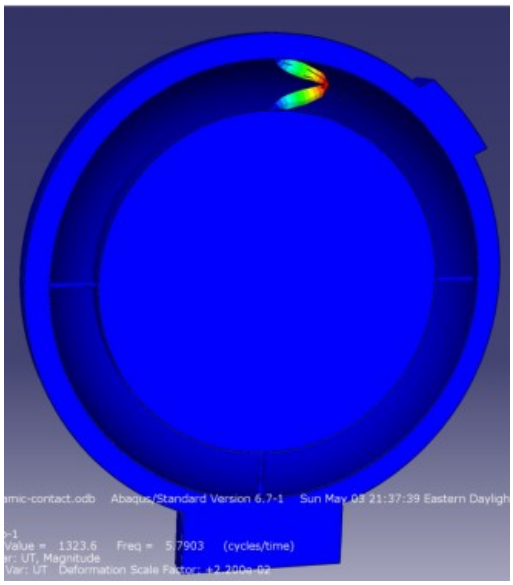

Figure 7.14 Buckling of trabeculae due to the movement of the brain.

7.5 2D transverse model the brain

To further estimate material properties of the trabeculae, a two-dimensional (2D) transverse model of the head was created using the magnetic resonance imaging (MRI) of a subject, see Figure 7.15. The model consists of the scalp, skull, dura mater, SAS and the brain Figure 7.16.

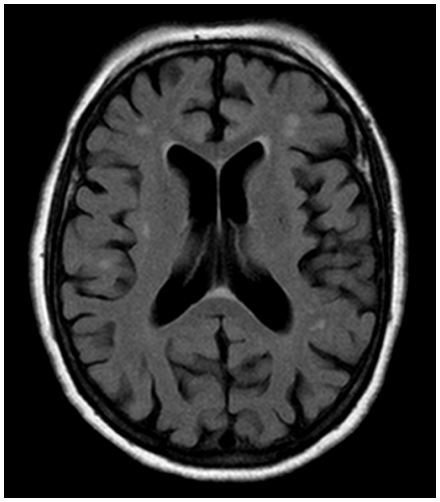

Figure 7.15 MRI image of the transverse plane of a human head.

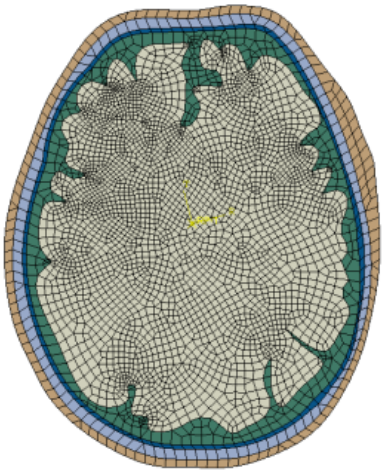

Figure 7.16 FE model of the transverse plane.

The model was created using the MRI images from an adult female patient (age 50's); all the dimensions were directly taken from the MRI. Abaqus 9.6-2 were used as pre processor, the details of the geometry and the dimensions were determined using eRAD/Image Medical Practice builder 1-2-3 software and were imported into Abacus sketch module. The model was then meshed using tetrahedral elements. The same

boundary conditions as a experimental study of Sabet et al. (2007) were used. To simulate the experiment, our model was subjected to a mild angular acceleration of 100 rad/s^2 to the head. Abaqus Multi point constrain (MPC) was used to control the center point, as shown in Figure 7.16. General contact was defined as an interface boundary condition between the SAS and dura mater. Abaqus explicit dynamic analysis was performed and it took 40 minutes to run the analysis in 80 intervals with a 3.4GHz processor.

The input boundary condition for the study was taken from Sabet et al. 2007 experimental study; where they apply mild angular acceleration to three human subjects and measured the strain in the brain, see Figure 7.17.

To estimate the material properties of the SAS 12 different cases were studied using the same load and boundary conditions, as shown in Table 7.1. The results were compared with the experimental study of Sabet. et al, (2007) and Bayly et al. (2005) as shown in Figure 7.18.

SAS Young modules	ε_{r0}-Node 1791	ε_{r0}-Node 3516	ε_{r0}-Node 3504
SAS 100	1	2.5	2
SAS 850	1.8	2.3	2.4
SAS 920	1.7	2.7	2.9
SAS 960	1.9	2.4	3.1
SAS 1000	1.8	2.5	3.2
SAS 1050	1.9	2.8	3.2
SAS 1150	2.1	2.9	2.8
SAS 1500	2.4	2.9	3.2
SAS 2500	2.8	3.5	4.2
SAS 5000	3	5	5.8
SAS 10000	3	5.5	6.2
SAS 100000	3.1	6	7.8

Table 7.1 12 Different cases for the SAS material properties.

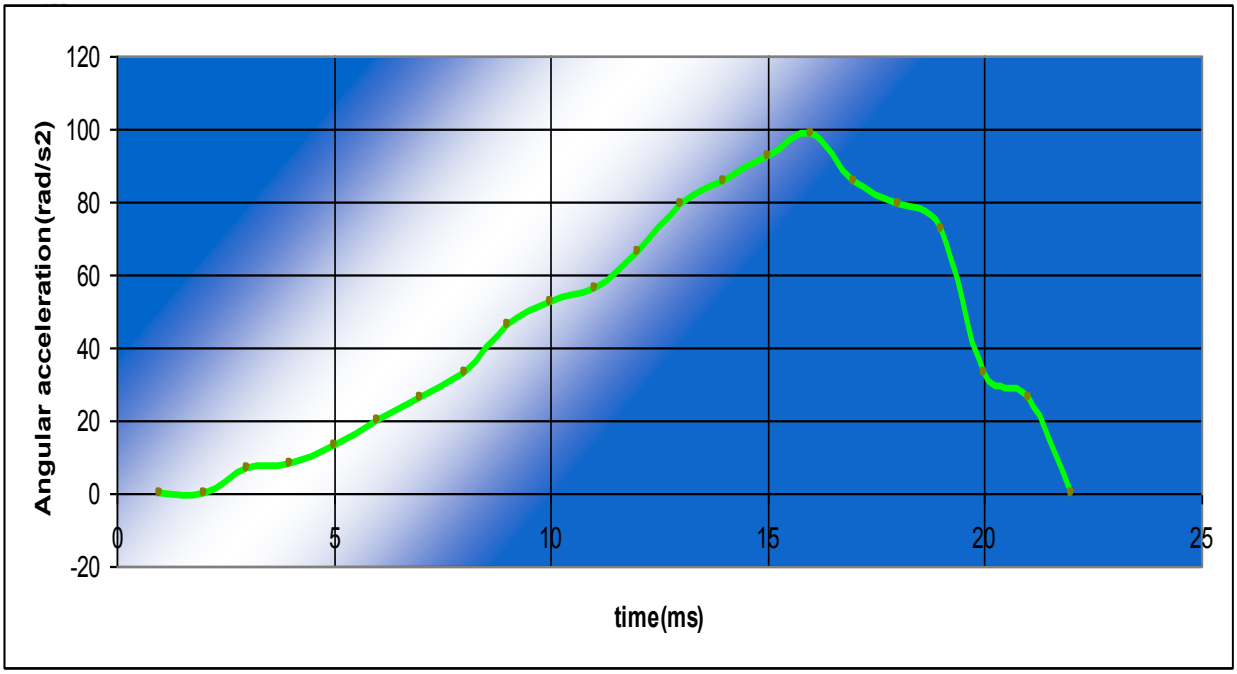

Figure 7.17 Input BC for the model, Sabet et al. 2007.

The nodal solutions of the strain in the brain were determined and compared with the 2% to 6% strain obtained from the experimental study. As shown in Figure 7.18 the results show that for the Young modulus range of 1000-1500 Pa the strain range is within the range reported by Sabet et al. (2007). The middle range of 1150 Pa was selected for our analyses since it was the closest range to experimental results. This value was in the same range for the first analysis (2D cortex model). The nodal strain pattern of the brain is shown in Figure 7.19.

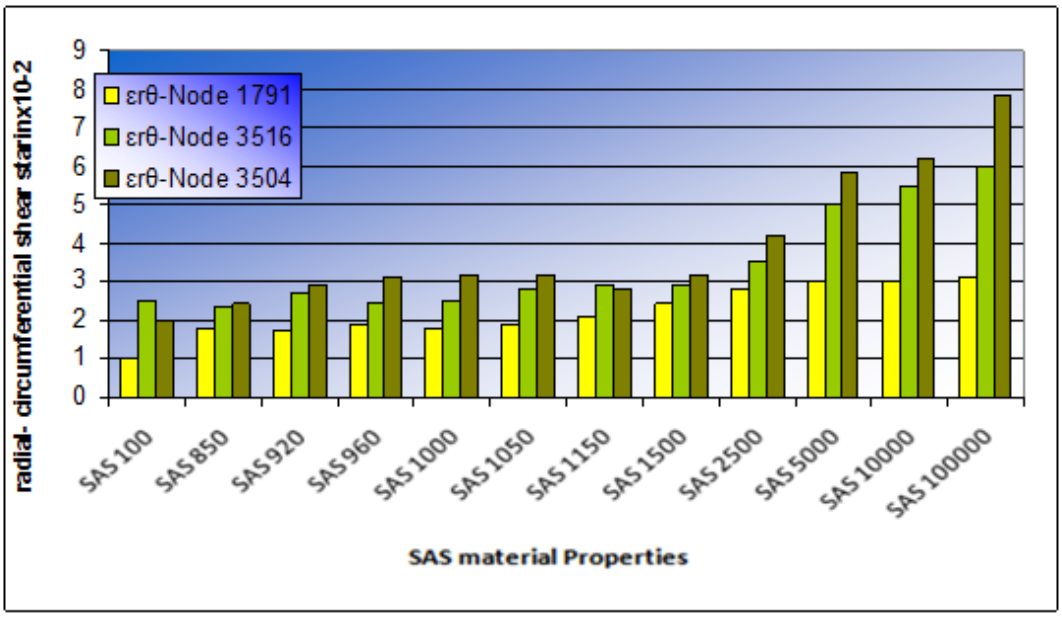

Figure 7.18 Radial circumferential shear strain corresponding to different nodes in the brain.

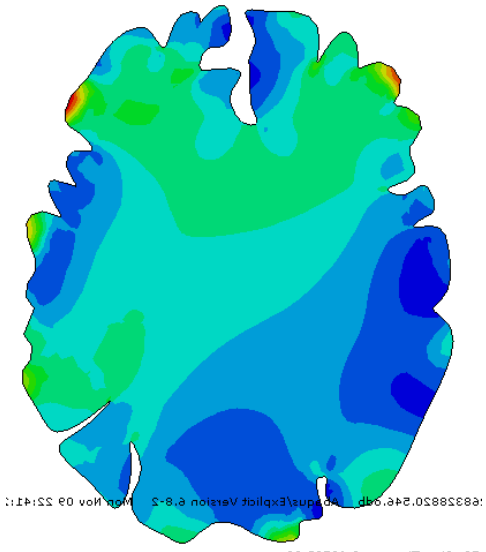

Figure 7.19 Contour strain for transverse model- nodal solution.

7.6 2D lateral model of the brain

To further investigate and validate the material properties of SAS a model of the head and neck in the lateral plane was created, Figure 7.20. The data for the modeling was taken from the same MRI subject, as shown in Figure 7.21. The material properties for the neck and muscles were taken from de Jager et al. (1994). To simulate experiment of Sabet et al. (2007), the frontal head was subjected to a mild angular acceleration of 100 rad/s^2. Abaqus multi point constrain (MPC) was used to control the center point. General contact was defined as an interface boundary condition between SAS and dura mater. Abaqus explicit dynamic analysis was performed and it took approximately 50 minutes to run the analysis in 80 intervals with a 3.4 GHz processor.

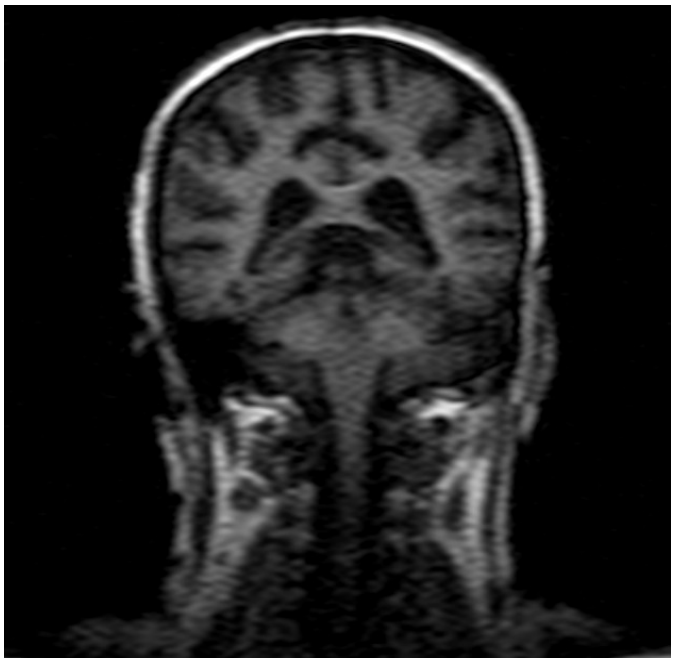

Figure 7.20 The lateral MRI image of the human subject head

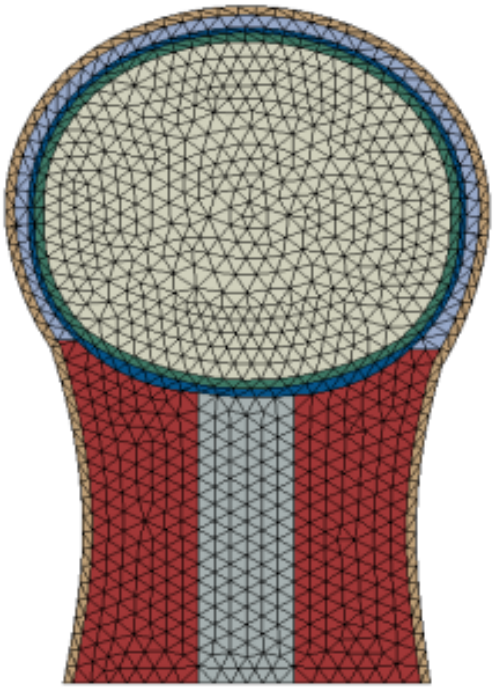

Figure 7.21 FE model of the lateral plane.

The model was analyzed using Abaqus and the nodal solutions of the strain in the brain were compared with the experimental study of Sabet et al. It was determined that the strain in the brain was in the range of 2% to 6% as reflected by the experiment study of Sabet et al. (2007), see Figure 7.22.

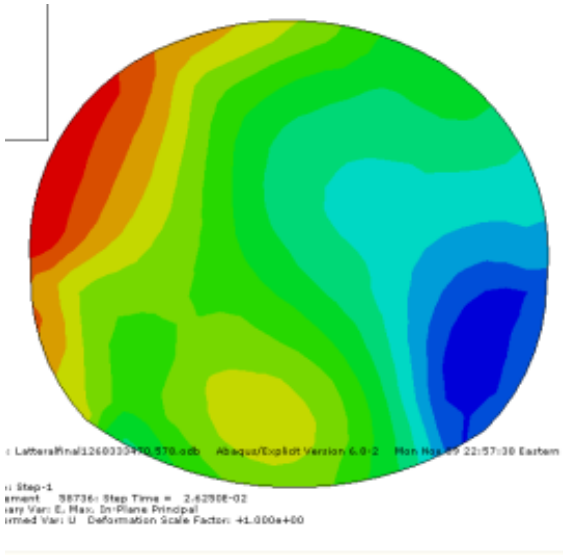

Figure 7.22 Contour the strain in the brain for the lateral model .

7.7 2D Sagittal plane- NHTSA test

To investigate a real case of head impact during an automotive frontal barrier test, National Highway Traffic Safety Administration (NHTSA), test # M30507. (VERIDIAN TEST NUMBER: 8642-NCAP-28) was used. The sagittal plane was created as shown in Figure 7.23. The data for the modeling was taken from the same MRI subject, as shown in Figure 7.24. The material properties for the neck and the muscles were taken from de Jager. et al. (1994), Table 6.4.

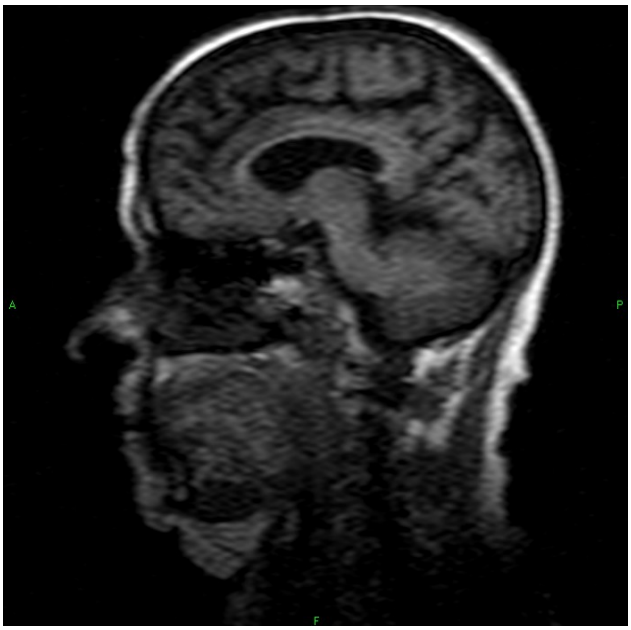

Figure 7.23 MRI image of the sagittal plane of human head.

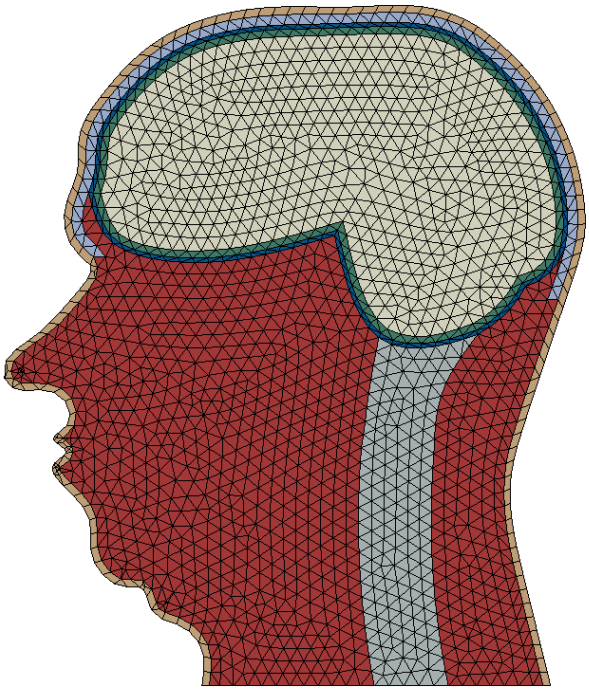

Figure 7.24 FE model of the sagittal plane image of MRI.

To simulate NHTSA test # M30507, the head was subjected to a velocity impact equivalent to 27 MPH. General contact was defined as an interface boundary condition between SAS and dura mater to imitate the real anatomical contact condition. The inferior section of the neck was fixed to constrain the model and Abaqus explicit dynamic analysis was performed. It took approximately 87 minutes to run an analysis in 100 intervals with a 3.4GHz processor.

The model was analyzed and the nodal solutions were compared with the NHTSA# M30507 result. It was determined that the brain strain was between 10% to 15% as reflected by the NHTSA test, see Figure 7.25 and Figure 7.26. Same data were used for lateral plane and the result confirm the 10% to 15% strain range in the brain as well.

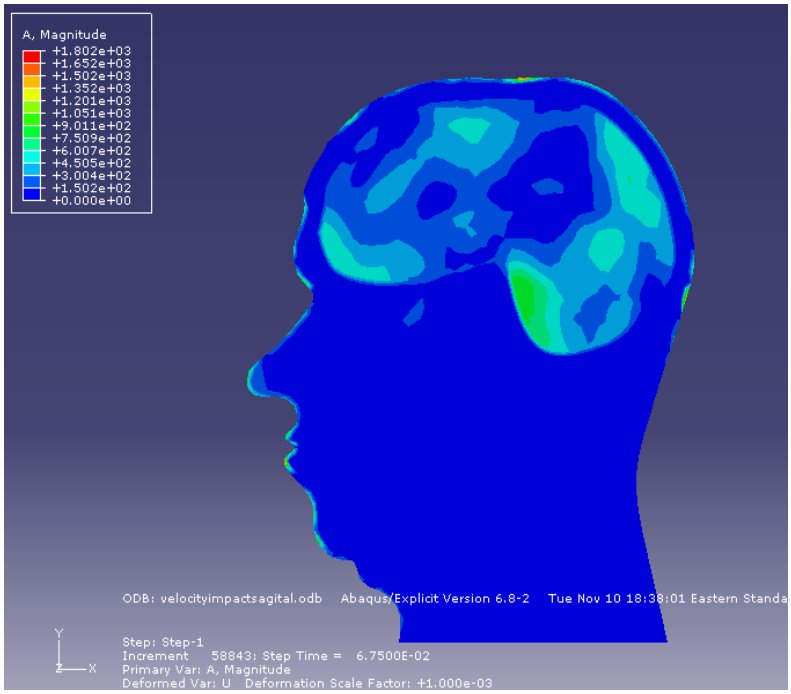

Figure 7.25 Contour Acceleration for sagittal model in the brain - nodal solution.

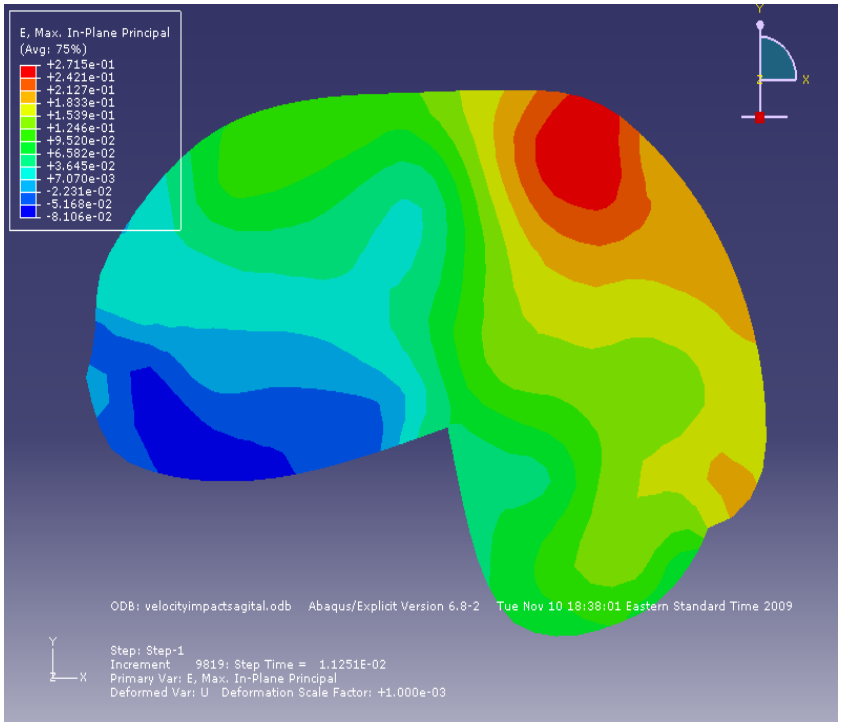

Figure 7.26 Contour strain for sagittal model in the brain - nodal solution.

7.8 Conclusion

Due to the safety consideration, human and animal experimental studies are limited to mild impacts or accelerations. Therefore the validated computer models are valuable tools for investigators to quantify the strain in the brain and the study of TBI. In this section the validation of the wide range of material properties of SAS, up to three orders of magnitude, which has been reported in the literature, was investigated. Through several 2D FE models, a wide range of the mechanical properties of the trabeculae was employed and the transductions of blunt impact loads from the skull to the brain were determined. Finally the optimum material property of the SAS trabeculae was determined based on the validation of the models with the experimental results of Sabet et al. (2007).

The result indicated that the optimum elastic modulus of the trabeculae is 1150 Pa. It was determined that the SAS material properties used by some investigators is very stiff and could lead to an unreliable results. It was also concluded that the material properties of the trabeculae should be simulated as tension-only elements since the trabeculae buckles with minimal compressive load. The real impact case was simulated using NHTSA test where the model was subjected to the velocity impact. The analysis of the NHTSA case revealed that the strain in the brain was in the range of 10% to-5% which is less than the %20 threshold of traumatic brain injury (TBI) addressed in the literature, Bayly et al. (1995). The results of this study confirmed the lack of TBI, corresponding to the safe HIC value of less than 1000, as reflected in the NHTSA test (M30507) where the corresponding HIC value was 442.

CHAPTER 8 2D Subarachnoid Space Material Modeling

8 2D SUBARACHNOID SPACE MATERIAL MODELING

The experimental studies revealed that the SAS contains abundant trabeculae with complicated architecture, which makes the modeling of the subarachnoid space very difficult. To understand the mechanics of movement of the brain within the skull, i.e. the mechanics of the flow of CSF within the trabecular structure, global and local models were proposed. In many analyses the subarachnoid space was modeled as soft solid or fluid, where the functionality of the CSF fluid was reduced or the functionality of the trabeculae was ignored, respectively. To investigate the best material model for the SAS, in this chapter we compare four different types of material modeling as they transfer the load to the brain. In the first model the SAS was consider to be soft solid. In the second model fluid elements were used and viscous fluid material was used to simulate the SAS. For the third model, the SAS was considered to have porous elastic material properties and 3D solid elements were used for the modeling of the SAS. Finally the last model was performed based on Darcy's permeability where the SAS was modeled by using pore/ stress elements.

Because of the limitation of the fluid element in Abaqus software and to be able to compare our result with fluid and Darcy models, a 3D transverse model of the brain was created. The same model was used for all four different studies of SAS material modeling. The model was created using the MRI images from an adult female patient, all the dimensions were directly taken from the MRI. The geometry details and dimensions were generated using eRAD/Image Medical Practice Builder 1-2-3 software and imported

into Abaqus sketch module, then the 3D model and mesh was created using tetrahedral element in Abaqus.

The model consists of the brain, subarachnoid space, dura mater, skull and the skin. Each layer was modeled according to real geometry from an adult patient and then assembled to the final model as shown in Figure 8.1 to Figure 8.5. General contact was defined as interfaces between SAS and Dura mater and Abaqus Tie constrains were defined to attach all the boundary nodes. To simulate the same study as a Sabet et al. (2007), MPC constrain was defined and a mild angular acceleration was applied to the skull layer that was created around the model, Figure 8.5. Same concept was used to construct the other two models (lateral and sagittal) Figure 8.6.

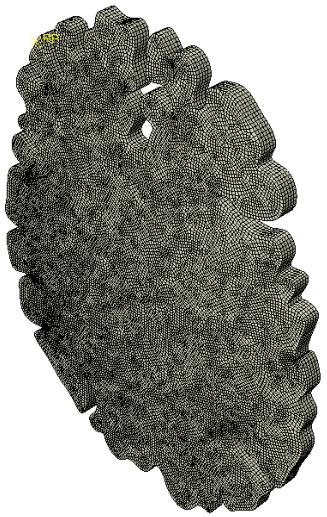

Figure 8.1 3D transverse brain model.

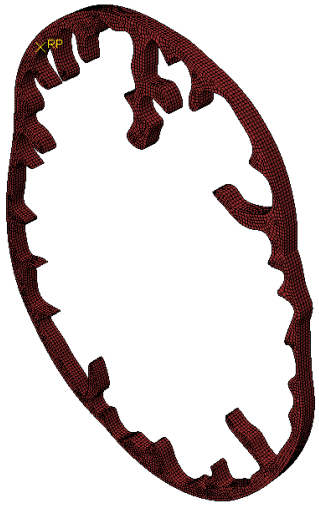

Figure 8.2 3D transverse model of SAS

Figure 8.3 3D transverse model of dura.

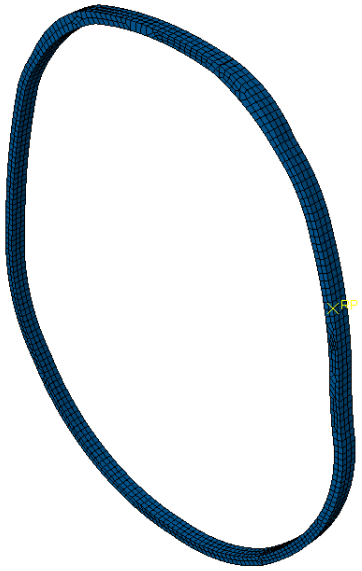

Figure 8.4 3D transverse model of skull.

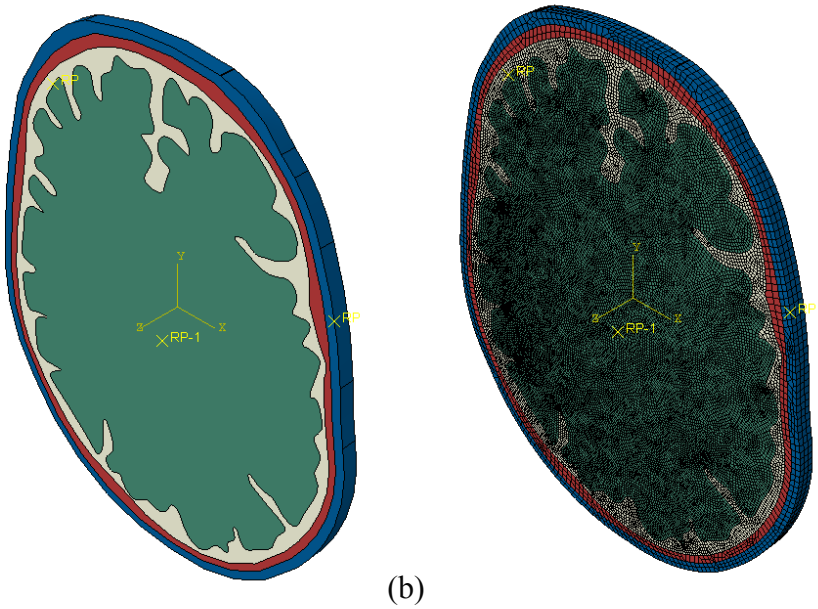

(a) (b)

Figure 8.5 3D transverse model of the head after the assembly (a) The 3D model, (b) The mesh.

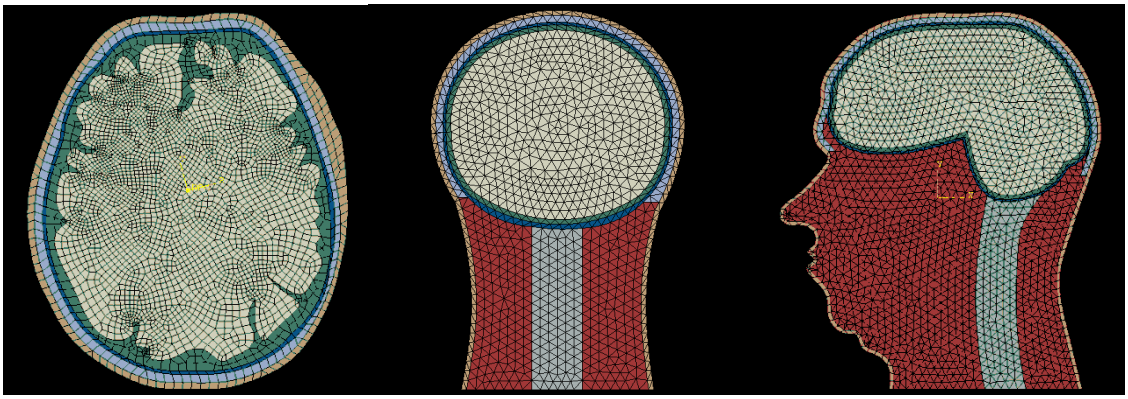

Figure 8.6 3D model of human head using Abaqus/CAE software from the left to the right are: Transverse, Lateral and Sagittal sections.

8.1 2D Material modeling the SAS - Soft solid

The first model was created using same data and considering the SAS to be soft solid. The SAS was creating using sketch modules in Abaqus/CAE. The region was then meshed with tetrahedral element and soft solid material property was defined for the SAS layer. The same boundary condition as Sabet et al. (2007) experimental study was applied to the model, Figure 8.7.

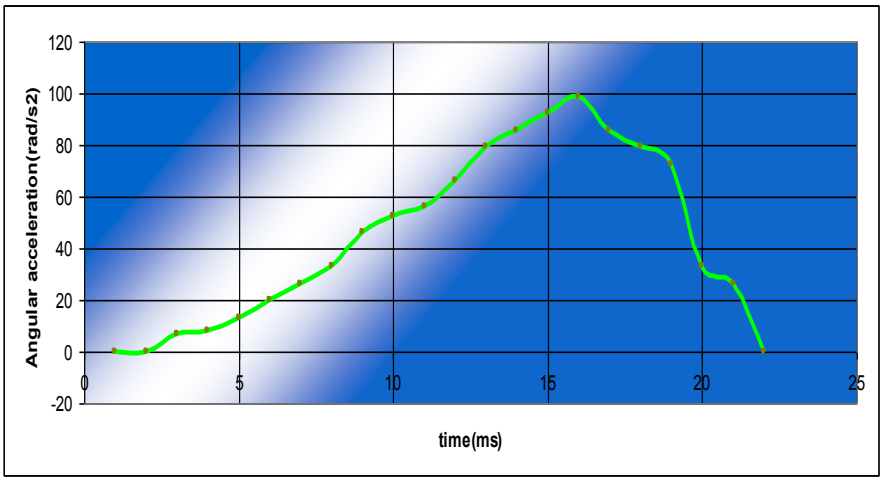

Figure 8.7 Input BC for the SAS modeling.

Abaqus explicit dynamic analysis was performed and it took about 1.5 hours to run the analysis in 120 intervals with a 3.4GHz processor. The result was also compared to experiment study and 2% to 6% strain filed in the brain was confirmed.

8.2 2D Material modeling of subarachnoid - fluid media

The second model was created using Pore Fluid/Stress element for subarachnoid space. To simulate the same functionality for the combination of the trabeculae and CSF while they performed as shock absorber, the SAS was modeled as completely viscous fluid region. The viscosity for CSF was taken from Zoghi and Sadegh (2004), viscosity of 0.25 kg/(s·m). General contact was used to define the interaction between CSF fluid with boundary layers of dura mater and the brain. The same load and boundary conditions as the 3D soft solid model was used in this study. Fluid/ solid interaction defined for the boundary caused the problem to be more time consuming. Abaqus explicit dynamic analysis was performed and it took approximately 2.5 hours to run the analysis in 120

intervals with a 3.4GHz processor. Because of Abaqus and processor limitation we did not get very good results in this study, the simplified model was then used, solid/ fluid interaction problem usually need higher speed processor for analysis. Figure 8.8 shows strain filed in simplified transverse model that confirm 2-6% threshold strain in the brain.

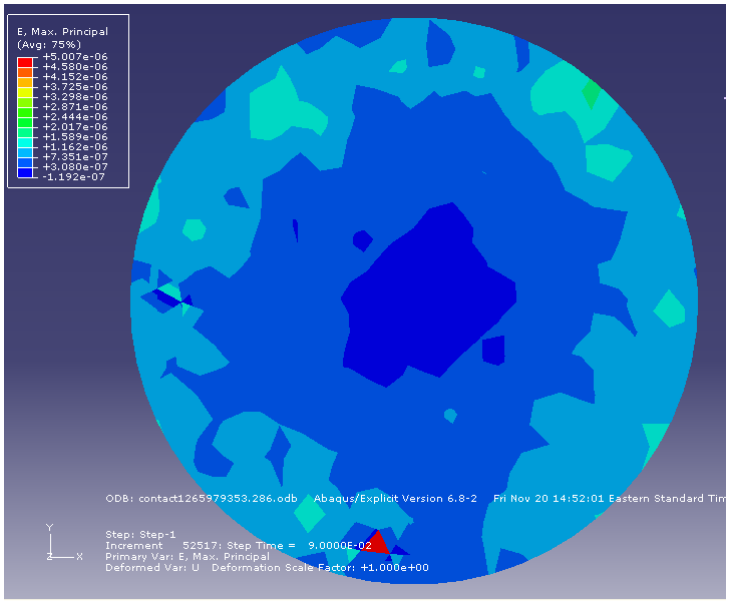

Figure 8.8 Strain in the brain-modeling the subarachnoid space as a fluid.

8.3 Modeling of subarachnoid as porous material using Darcy law

The subarachnoid space is not a soft solid region nor a fluid media, our experimental studies reveals that the SAS contains of very dens layers of soft trabeculae tissues within the CSF fluid. These solid / fluid interactions provide damping against external impacts. One of the best models that can be used for the SAS is porous elastic model where we have the effect of the CSF fluid and soft trabeculae tissue as one mechanism. To model the SAS as a porous elastic material we need to estimate the void ratio, density and Darcy permeability. The result of our experimental study of histology section using fluorescent light was used to estimate the void ratio and density, Figure 8.9. The Darcy's permeability parameter estimation is explained in the next chapter (Mechanics of CSF flow through the trabeculae, 9-1-1)

In Abaqus software, porous elastic material model is valid for small elastic strain of about 5% and it defines the elastic parameters for a porous material. Note that concussion usually happened in the small strain about 2-6%, therefore, the use of the porous elastic material properties for the SAS is appropriate.

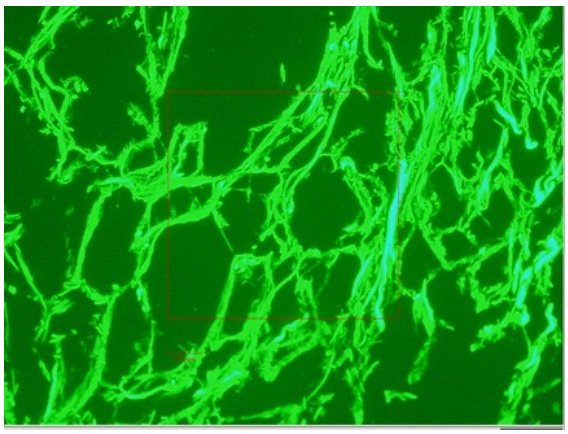

Figure 8.9 Trabeculae tissue under fluorescent light form the brain (cadaver), estimate density and void ratio.

Using hexagonal pattern of fiber in the CSF fluid we could determine specific surface and void ratio. Using these data along with trabecula radius (r =5 micron) and space between each trabecula (Δ=40 micron) we solved for SAS permeability. Our estimation determined the permeability of K_p = 3.125e^{-10} an it's in the range of permeability for soft tissue in fluid media, Weinbaum et al. (2006). This value was used to simulate the SAS in the analytical and FE models.

Having permeability and void ratio, the same 3D model was used for porous analysis, each layer was created separately, the SAS was mesh using 3D stress element and Abaqus Tie constrain were used to attach boundary nodes, the model then was assembled. Abaqus pre and post processor was used. Abaqus Static/General step defined for analysis type and it took about an hour to solve the problem with 3.4GHz processor.

The nodal solution of the strain in the brain was compared with experimental study of Sabet et al. (2007). The strain in the brain was very small, Figure 8.10. Further investigation is needed to validate this model.

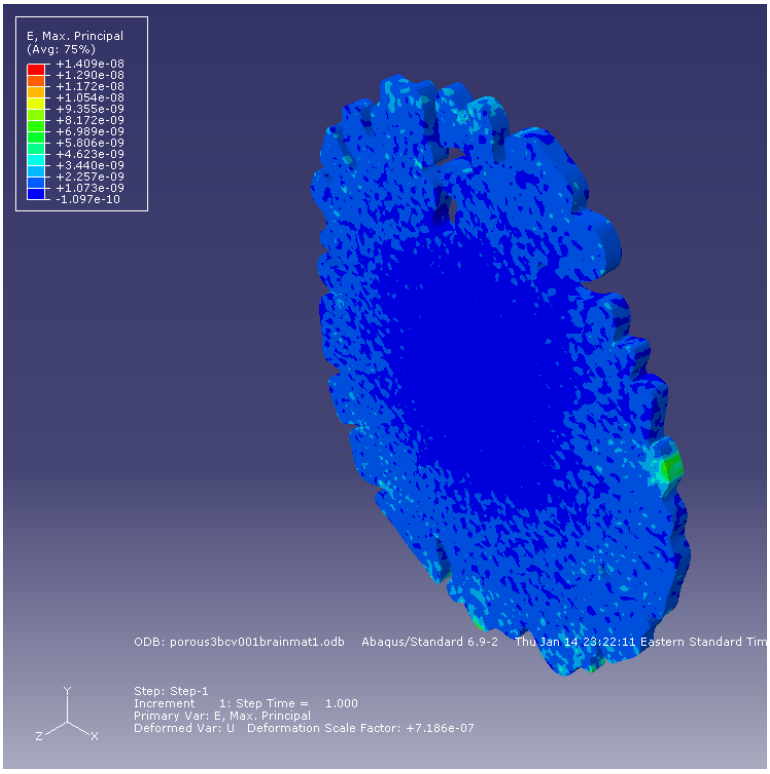

Figure 8.10 Strain in the brain-modeling the subarachnoid space as a porous media.

8.4 2D Modeling the SAS as Darcy's permeability

The last prospect for the material modeling of SAS was using Darcy's permeability. Fluid flow in porous media has been studied for many years, the traction between solid and liquid parts in porous media can be solved by two different methods, one approach is to numerically solve the governing equation for fluid flow in individual pores if the structures of pore network are known. In the other approach we could

assume that porous medium is a uniform material where the flow rate is proportional to the pressure gradient. Darcy's permeability and void ratio value were taken from previous section. To investigate the effect of the SAS material property on the transferring load to the brain the last analysis was performed using the same simplified transverse model, same boundary and load were applied. The SAS space was mesh using Abaqus Pore Fluid/stress element and Abaqus Geo Static step was used for the analysis type. The nodal solution of the strain in the brain was compared with 2-6% strain threshold from the experimental study. The strain filed in Darcy's model was very small compare to the other model studies, which might be as the result of defining Geo static step for the analysis type in Abaqus or the parameters that we had to use for some specific steps in the analysis.

8.5 Conclusion

In this section we study the effect of the different SAS material properties on transferring the load/impact to the brain as it relates to TBI. Four different materials were proposed for SAS modeling and the strain in the brain was compared with the experimental study of Sabet et al. (2007). The nodal solution for the soft solid modeling was in good agreement with 2-6% threshold strain in the brain. Because of the processor limitation we had to use simplified model for Fluid/ solid interaction where the SAS was modeled as a complete viscous fluid region. In the last two models Darcy's permeability was calculated and used in the analyses. Because of the software and processor limitations we were not able to apply the same step and boundary conditions for all the models which make the comparison difficult. In order to apply the same step and

boundary condition, 3D model of the SAS region will be created and displacement boundary conditions will be applied to the model. The result of this study, then, will be used as an input boundary condition for the 3D head model.

CHAPTER 9 Mechanics of CSF Flow Through the Trabeculae

9 MECHANICS OF CSF FLOW THROUGH THE TRABECULAE

In this chapter, we propose a structural model for the analysis of mechanotransduction of CSF's hydrodynamic forces through the SAS. Consider a transverse and/or lateral slice of the head where the brain is encased by the SAS. For simplicity of the analytical model we assume that the SAS is a uniform strip of a continuum around the brain. When the head is subjected to an impact the deformation of the brain at the coup location causes the CSF to flow around the brain and stagnates at the countercoup location. Assume that at the CSF's stagnation point (countercoup) the SAS is cut, then the strip band around the brain is straightened out as a long channel. Therefore, the mechanics of the CSF flow through the SAS can be simulated as the flow of the CSF through a deformable channel (a long strip) when the plane of the channel is subjected to an impact or deformation. Based on the anatomy of the head and brain, the dimensions of the deformable channel are: 3 mm thick, 10 mm wide and 600 mm long, as shown in Figure 9.1.

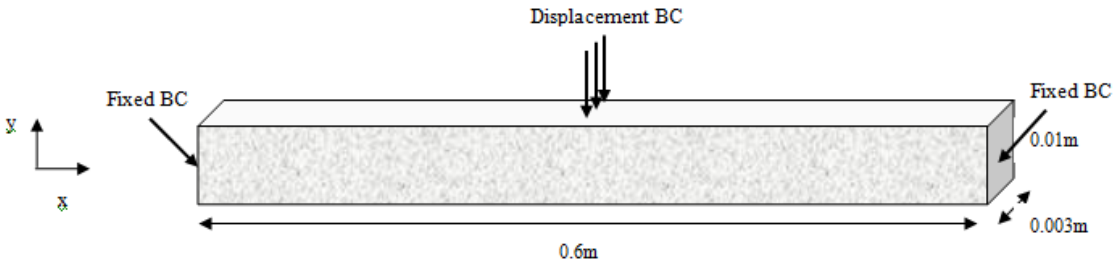

Figure 9.1 The channel (strip) model.

It is assumed that the flow of the fluid through the deformable channel is governed by Darcy's permeability law. The reason for this choice is that in our previous chapter 8, several material models of the SAS including; Darcy's permeability, viscous fluid, fluid solid interaction and porous elastic materials, were considered and analyzed. These material models were compared/validated with the experimental results of Sabet et al.2007 who applied a mild angular acceleration to three human subjects and measured the strain in the brain. It was observed that the Darcy's model could be one of the best models for the SAS and thus was selected. In addition, our in-vivo and in-vitro studies revealed that abundant trabeculae exist in the SAS region, which create a hydrodynamic resistance force against the CSF flow similar to Darcy's permeability model.

9.1 Structural Model

9.1.1 Analytical approach

We propose a hexagonal structural (unit cell) model for the structural organization of the trabecular architecture, Figure **9.2**. This is a structure model, where it provides a base to formulate a mathematical model for analyzing the transduction of mechanical and hydrodynamic forces through the SAS. It is also assumed that each trabecula is a fiber (rod) with a circular cross-section of radius *a* connecting the arachnoid to the pia mater. This structural model provides a reasonable prediction of the SAS permeability.

Darcy's permeability k is estimated by $k = \frac{C\varepsilon^3}{\mu s^2}$ Kozeny (1972), were C=1/2 for circular void, ε = void volume/total volume, μ= dynamic viscosity and S = total reference area /total volume.

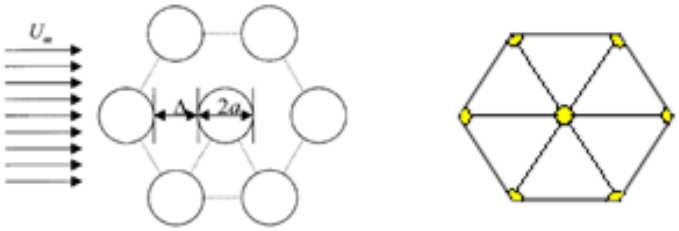

Figure 9.2 Hexagonal structural model of trabeculae.

Based on the experimental results, the radius of the fiber is approximately about 5 microns and the fiber gap (spacing between two fibers) is Δ=40 microns. Using the hexagonal geometry the void volume/total volume ε, and total reference area /total volume S, can be written as,

$$\varepsilon = \frac{2\Pi r^2}{\sqrt{3}(2r+\Delta)^2} \qquad S = \frac{4\Pi r}{\sqrt{3}(2r+\Delta)^2}$$

Therefore, using these equation the SAS permeability was determined as K_p = 3.125e^{-10} m^2. which is in the range of permeability for soft tissue in fluid media, Weinbaum et al. (2002)

9.1.1.1 Mathematical formulation

Consider a long channel containing trabeculae and the CSF, as shown in Figure 9.1, where the channel is subjected to a transverse load (q(x, t) or displacement on the top surface. The governing Darcy's law is,

$$u(x,t) = -\frac{K_p}{\mu}\frac{dP}{dx} \tag{9.1}$$

where u (x,t) is the velocity and p is the pressure of the CSF. The continuity equation is:

$$u(x,t) \cdot h(x,t) = C \tag{9.2}$$

where h(x,t) is the height (thickness) of the channel. Finally, the balance of the forces lead to:

$$(\, q(x,t) - P(x,t) \cdot l)dx = E \cdot A\frac{dh(x,t)}{h(x,t)} \tag{9.3}$$

In this case we assumed there is no load applied, q(x,t) = 0. Utilizing several mathematical manipulations and change of variables the solution to the three coupled differential equations 9.1 to 9.3 are:

$$P = -\sqrt{\frac{2C_1EA}{l}}\,tanh\left(\sqrt{\frac{C_1 l}{2EA}}(x + C_2)\right) \tag{9.4}$$

$$u = \frac{K_p C_1}{\mu}\,sech^2\left(\sqrt{\frac{C_1 l}{2EA}}(x + C_2)\right) \tag{9.5}$$

$$h = \frac{\mu C_3}{K_p C_1}\,cosh^2\left(\sqrt{\frac{C_1 l}{2EA}}(x + C_2)\right) \tag{9.6}$$

To solve for the constants C1, C2 and C3 the following boundary conditions were used.

$$h(0,t_i) = \frac{\mu C_3}{K_p C_1} cosh^2\left(\sqrt{\frac{C_1 l}{2EA}}(C_2)\right) = \mathrm{h_i} \tag{9.7}$$

$$h(0.3,t) = \frac{\mu C_3}{K_p C_1} cosh^2\left(\sqrt{\frac{C_1 l}{2EA}}(0.3 + C_2)\right) = 0.003 \tag{9.8}$$

$$\frac{dh}{dx}(0.3,t) = \frac{\mu C_3}{K_p C_1} cosh^2\left(\sqrt{\frac{C_1 l}{2EA}}(0.3 + C_2)\right) = 0 \tag{9.9}$$

The constants were determined as: C2= - 0.3,

$$C_3 = \frac{h_i K_p C_1}{\mu} \frac{1}{cosh^2\left(\sqrt{\frac{C_1 l}{2EA}}(-0.3)\right)}$$

$$C_1 = \frac{2EA}{0.09l}\left(cosh^{-1}\left(\sqrt{\frac{h_i}{0.003}}\right)\right)^2$$

The input velocity, corresponding to a blunt impact was used, and the results were compared to FE solution. The result of this analysis is shown in Figure 9.4, which shows the maximum displacement at the middle of the model.

9.1.2 Numerical approach

The three dimensional model of Figure 9.1, was created and subjected to the same boundary condition and permeability as numerical study. The model was meshed using Pore Fluid/ Stress element and Abaqus General Static was defined for step analysis. The model solved using Abaqus 6.9-2 pre and post processor. The result indicated the same deformation as analytical model, Figure 9.3. The compression result between numerical and analytical model was in very good agreement. As shown in Figure 9.4.In Figure 9.4, the t10 to t20 are displacements of the model at the time equal to 10 to 20 millisecond.

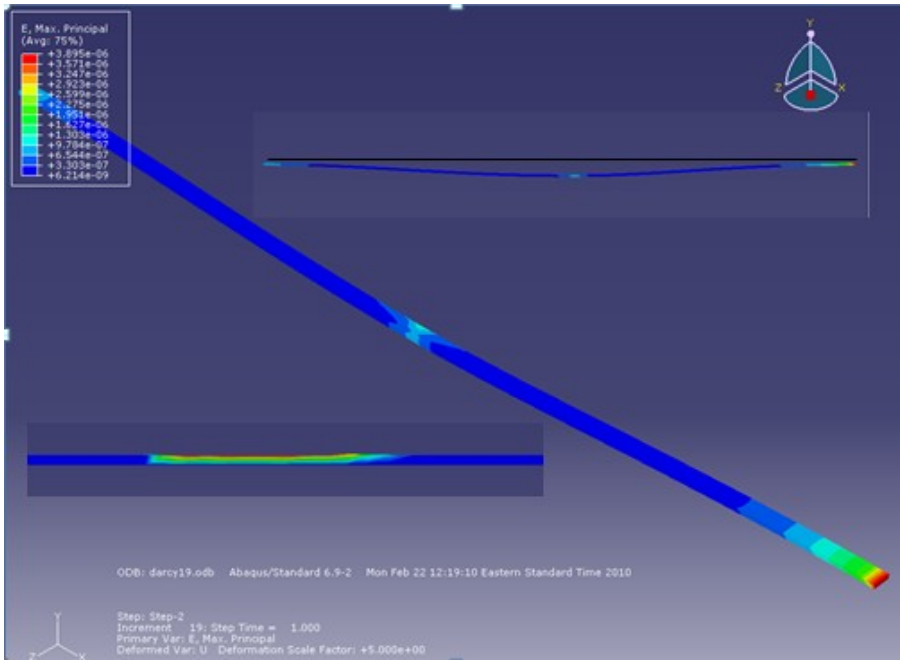

Figure 9.3 Deformation of the structural model due to displacement BC.

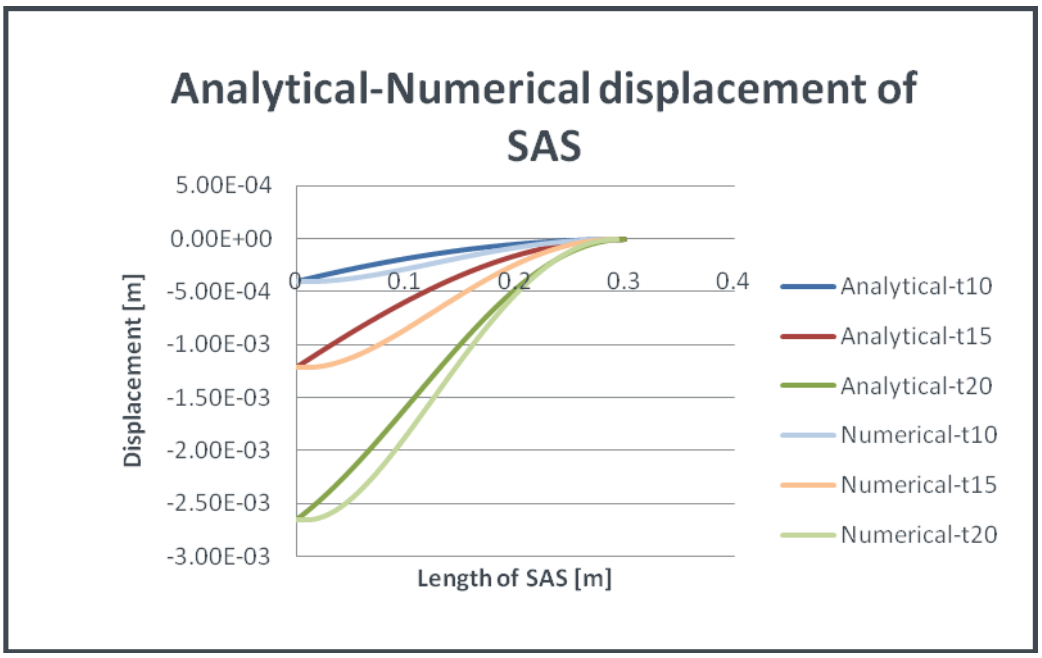

Figure 9.4 Compression between analytical and the FE results at different time.

9.2 2D single trabecula model

In this section we investigate the buckling phenomena of a single trabecula that is connecting the arachnoid to the pia mater. Specifically we investigate at the buckling of a single trabecula as a result of the flow velocity of the CSF. The reason for this study is that SAS trabeculae could buckle not only due to brain movements but also due to the hydrodynamic force of the flow velocity of the CSF.

9.2.1 Input velocity for the model

In this section the flow velocity of CSF, that is used in the analytical and the FE models, is determined. Circumferential strap model of Figure 9.1 was employed and

Fluent 9.3.26 was used to determine the flow velocity of CSF. Three different (viscous) fluids were used to study the velocity profile. The models were created and meshed using Gambit 2.4.6 and then imported to Fluent 6.3.26. Material property and boundary conditions were defined. Fluent software was used for post processing analysis and it took about 8 minutes to run each analysis. The first material property was an equivalent to viscous fluid (μ=0.25), taken from Zoghi et al. (2004), representing a combination of the trabeculae and CSF. For the second analysis, CSF was considered as water like. Finally, as the third analysis, an equivalent viscosity of μ=0.01 was defined to simulate the same functionality for the structural model. The velocity profiles are shown in Figure 9.5 to Figure 9.7. The result velocity profile for the viscous fluid and water like fluid were either too high or too low. That is, if we apply the viscous velocity output as an input boundary condition for the 2D single trabecula l model ($3E^{-11}$ m/s) , this will be too low to give us any deflection. Also for the water like fluid (μ=0.001) the velocity profile of Figure 9.6 (16 m/s) the deformation results would be extremely high. The third model with the viscosity equivalent to μ=0.01 give us sensible velocity range for trabeculae (0.8 m/s). We used this velocity as input boundary condition for the 2D analytical and FE models.

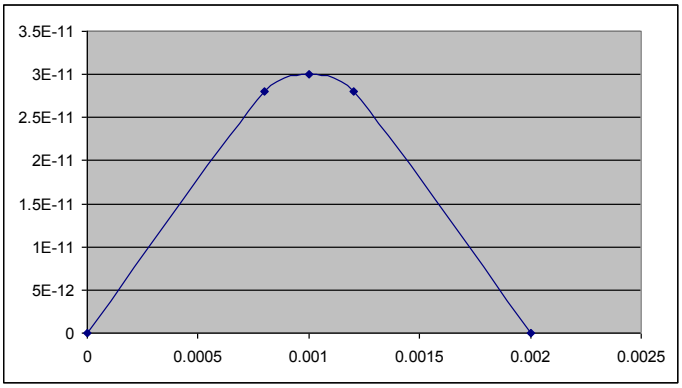

Figure 9.5 Velocity profile for viscous fluid μ=0.25 max velocity 3E-11 m/s.

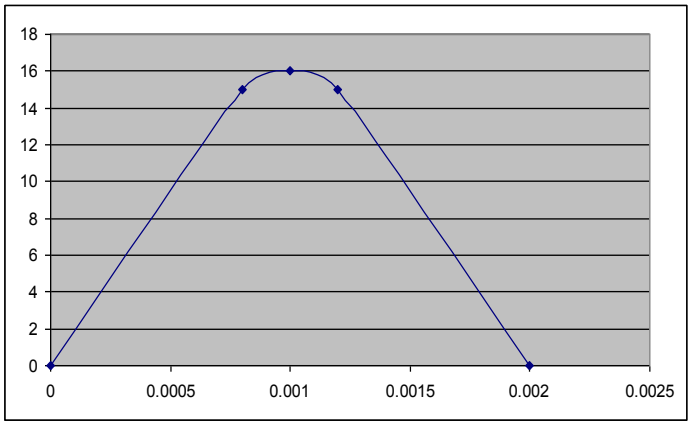

Figure 9.6 Velocity profile for CSF fluid μ=0.001 max velocity 16 m/s.

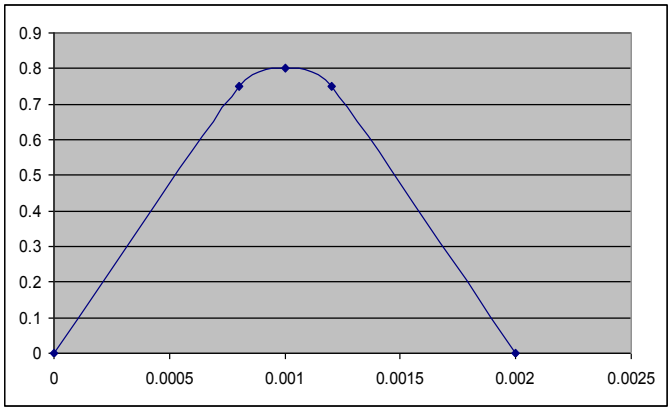

Figure 9.7 Velocity profile for equivalent viscous fluid μ=0.01 max velocity 0.8 m/s.

9.2.2 2D single trabecula model -Analytical approach

The hexagonal unit cell model that is represented by a single fiber was employed and was subjected to a non-uniform velocity profile $u(x)$as shown in Figure 9.7. Based on that profile, a drag force profile $F(x)$ was applied on the trabeculae. This profile is given by:

$$F(x) = \frac{\pi \cdot \mu \cdot r_f^2}{c \cdot K_p} \cdot u(x) \tag{9.11}$$

where, r_f is the radius of the trabeculae, $c = \frac{2 \cdot \pi \cdot r_f^2}{\sqrt{3} \cdot (2 \cdot r_f + \Delta)^2}$is the fiber volume fraction of the trabeculae in the periodic unit. K_p and μ have the same value as in the previous section (the strap model.) Assuming that $u(x,t)$ is the instantaneous local fiber velocity and $y(x,t)$ is the local deflection of the fiber, we can write $u = \frac{\partial y}{\partial t}$. Then, using the similar approach presented in Finnie et al. (2004), the viscoelastic recoil of a trabeculae is determined by the following equation:

$$EI \frac{d^4 x}{dz^4} = -\frac{\pi \mu r_f^2}{c K_p} \frac{\partial y}{\partial t} \tag{9.12}$$

To solve this equation we first introduce some dimensionless variables, $X = x/L$, $Y = y/y(\frac{L}{2}, 0)$, $T = t/\tau$ with $\tau = \frac{kL^4}{EI}$ and $. k = \frac{\pi \mu r_f^2}{c K_p}$ Note that τ and k are the coefficients of the velocity term, L is the height of the SAS, and $y(\frac{L}{2}, 0)$ is the maximum deflection at the beginning of our analysis. The dimensionless equation to solve is then reduced to

$Y_{XXXX} = -Y_T$. For the boundary conditions we assume that there is no deflection at the top and bottom of the SAS, that the slope at the top of the SAS is zero and that there is no shear force in the middle of the fiber: $Y(0,T) = Y(1,T) = \frac{\partial Y(0,T)}{\partial X} = \frac{\partial Y(1,T)}{\partial x} = 0$

After some manipulation the solution of the differential equation is expressed as: four times, the deflection of the fiber can be expressed as:

$$Y(X,T) = \frac{f_1}{2}X^2 + \frac{f_2}{6}X^3 - \frac{f_1'}{720}X^6 - \frac{f_2'}{5040}X^7 \tag{9.13}$$

where f_i's are unknown time-dependent functions that are determined through the boundary conditions. The results are shown in Figure 9.8 and Figure 9.9, which indicates that it takes approximately 19-20 milliseconds for the fiber to come back to its original shape in the SAS region.

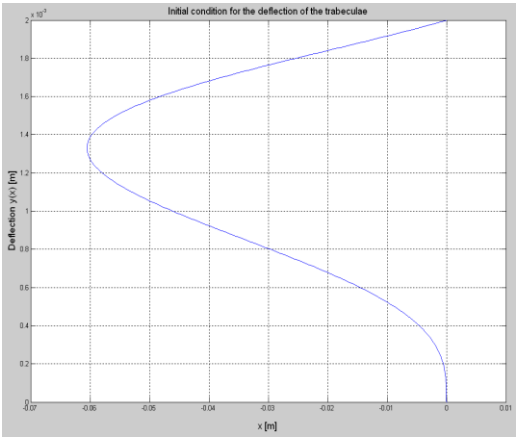

Figure 9.8 Buckling of trabecula due to velocity BC.

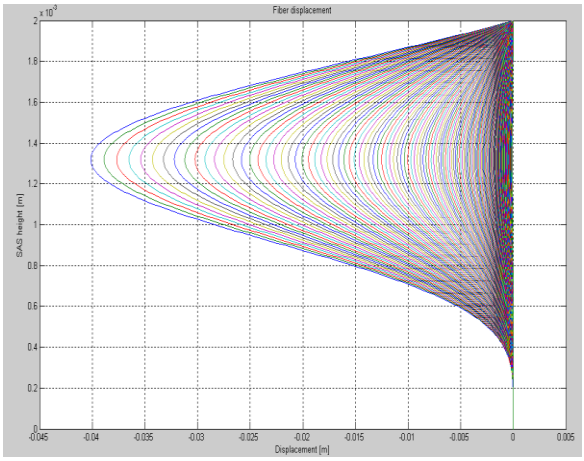

Figure 9.9 Trabecular buckling and recoil,19-20 millisecond.

9.2.3 2D single trabecula model - Numerical approach

2D single trabecula model was created using MRI images and Abaqus software. Velocity boundary condition was applied as input to compare rebounding effect of trabeculae with analytical study, in order to understand the buckling phenomena of trabeculae. The single trabecula l was fixed at its two ends. Abaqus 6.9-2 was used as a pre and post processor to investigate the buckling phenomena of the single trabecula and compared the result with the analytical study. The result indicated the same deformation as the analytical model, Figure 9.10 and Figure 9.11. The results of the numerical and the analytical models are in good agreement, as shown in Figure 9.12. The different slope of the buckling curve at the two ends of the trabecula was as a result of difference between the boundary conditions in the analytical and the numerical studies. For the analytical study the trabecula was simply supported at two ends, however the boundary condition was totally fixed for the finite element model.

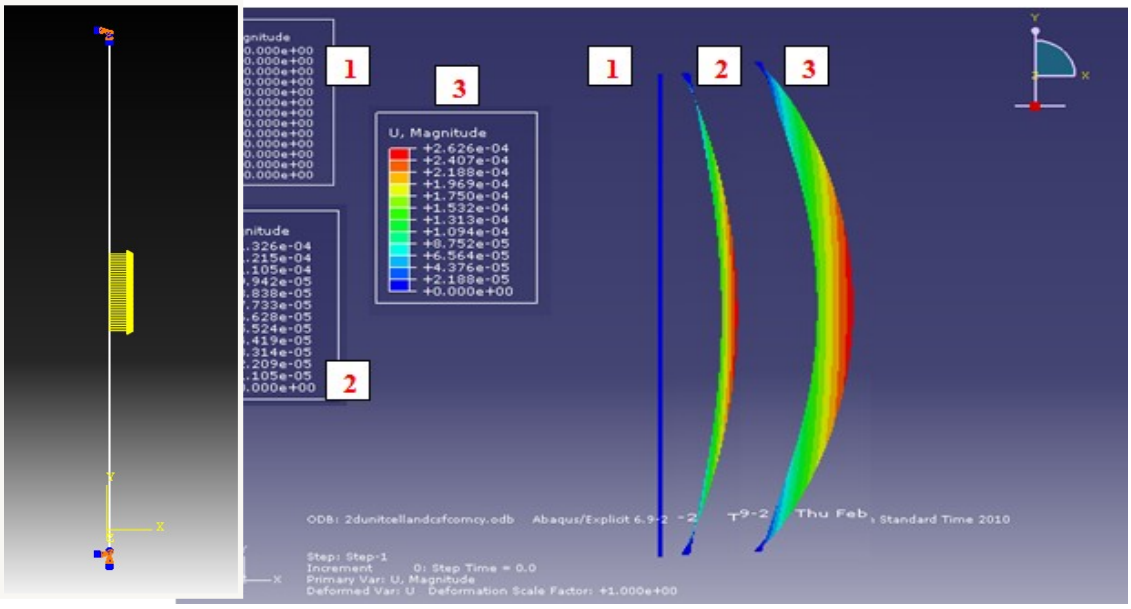

Figure 9.10 Trabeculae buckling due to velocity input BC in different time step.

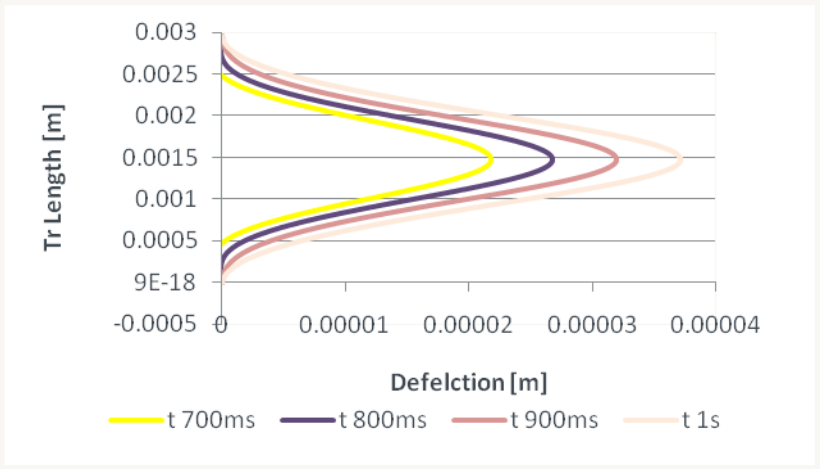

Figure 9.11 Trabecular buckling due to velocity BC.

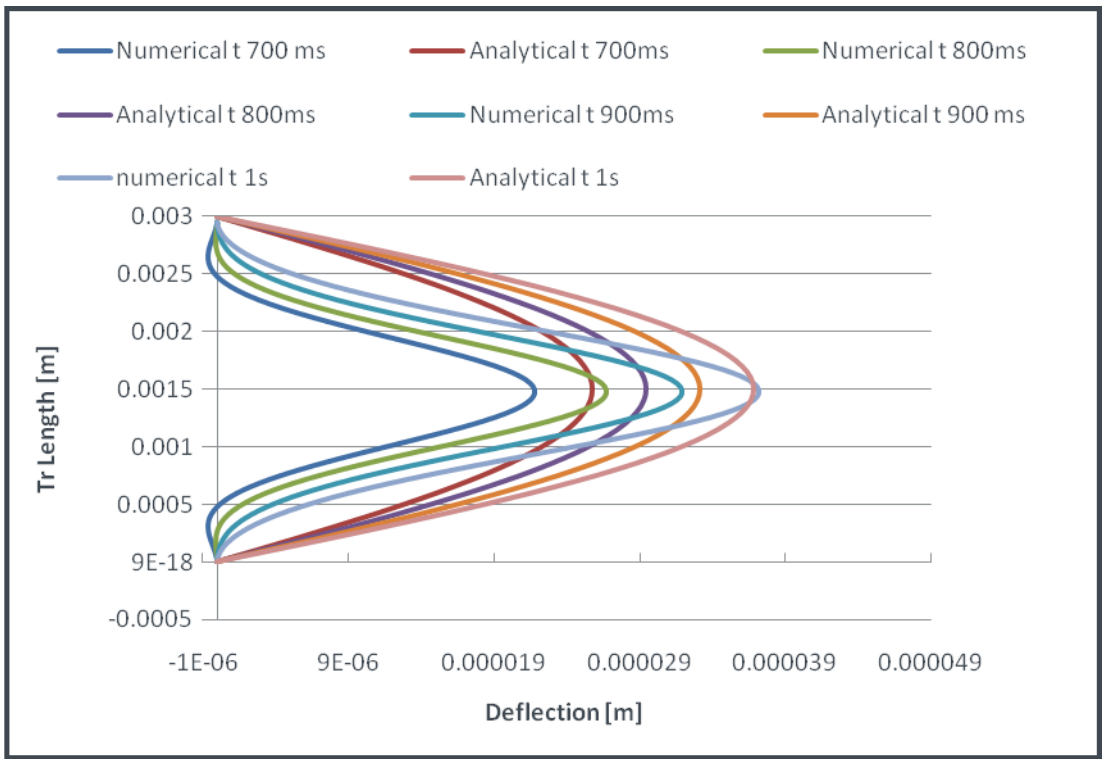

Figure 9.12 Comparison between analytical and numerical study.

9.3 Conclusion

The objective of this chapter was to find a suitable model for SAS region to be utilized in our global head model, where we investigate the strain in the brain due to contact and/or noncontact head accelerations (impacts). Several models, soft solid, viscous fluid, Darcy's permeability and porous elastic models were investigated. It was determined that Darcy's model is a realistic representation of the SAS region and can explain the hydrodynamic forces of CSF through the SAS region.

Further we proposed a hexagonal structural (unit cell) model for the structural organization of the trabecular architecture. In addition, for the mathematical formulation we assumed that the SAS is a uniform strip of a continuum around the brain. The mathematical formulation of the strip model was based on: Darcy's permeability, continuity equation and the balance of force equation. The solution of the analytical model was in good agreement with the FE solution. Finally, the buckling and recoiling of the unit cell fiber was formulated and solved analytically and compared with the FE solution.

The results of this chapter confirm the validity of the proposed structural unit cell model and the results of the analytical solution. In addition, the results indicate that Darcy's permeability is an appropriate model for the SAS. This study can be used as a basis to further investigate the transduction of mechanical and hydrodynamic forces through the SAS.

CHAPTER 10 Trabecular Architecture Models

10 TRABECULAR ARCHITECTURE MODELS

In this chapter the mechanotransduction of the external load to the brain through the trabeculae (with a specific architecture) in the subarachnoid space (SAS), was investigated. This has been accomplished by employing the results of our animal studies, i.e. the histology and architecture of trabeculae, and by creating local models consist of a trabecula. From our experimental study it was concluded that the trabeculae are mainly configured as tree-shaped, where the branches are attached to the arachnoid mater and the stem is attached to the pia mater. The result of the analysis reveals that tree-shaped configuration of the trabeculae creates less strain in the brain when the head is subjected to external loads, and thereby damps the impact.

It has been shown that subarachnoid space (SAS) trabeculae plays an important role in damping and reducing the relative movement of the brain with respect to the skull, thereby reducing traumatic brain injuries, (Zoghi & Sadegh 2009 and 2010). Several models have been created to predict different types of head injuries. In these models the space between the skull and the brain, i.e., the meningeal layers including the cerebrospinal fluid (CSF) and the subarachnoid space (SAS) have been over simplified as an elastic materials having the bulk modulus of water and very low shear modulus, or in some cases as water only, Kleiven et al. (2003) and Trosseille et al. (1992). These over simplification could lead to inaccurate results.

The results of our experimental study revealed that the SAS is a complex region contains of abundant trabeculae in the form of septa, rods, plates and tree-shaped

trabecula. Seventy percent (70%) of these trabeculae are tree-shaped where the stems are connected to the pia mater and branches are attached to the arachnoid mater as it is reflected in i.e. Alcolodo et al. (1988), Frederickson et al. (1991) and is confirmed with our experimental study, Figure 10.1 (b-d). Note that this trabecula is formed as bundle of collagens. The tree-shaped trabeculae appears counterintuitive, that is, the inverted tree-shaped seems to have less strain in the brain. To understand why the majority of the trabecula are tree-shaped, in this chapter, we compare these two architectural structures. This is an important question since it affects the global models of the head and biomechanics of the brain.

10.1 2D Local Models of single trabecula

To further investigate the mechanotransduction of the external load to the brain and have a better understanding of the effect of the trabecular architecture and their orientations on transferring loads or impacts to the brain, in this chapter, two basic local models i.e. one with a tree-shaped and the other with an inverted tree-shaped of a single trabecula connecting the pia mater to the arachnoid were created. The first model was created using our experimental images where the branches of the single trabecula were merged to the arachnoid and the stem was attached to the pia mater. The second model was created as a inverted tree-shaped where the branches of single trabecula are attached to the pia mater and the stem was merged to the arachnoid mater. Both models were consist of single trabecula, CSF as a soft solid, brain, pia mater and arachnoid mater. The models are shown in Figure **10.2** (a-b). The reason for the two configurations is that we need to understand why the majority of the trabeculae are oriented such that the stem is

attached to the pia mater and the branches are attached to the arachnoid. The meshes then were generated in the two local FE models and Abaqus 6.10-EF1 was used for pre and post analyses. These two models were subjected to the same boundary conditions, displacement of 3 mm, on the arachnoid side and the bottom layer of the brain was fixed to restrain the model. Explicit dynamic analysis was performed and it took about 14 minutes to solve for each local model with 3.4GHz, 6 core processor. The same material properties, as shown in Table 6.3, were used for two local models. The percentage of the strains in the brain in the two models were compared , Figure 10.3and Figure 10.4.

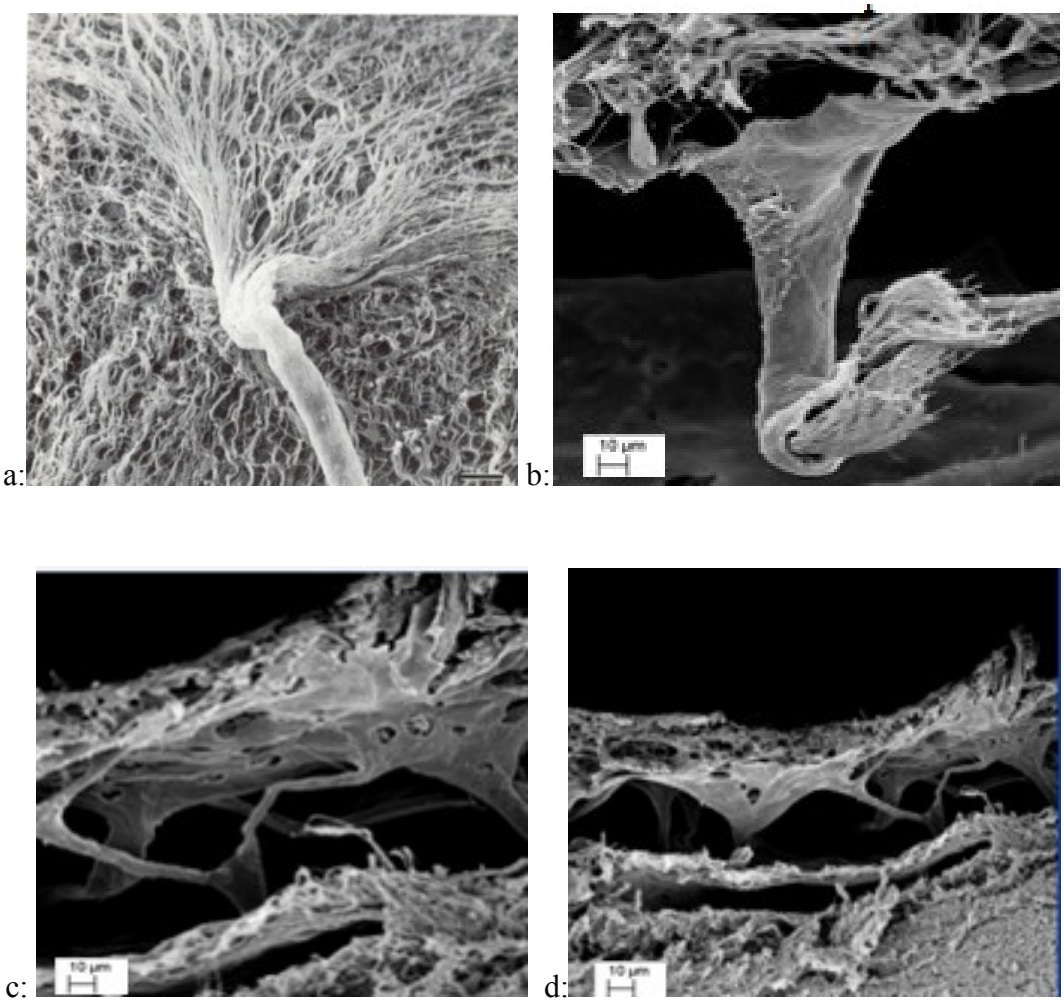

Figure 10.1 SEM images of SAS showing branching the trabeculae into the arachnoid a: (Alcolado et al. 1988). b: single trabecula connecting pia to arachnoid. c and d: (zoom out) of the SAS depicting the trabeculae.

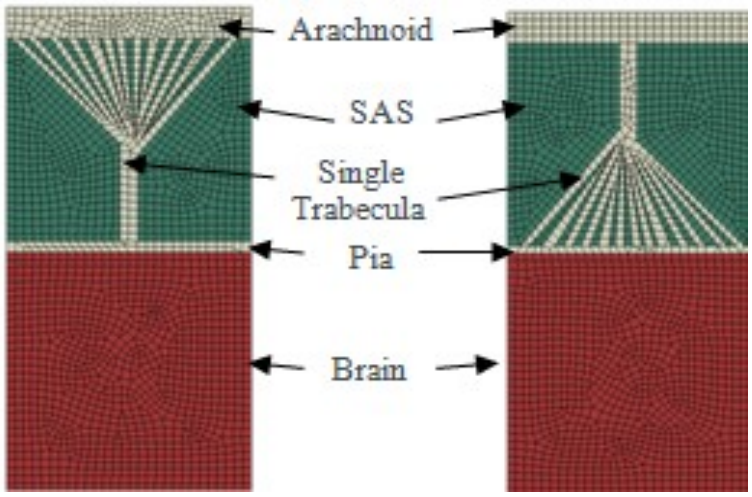

a b

Figure 10.2 FE models, a: tree-shaped model of single trabecula, b: inverted tree-shaped model of single trabecula

10.2 Result of the Architectures of a single Trabeculae a

The results of the analysis of the two local models of single trabecula revealed that the strain field in the brain and in the SAS near the brain, of the tree-shaped trabecula is less than that of the inverted tree-shaped trabecula, as shown in Figure 10.3 and Figure 10.4. The reason is that in the inverted tree-shaped the CSF is trapped in the branches of trabecula. This would increase the resistance (shear) to the flow of the CSF near the brain, and thereby would increase the pressure on the brain. Where as in the tree-shaped trabecula as soon as the brain moves closer to the skull the stem buckles immediately and there is no additional pressure concentration on the surface of the brain. In addition, in the tree-shaped trabecula, when the brain start to move toward the skull, the CSF can freely flow over the surface of the brain and applies a more uniform and well distributed

(reduced) pressure on the brain. Note that TBI and concussions occur due to the excessive strain in the brain (approximately 15 to 20 percent). Therefore, we chose strain contour as the base for the evaluation of the results.

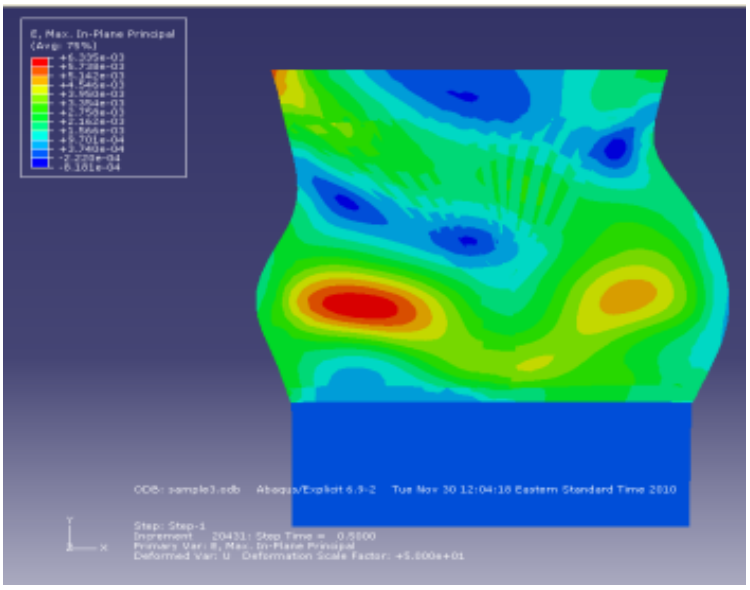

Figure 10.3 Strain contour in the tree-shaped model.

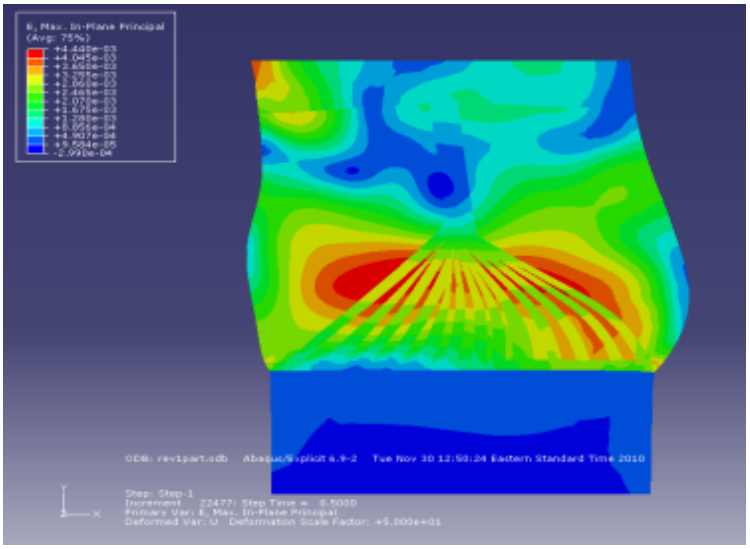

Figure 10.4 Strain contour in the inverted tree-shaped model.

10.3 Trabecular architecture 2D global model

To further investigate the effect of the trabecular structure on transferring the load/impact to the brain two global models of the several single trabecula were created and the transmission of the load through trabecula structure were analyzed.

The two global models were created assuming the head is perfectly spherical. The first model consisted of an inner disk representing the brain, CSF as a soft solid, several tree-shaped trabecula, the dura mater and the skull. In the second model the tree-shaped trabeculae were replaced with inverted tree-shaped trabeculae, Figure 10.5 and Figure 10.6. The models were then meshed and Abaqus 6.10-EF1 was used for pre and post processor analyses. All the layers of the model assumed to be homogenous and isotropic. The same material properties as shown in Table 6.3were used. A displacement boundary condition of 3 mm was applied to the skull and the center of the brain was restrained using Abaqus Multi Point Constrain (MPC). It took about 2 hours to solve for the Global models with 3.4GHz, 6 core processor.

.

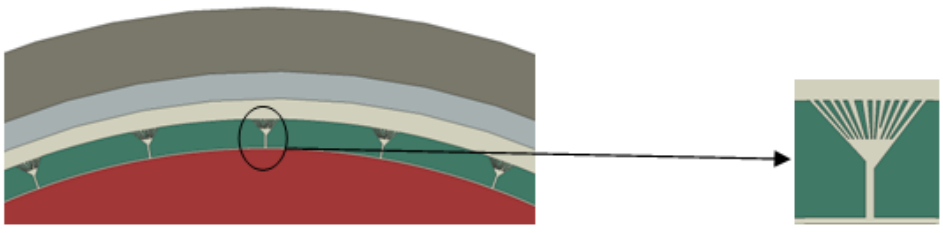

Figure 10.5 Global FE model of the tree-shaped model of single trabecula.

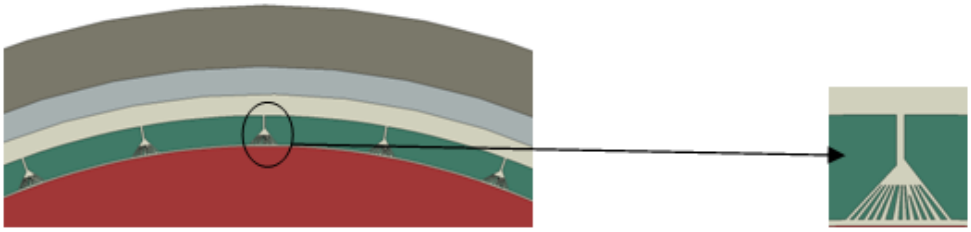

Figure 10.6 Global FE model of the inverted tree-shaped model of single trabecula.

10.4 Result of Trabecular architecture 2D global model

The results of the analyses of the two global models along the path is presented in following figures. The path is located as a curved line near the outer boundary of the brain as shown in Figure 10.7. Figure 10.8, Figure 10.9 and Figure **10.10** revealed that the strain, displacement and stress in the brain in the tree-shaped trabecula is less than that of the inverted one. Figure 10.8 depicts the strain variation in the brain along a normalized path. This figure shows that the strain in the brain in the inverted tree-shaped trabecula is higher than the tree-shaped. Figure 10.9 compare the displacement variation along the normalized path between the tree-shaped trabecula and the inverted one. The analysis reveals that the displacement in the brain in the tree-shaped trabecula is less than the inverted one. And finally the stress variation between the two models was compared in the Figure **10.10**. It was observed that the stress in the tree-shaped structure also is less than the inverted tree-shaped.

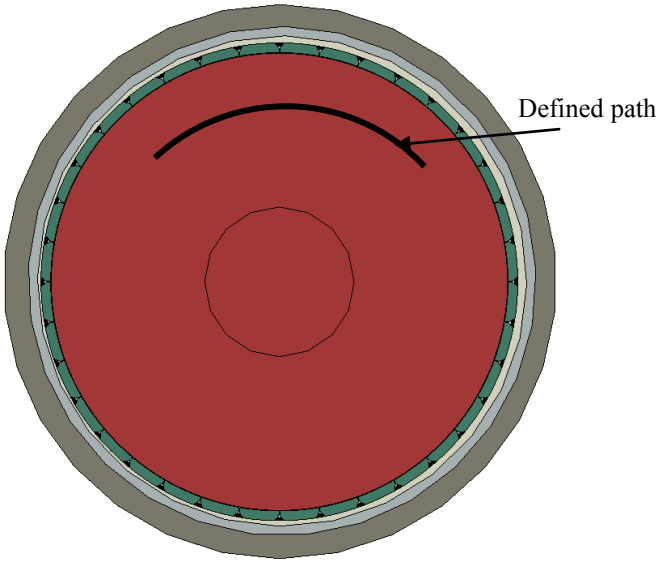

Figure 10.7 The path as a curved line near the outer boundary of the brain.

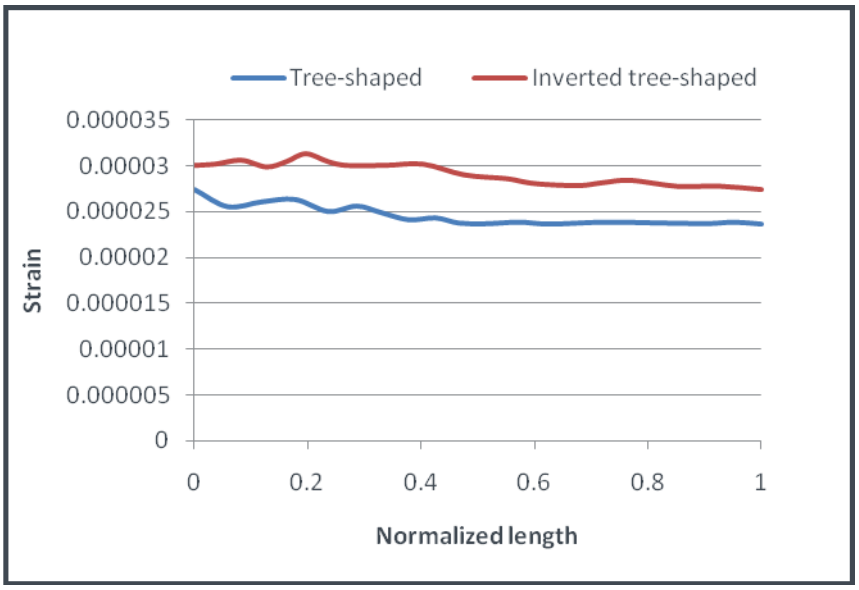

Figure 10.8 Strain variation of the two models along the define path.

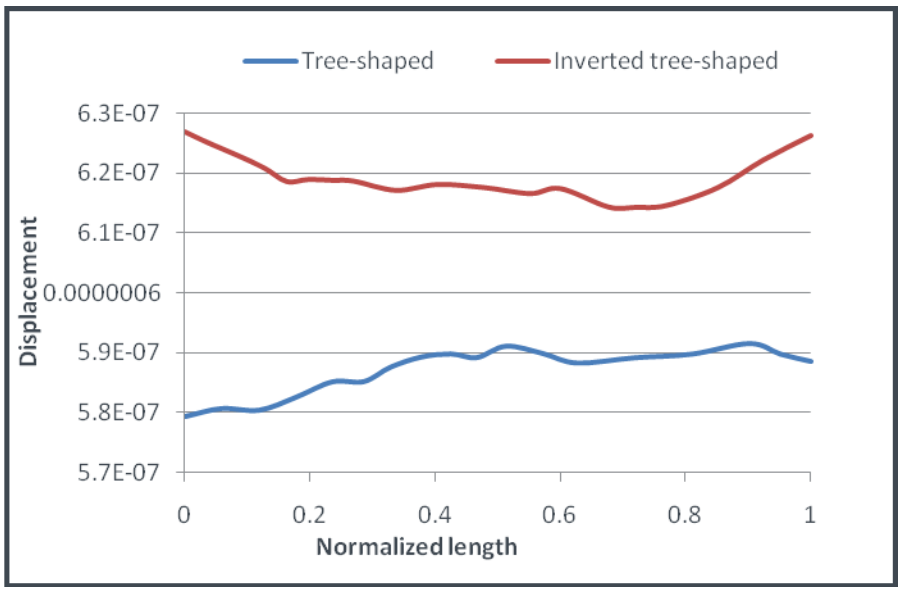

Figure 10.9 Displacement variation of the two models along the define path.

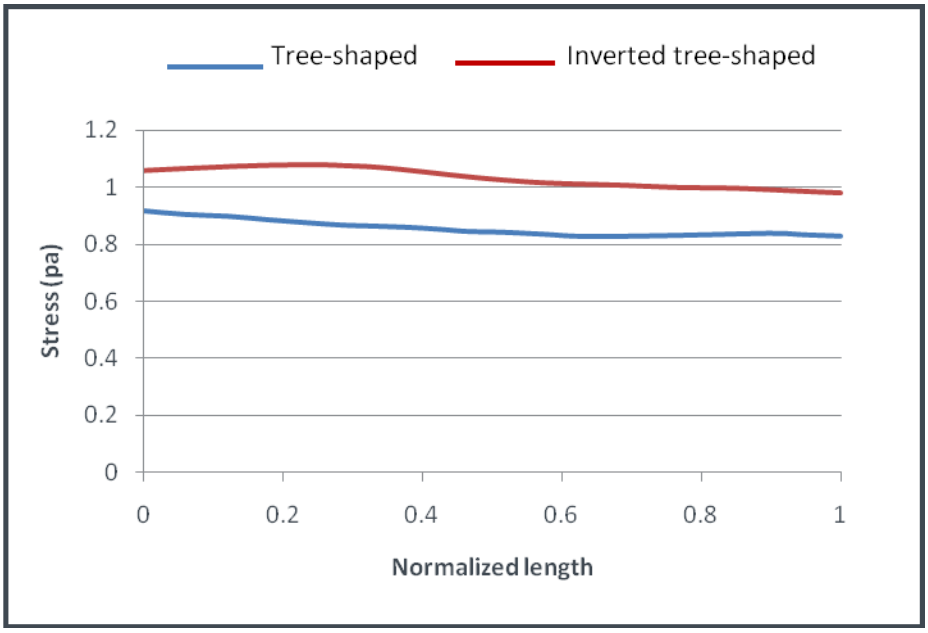

Figure 10.10 Stress variation of the two models along the define path.

10.5 Conclusion

Our animal studies revealed that a trabecula consists of a bundle of very thin collagen fibers braided together, and as they extended from the pia mater, they spread out and merge to the arachnoid mater in a form of branches. Based on the experimental results two local and global models of the trabeculae architecture were created and analyzed. The results of the analysis of the models revealed that the strain, displacement and stress fields of the tree-shaped trabecular architecture is less than that of the inverted one, as shown in Figure 10.8, Figure 10.9 and Figure **10.10**. It also reveals that the tree-shaped orientation of the trabecula where the branches are attached to the arachnoid mater provides more protection for the brain tissue when the head in subjected to an impact. Note that TBI and concussions occur due to the excessive strain in the brain (approximately more than 20 percent). The results of this study will lead to accurately modeling of the SAS and thereby determining the strain in the brain.

CHAPTER 11 3D Model of The Head

11 3D MODEL OF THE HEAD

As explained in the previous chapters the goal of this study is to quantify the relationship between the external loads to the brain and relate that to concussion or mild TBI. That is, to quantify the relationship between the magnitude of external impact to the strain in the brain leading to concussion or TBI. This goal was accomplished though three aims. The first aim was to study the architecture of the SAS trabeculae through the experimental study using SEM and TEM. The second aim was to investigate the effect of the SAS material properties and its architecture (tree-shaped and inverted tree-shape trabecula) on transferring load/impact to the brain through several 2D and 3D FE models.

To explain these results in more global sense, in this chapter, as a third aim, a three-dimensional (3D) model of the head-neck using magnetic resonance imaging (MRI) and Abaqus/CAE Sketch modules was created. The 3D model had to be validated to be used for further investigations. In the first part of this chapter the validation of the 3D head model against the experimental study of Feng et al. (2010) is explained. Next, the effect of the different types of material modeling of SAS on transferring the load to the brain is studied and is compared with the experimental study. Also, in the last section, the strain in the brain as a function of applied velocity impacts is determined.

11.1 The 3D head model

11.1.1 The 3D head model generation

The 3D head-neck model was created using the MRI images of a female adult patient in her 50's. The details of the geometry and the dimensions were determined using eRAD/Image Medical Practice builder 1-2-3 software. To create 3D model of the head, initially transverse, sagittal and lateral planes of the head were defined. Several cross sections from each plane was imported in to the Abaqus/ CAE sketch modules, Figure **11.1** to Figure 11.5. Each cross-section was measured and the data was used to create the same section in the Abaqus/CAE. From eleven cross sections that was imported into Abaqus sketch modules, Solid Loft commend was used to create the left portion of the white mater of the brain, Figure 11.6. The brain assumed to be homogeneous and isotropic. The right portion of the white mater was created by mirroring the object along the XY plane. Completed model of white mater was measured and compared with the 3 known planes of the human subject (transverse, sagittal and coronal). Due to the complexity of the model of the white mater the model was then simplified base on the MRI images. The simplified model of the white mater was used as a base model for the construction of the whole brain, Figure 11.7. Gray mater, SAS, dura mater and the skull were created using offset option of the sketch modules. Different layers of the head was assembled together to create a completed head model, Figure 8a-f. The model of the face was then created using the same method that we used for the white mater. Different cross sections of the MRI image of the face were imported to the Abaqus/CAE sketch modules and the complete face model was created, Figure 11.8-d.

Then, the different layer of the head-neck was subtracted from the 3D model of the face, Figure 11.8-e. Finally all the layers were assembled together to create the complete head model, Figure 11.9.

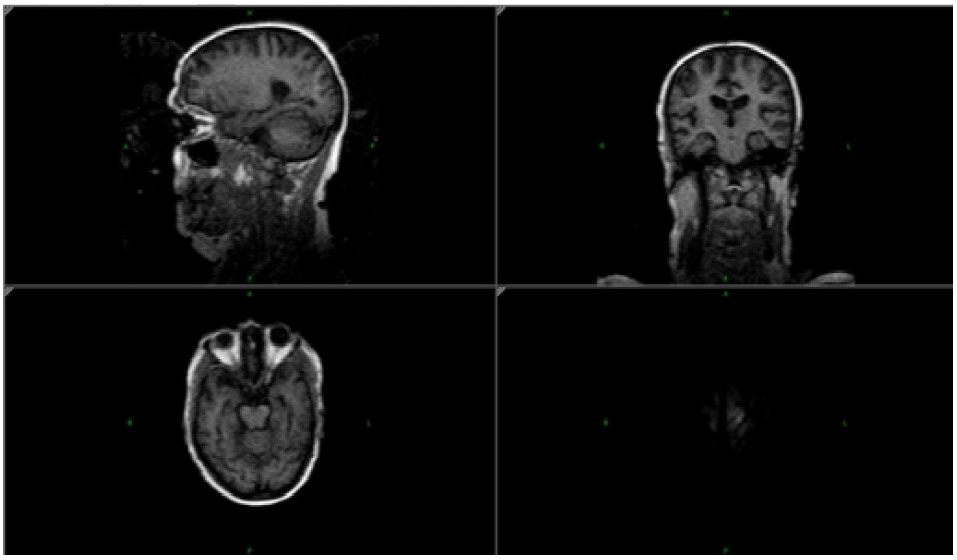

Figure 11.1 The MRI images of sagittal, coronal and transverse plane shown in eRAD/Image Medical Practice Builder 1-2-3 software

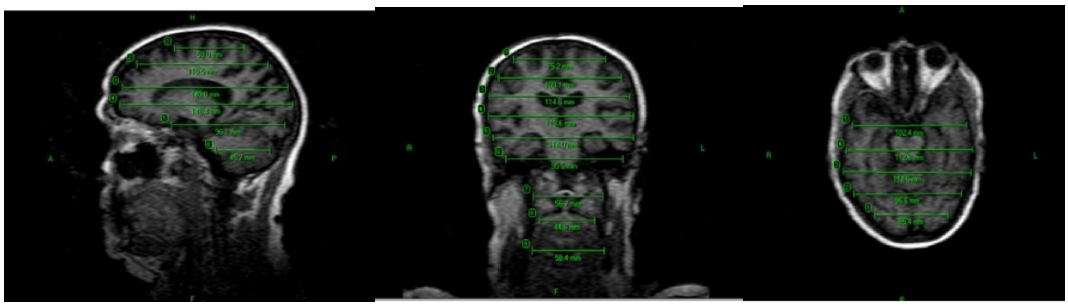

Figure 11.2 The MRI sagital, lateral and transverse images of head with some dimensions.

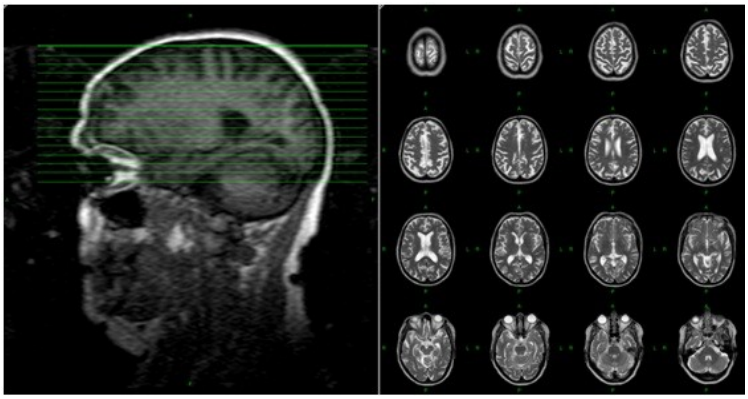

Figure 11.3 The MRI images of coronal cross sections along the sagittal plane.

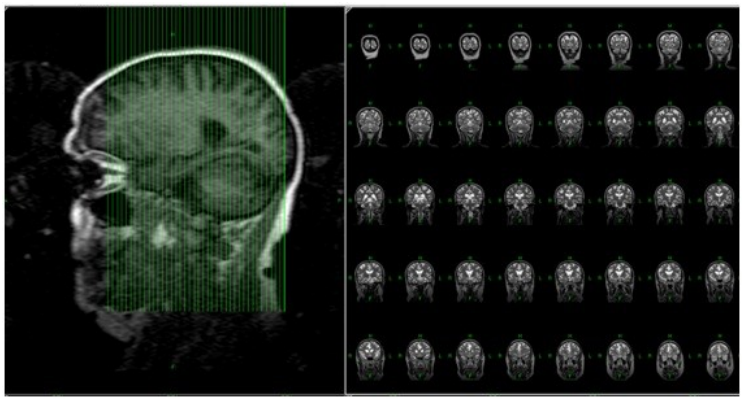

Figure 11.4 The MRI images of lateral cross sections along the sagittal plane.

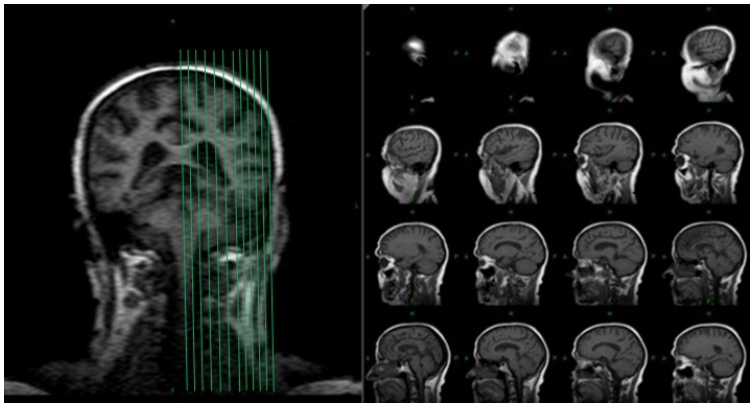

Figure 11.5 The MRI images of sagittal cross sections along the lateral plane.

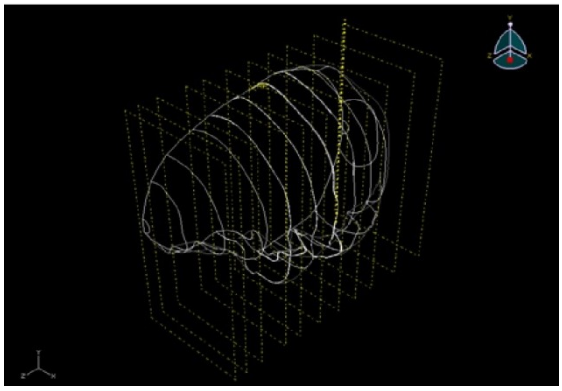

Figure 11.6 Contour of lateral cross section of left side the brain.

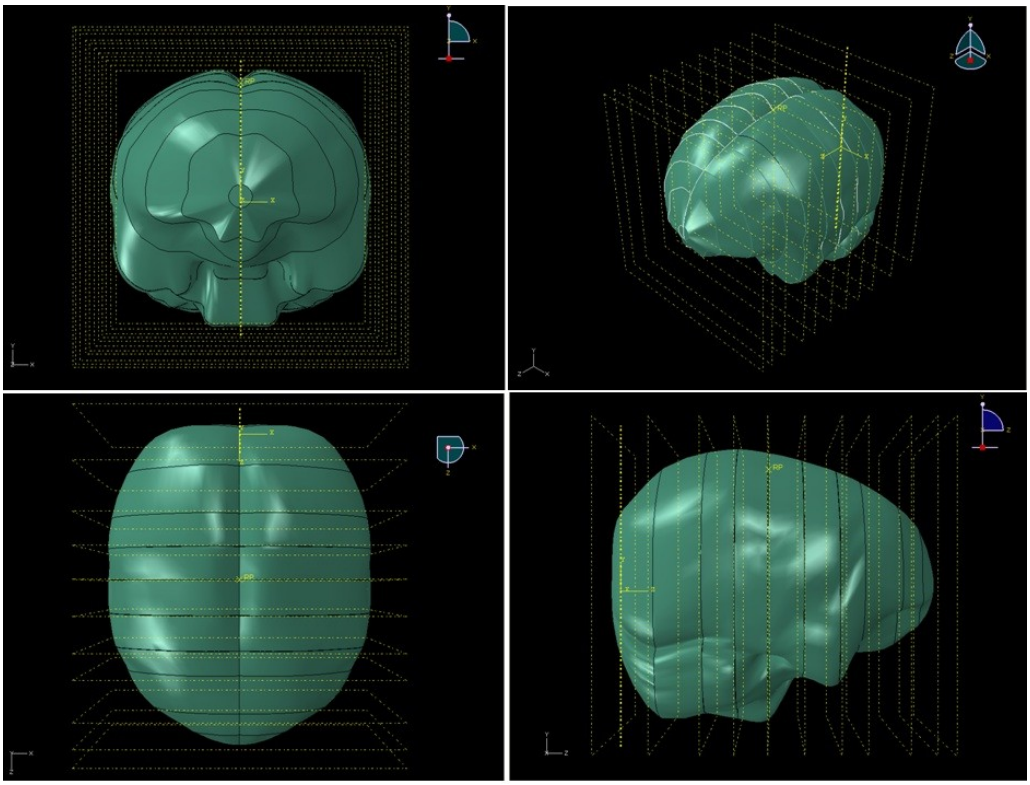

Figure 11.7 Completed white mater model.

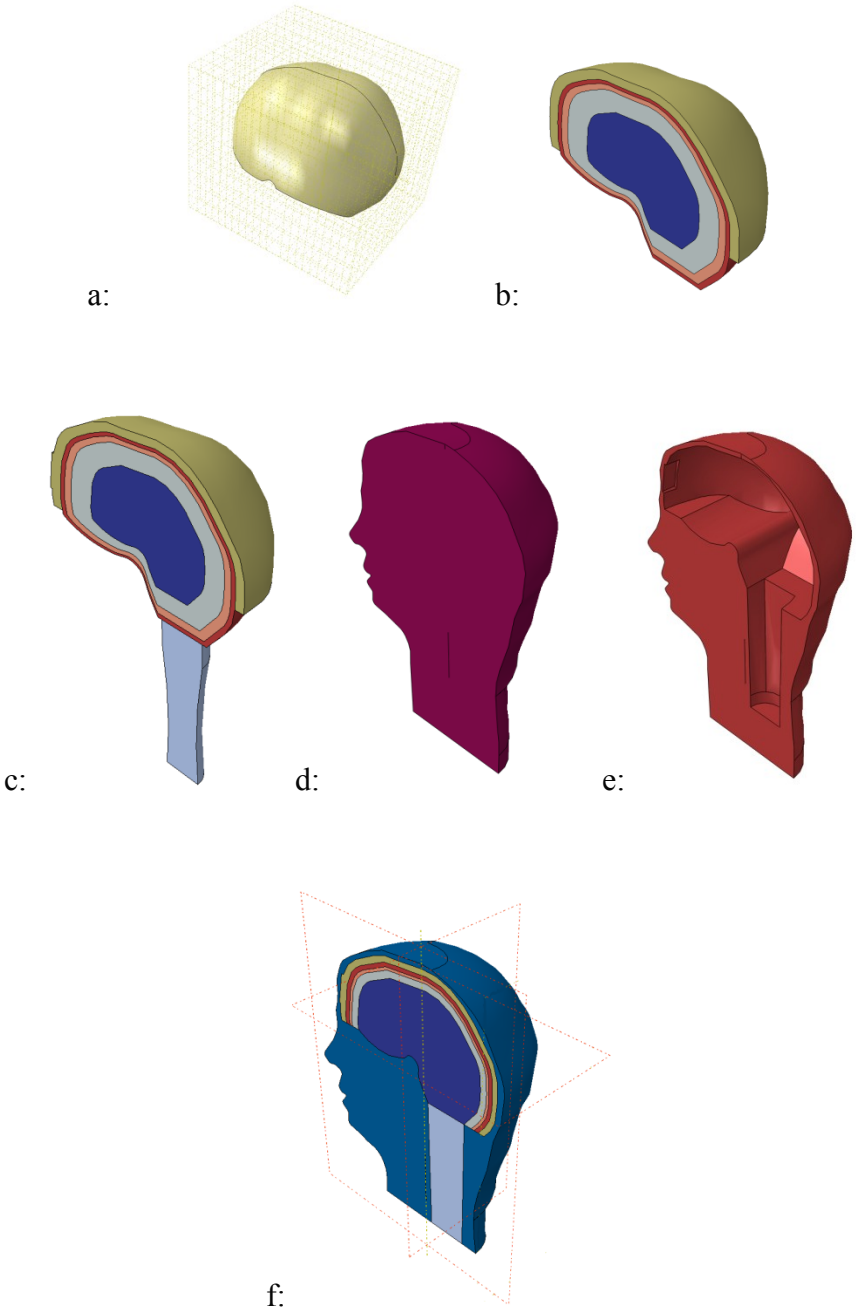

Figure 11.8 a-f: Steps to completed the 3D head model a: The whit mater, b: The white mater, gray mater, SAS, dura and the skull model c:The head and neck, d and e: The face model and f: completed head face model.

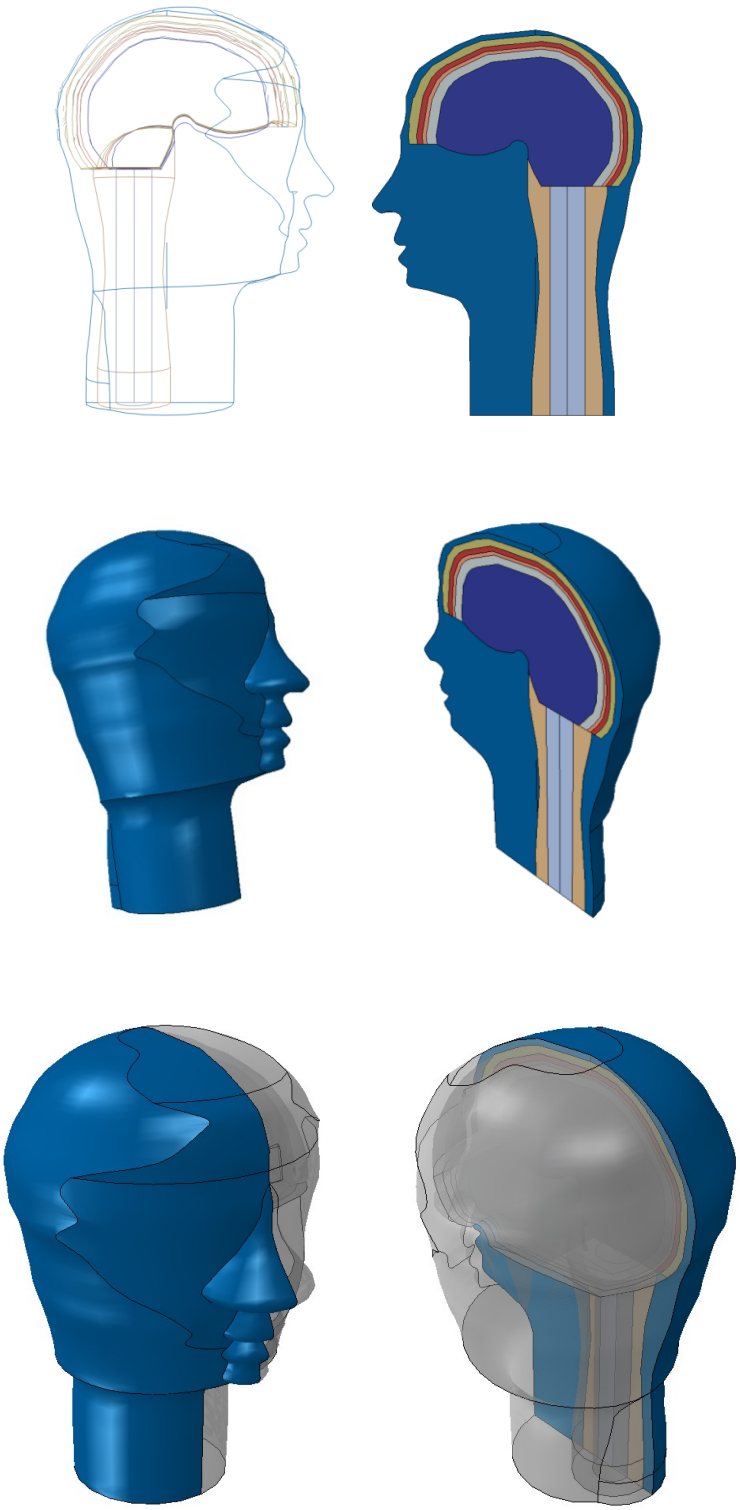

Figure 11.9 Different view of the 3D head model.

Abaqus 6.10-EF1 was used as the pre and post processors. The next step was to generate the nodes and the elements. The model was meshed using quadratic tetrahedral elements type C3D10M. The Total number of 48728 nodes and the total number of 33319 elements were created, Figure 11.10. Abaqus explicit dynamic analysis was performed using 3.4GHz, 6 core processor. It took approximately 2.5 hours to run an analysis. To reduce computational time, only the half of the model using the symmetry boundary condition was subjected to the displacement.

The material property of brain was assumed to be isotropic, and linear viscoelastic. All other components assumed to be linear, isotropic and elastic. Table 11.12, tabulates the material properties of the different components used in the 3D head model. The material properties are taken from Zhang et al. (2001-2002) and Takhounts et al. (2008). The average Young's modulus of the skull bone, the cortical and the trabecular bones layers is used as shown in Table 11.12. Figure 11.10 represents the 3D head model with its elements.

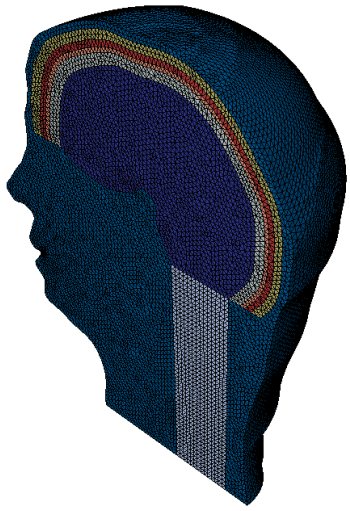

Figure 11.10 Completed 3d meshed model to be used for FEM analysis.

Brain tissue	
Shear modulus at t=0 (G0) (Pa)	$10.0*10^3$
Shear modulus at t=∞ (G∞) (Pa)	$2.0*10^3$
Bulk modulus at t=0 (K0) (Pa)	$5.0*10^7$
Bulk modulus at t= ∞(K∞) (Pa)	$5.0*10^7$
Relaxation time (λ) (s-1)	16
Density (ρ) (kg/m3)	$1.04*10^3$

Table 11.1 Tissue material properties of the brain as a linear viscoelastic model.

Skin	Young's modulus (E) (Pa)	$5.67*10^3$
	Poisson's ratio (υ)	0.48
	Density (ρ) (kg/m3)	$1.06*10^3$
Skull	Young's modulus (E) (Pa)	$12.2*10^9$
	Poisson's ratio (υ)	0.22
	Density (ρ) (kg/m3)	$2.12*10^3$
Dura mater	Young's modulus (E) (Pa)	$31.5*10^6$
	Poisson's ratio (υ)	0.45
	Density (ρ) (kg/m3)	$1.13*10^3$
SAS	Young's modulus (E) (Pa)	$1.15*10^3$
	Poisson's ratio (υ)	0.48
	Density (ρ) (kg/m3)	$1.13*10^3$
Muscles	Young's modulus (E) (Pa)	$1.0*10^7$
	Poisson's ratio (υ)	0.38
	Density (ρ) (kg/m3)	$1.01*10^3$
Neck	Young's modulus (E) (Pa)	$6.04*10^9$
	Poisson's ratio (υ)	0.38
	Density (ρ) (kg/m3)	$1.18*10^3$

Table 11.2 Material properties of the 3D head model.

11.1.2 Validation of the 3Dhead model

The model was validated against the experimental study of Feng et al. (2010). In their study, a human subject's head dropped on its own gravity approximately 2 cm and came in contact with a rubber band that is used as a stopper. Displacement data were then obtained from this mild frontal head angular acceleration of the head and the impact with the rubber band. Tagged magnetic resonance imaging method was used to measure in vivo relative displacement between the brain and the skull of three adult male human subjects. Their study provides an important set of displacement measurements in the human brain during the mild frontal skull impact. The result of Feng et.al (2010) shows that, at the four specific locations of the brain, the rotation and the displacement of these points relative to the skull is approximately 1-3 mm.

To validate our 3D head model the experiment of Feng et al. (2010) was simulated. The 3D head model was subjected to the displacement of 2 cm and the displacements of different sections of the brain were compared to the four material locations (a, b, c and d) corresponding to the experimental study as shown in Figure 11.11. Figure 11.12 shows the input boundary condition for the 3D head model. The input boundary condition was applied at the origin of the model, as shown in the Figure **11.13**, to suite the same boundary condition as the experimental study. The model was restrained at the inferior point of the neck and only in-plane rotation was allowed. Abaqus explicit dynamic analysis was performed using 3.4GHz, 6 Cores Processors. Relative displacement between the skull and brain was measured in the four material locations as shown in Figure 11.11.

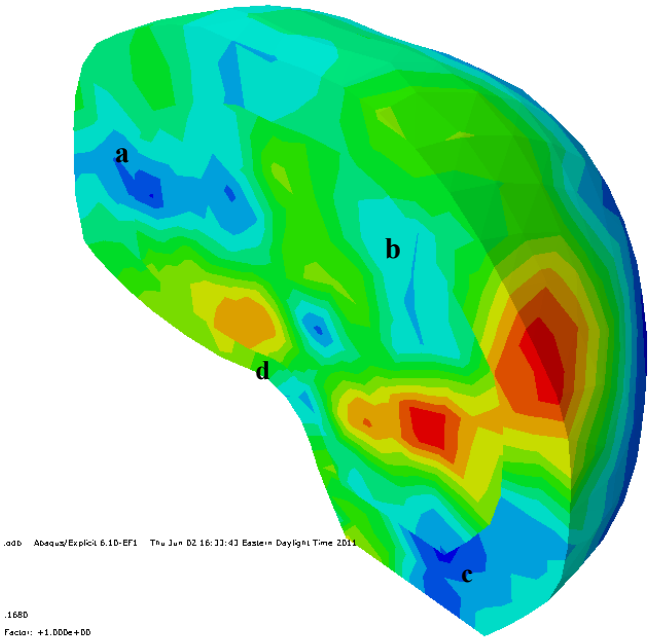

Figure 11.11 Four material locations in the 3D head model.

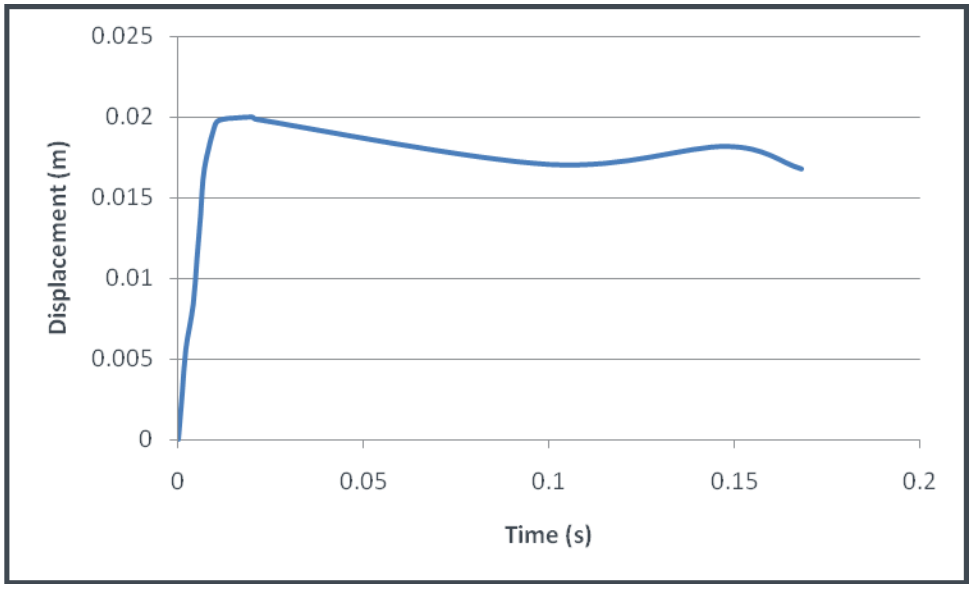

Figure 11.12 Input BC for 3D head model.

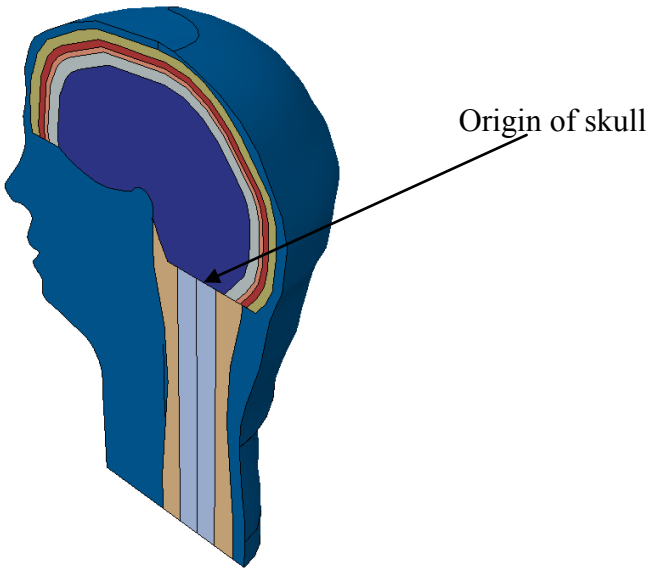

Figure 11.13 The origin of skull in the 3D head model.

11.1.3 Result of 3D head model validation

From our 2D analysis we understood that the SAS has significant factor on transferring the load to the brain. Based on our analyses in previous sections, in this section, the 3D model was analyzed using soft elastic material property, E=1000 Pa, for SAS. The displacement in the four material locations of the brain was compared with the experimental study of Feng et al. (2010). Figure 11.14 depicts the comparison of the relative displacements between the skull and the brain in location "a" of the experimental study and the FEM analysis. Figure 11.15 shows the comparison of the relative displacement between the skull and the brain of the experiment and the FEM analysis in location "b".

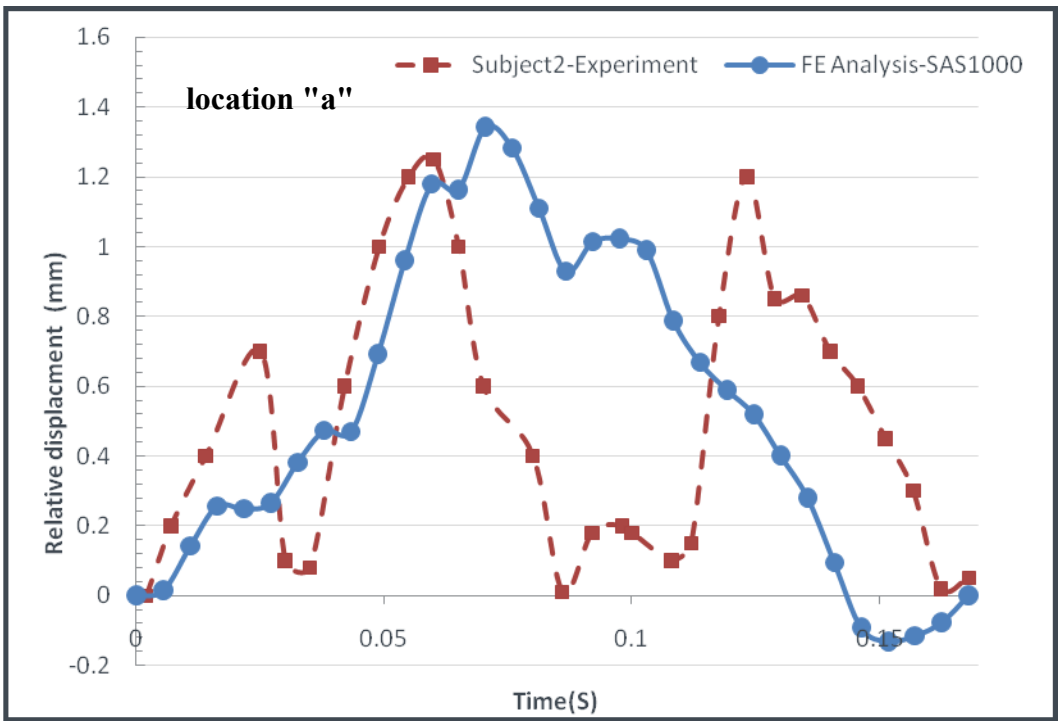

Figure 11.14 Relative displacement between the skull and the brain at the location "a".

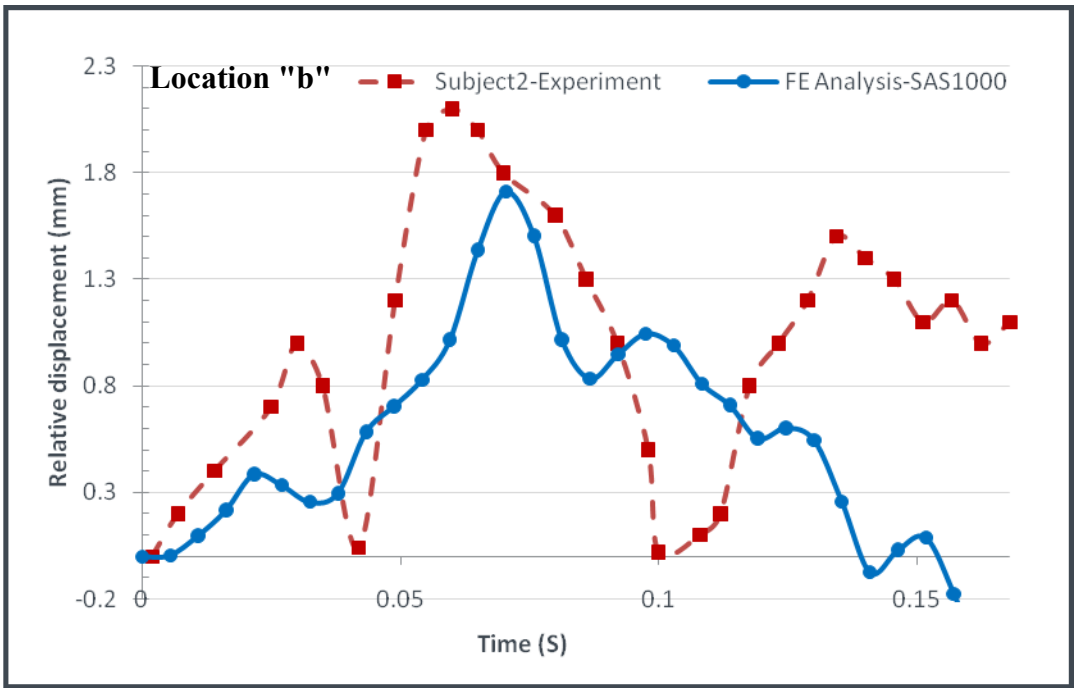

Figure 11.15 Relative displacement between the skull and the brain at the location "b".

The nodal solutions of the relative displacement in the brain and the skull were determined and were compared with the 2-3 mm displacement obtained from the experiment. Figure 11.14 and Figure 11.15 reveals that, for the Young's modulus of 1000 Pa the relative displacement between the brain and the skull is in good agreement with the 1-2 mm range of the displacement in subject 2 of the experimental study of Feng et al. (2010).

11.1.4 Conclusion

In our 2D modeling of the head a wide range of material property of SAS, up to three orders of magnitude, was investigated. the wide range has been reported by Zhang et al. (2002) and Xin et al. (2008). An optimum mechanical property of the SAS trabeculae was determined based on the validation of the models with the experimental results of Sabet et al. (2007). The result indicated that the optimum elastic modulus of the trabeculae is 1150 Pa. It was also determined that the SAS material property used by previous investigators is very stiff and could lead to unreliable results.

The human head as vulnerable body region is most frequently involved in traumatic brain injuries (TBI) and life threatening injuries. Because of the safety issues, animal and human experiments are always limited to mild angular acceleration or impacts. Therefore, the validated 3D FE model is a convenient tool to study the effect of the different types of the impacts to the brain. In this chapter we created an anatomically correct 3D model using magnetic resonance imaging (MRI) and Abaqus/CAE Sketch modules. The model was validated against experimental study of Feng et al. (2010) and

the displacement in the brain was compared to the 2-3 mm relative displacement between brain and skull of the experiment. The nodal solution of the strain in the brain was plotted in material location “a” and “b”. The relative displacement between the skull and the brain was in the good agreement with the experimental study of Feng et.al (2010).

The experimental curve of Feng et al. (2010) shown in Figure 11.14 and Figure 11.15 indicates two picks during the 168 ms period of the study. The first pick which occurs at about 40-60 ms is due to the moment when the head has its maximum angular acceleration. This moment is when the head of the subject hits the rubber band, see Figure 14-15. Once the elastic rubber band is stretched, it creates a rebound force pushing the head upward. Then the head of the subject separates from the rubber band fallowed by dropping down on its own gravity. This is the moment when the second pick occurs. Note that in our model, we did not consider the rebound force of the rubber band as it refers to the second pick. It is important to indicate that the time lag after the first pick, between experiment and our FEM results is due to the secondary force of the rubber that is not considered in our FE model.

These results indicate that the proposed young modulus's of 1000 Pa for the SAS is a reliable and appropriate value. The proposed value of E, also suggest that, the SAS material is soft and absorbs the brain movements. This confirms our hypothesis on the functionality of the SAS which act as damper and shock absorber of the brain. This model could be used for computer simulation of TBI.

11.2 Material modeling for SAS

To understand the mechanics of movement of the brain within the skull, i.e. the mechanics of the flow of CSF within the skull, and to further investigate the material properties of the SAS, three different types of materials for SAS were used in the 3D head model and the result were compared with the experimental study of Feng et al. (2010).

In previous studies, Trosseille et al. (1992), Kleiven et al. (2003), Zhang et al. (2001a, 2001b , 2002), Takhounts et al.(2008), Gupta et al. (2009) and Feng et al. (2010), the subarachnoid space (SAS) was modeled as soft solid or fluid. When the soft solid was used the functionality of the CSF was not consider. In the fluid model of the SAS the functionality of the trabeculae was ignored. To investigate the best material model, in this study we compare three different types of materials for SAS as they transfer the load to the brain. The first model where we used a soft solid material for SAS is presented in section 11-1. In the second material model the material of the SAS was defined as viscous fluid which has been used in most of head models. In the third model, the SAS was consider to be porous elastic material having the same void ratio and permeability that was used in chapter 9.

The 3D head model was used and the displacement boundary conditions were applied as an input for all the three material models. The displacement of the first-material location "a" in the brain was determined in all the three material's models and they were compared with the experimental study.

11.2.1 Material modeling of SAS -Soft solid

The first model was created using the same data as the previous section (11-1) which considers the SAS to be soft solid, with the young modules of 1000 Pa. The same boundary condition and loading were used. The relative displacement between the brain and the skull was compared with experimental study as shown in Figure 11.16. Strain contour of the brain with soft solid material for SAS is shown in Figure 11.17.

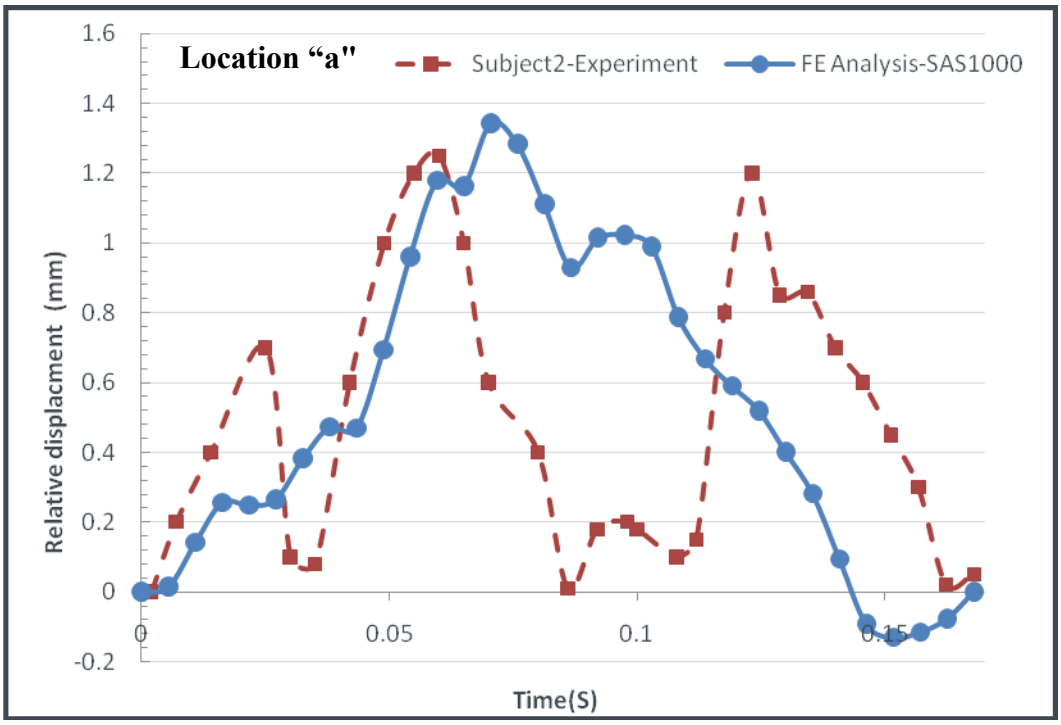

Figure 11.16 Comparison between the experiment and soft solid material model of SAS.

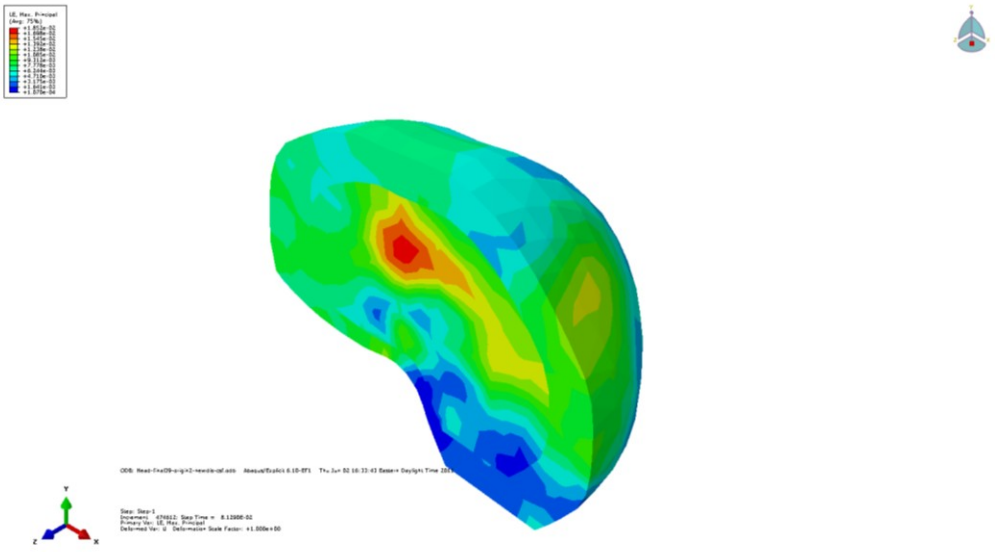

Figure 11.17 Strain contour in the brain, modeling the subarachnoid space as soft solid.

11.2.2 Material modeling of SAS-Fluid media

The second material model of the SAS was created using Pore Fluid/Stress element type of Abaqus. To simulate the same functionality for SAS i.e. combination of the trabeculae and CSF which acts as shock absorber, the SAS was modeled as viscous fluid. The viscosity of CSF was then taken from Zoghi and Sadegh (2004). The same boundary conditions as 3D soft solid material model was used. Fluid/ solid interaction boundary condition caused the computation to be more time consuming. Explicit dynamic analysis of Abaqus was performed. It took approximately 4.5 hours to run the analysis in 120 intervals with a 3.4GHz, 6 cores processor. The result of this analysis is shown in Figure 11.18. Also the strain contour of the brain is shown in Figure 11.19 for viscous fluid.

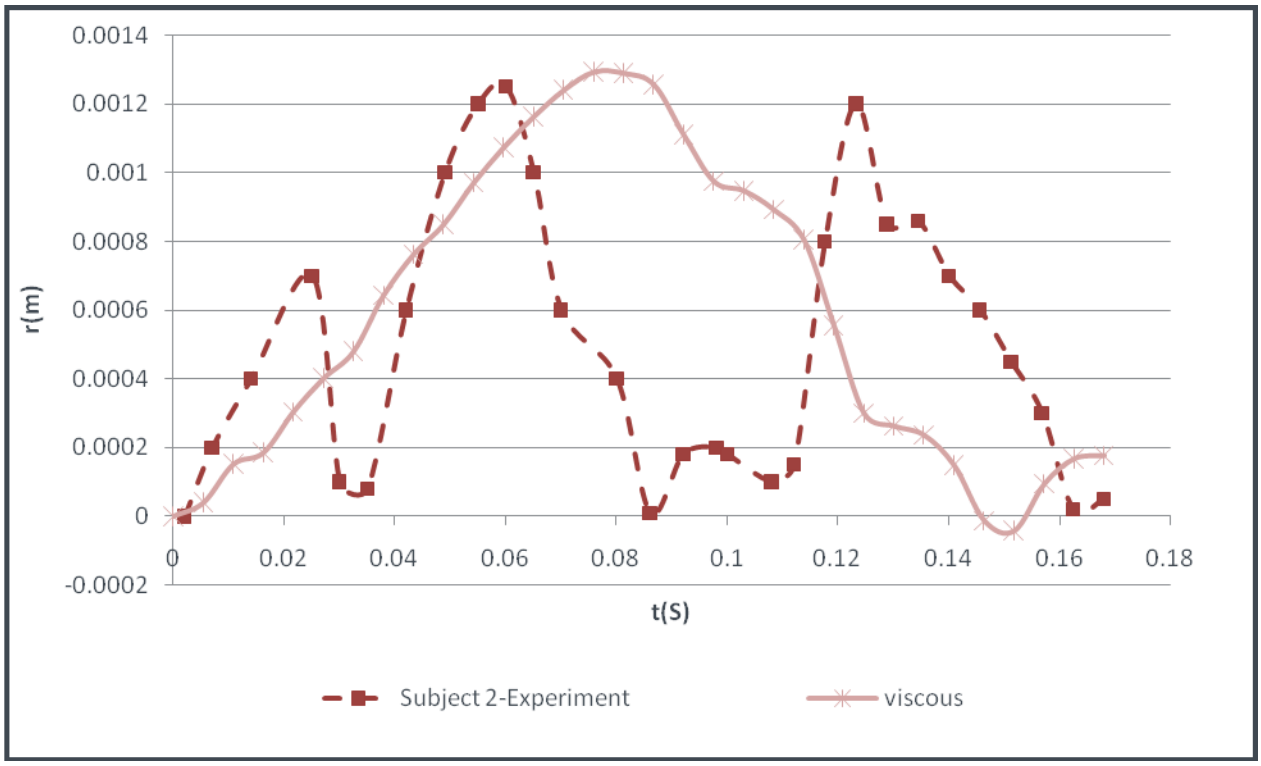

Figure 11.18 Comparison between experiment and viscous fluid model of SAS .

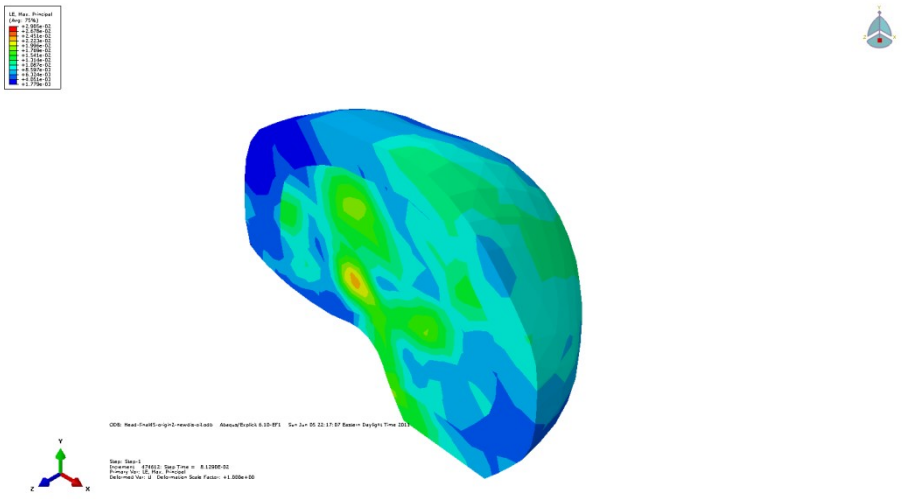

Figure 11.19 Strain contour in the brain, modeling the subarachnoid space as viscous fluid.

11.2.3 Material modeling of SAS- porous media

Our experimental studies reveals that the subarachnoid space is not a soft solid region nor a fluid media, however, it contains very dens layers of soft trabeculae tissues within the CSF fluid. These solid / fluid interactions provide damping against external impacts. One of the preferred models that can be used for the SAS is porous elastic model where the interaction of the CSF fluid and soft trabeculae tissue is considered as one mechanism. To model the SAS as a porous elastic material we need to estimate the void ratio, density and Darcy permeability. These data were used as described in chapter 9-1-1(Mechanics of CSF flow through the trabecula)

Having permeability and void ratio, the 3D model was used for porous analysis. Abaqus/CAE was used as pre and post processors and dynamic analysis was performed. It took approximately one hour to solve the problem with 3.4GHz, 6 core processors. Relative displacement between the brain and the skull was compared with the experimental study of Feng et al. (2010) as shown in Figure 11.20. This Figure shows good agreement with the experimental result. The strain contour of the brain with SAS as porous elastic is shown in Figure 11.21

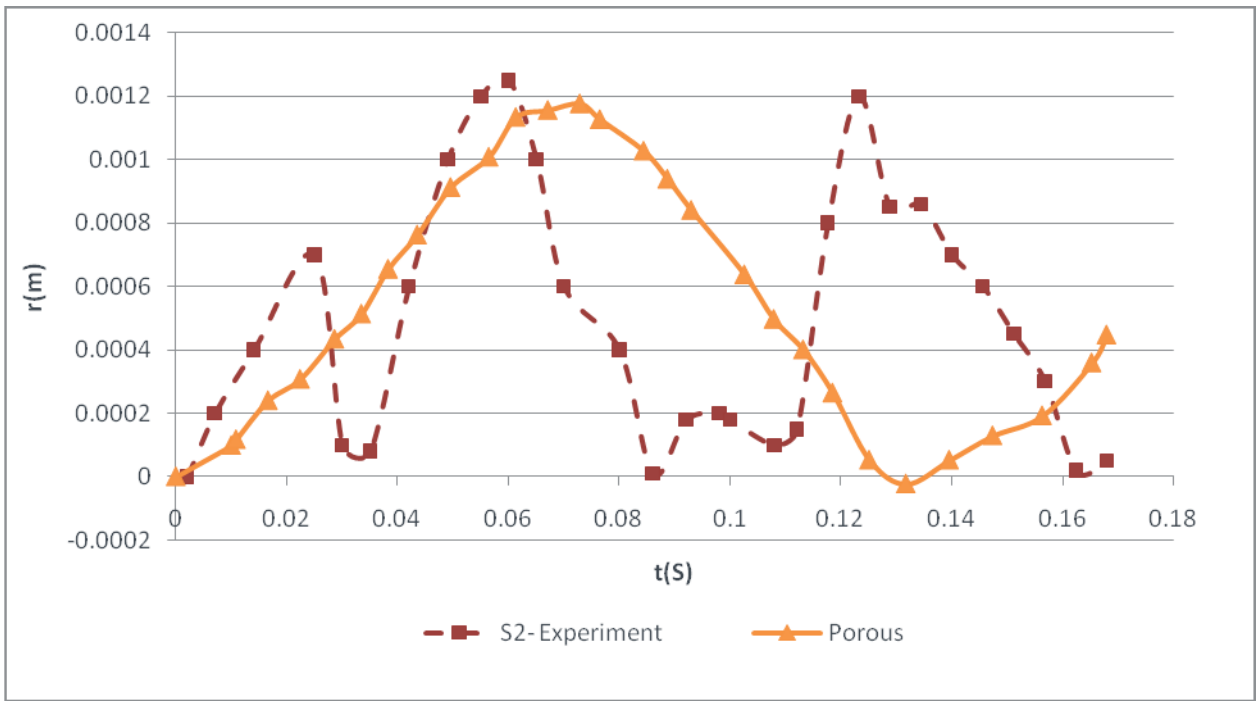

Figure 11.20 Comparison between the experimental study of the Feng et al. (2010) and SAS material as a porous media.

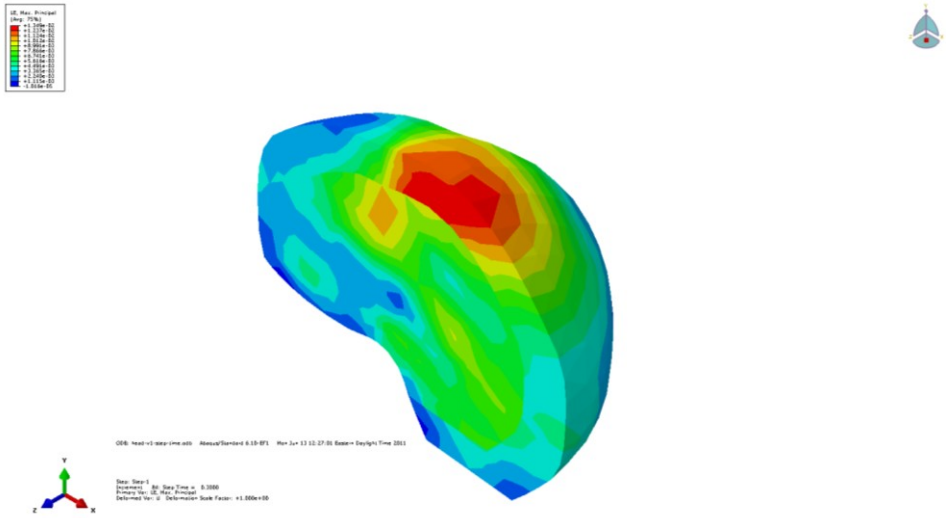

Figure 11.21 Strain contour in the brain, modeling of the subarachnoid space as porous media.

11.2.4 Conclusion

In this section we study the effect of the different material modeling and properties of SAS on transferring the load/impact to the brain, as it relates to TBI. Three material types were proposed for SAS modeling and relative displacement between the skull and the brain was compared with the experimental study of Feng et al. (2010), Figure 11.22. The displacements for all the three SAS material models are in good agreement with the experiment. That is, if one decides to use any of these materials to model the SAS, in local or global FE analyses, the properties found in this study are appropriate for future investigation.

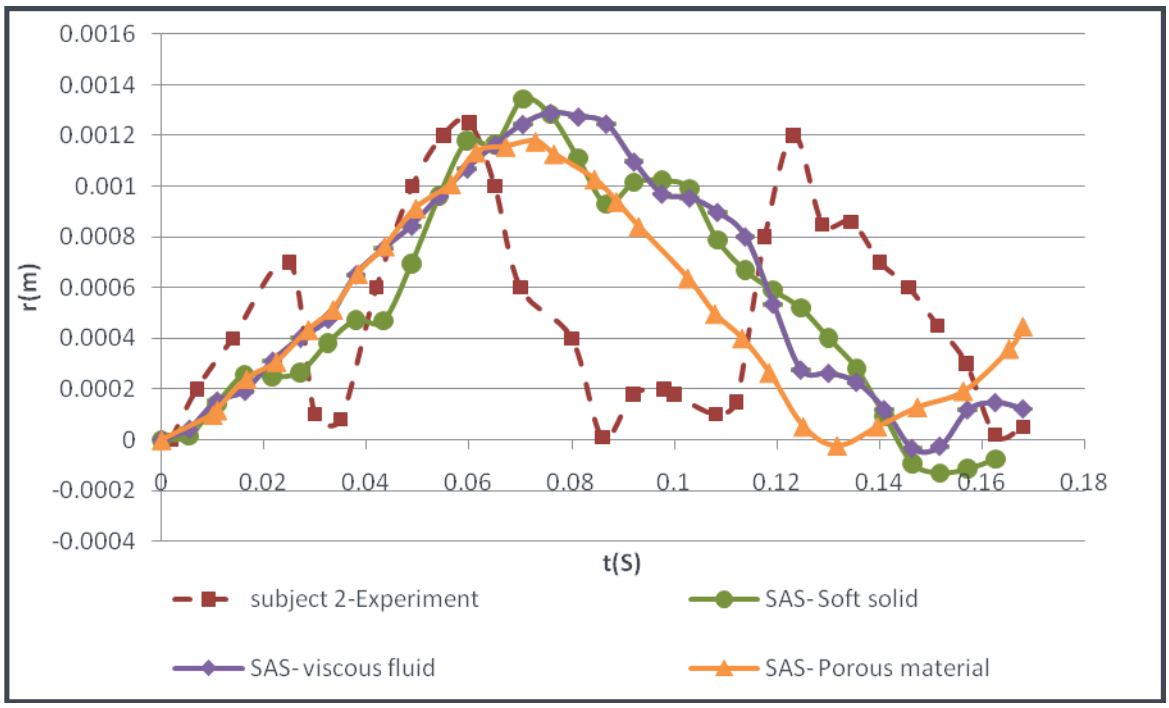

Figure 11.22 Comparison between the experimental study of the Feng et al. (2010) and , soft solid, fluid and porous material models for SAS.

11.3 The blunt head impact

11.3.1 Blunt impact analyses

In this section the 3D Head model was used to study the strain in the brain when the head in subjected to a wide range of impacts. The duration of typical blunt impacts are known to be approximately between 30-50 ms, Zhang et al. (2001) and Hardy et al. (2001). The displacement curve of these typical impacts is approximately a sine curve, Hardy et al. (2001). Considering these data, we established a series of curves for each case of the velocity impacts. The pick value of the displacement-time curve for the case of 15 mph is shown in Figure 11.23.

The 3D finite element model was subjected to the 12 different impact cases, corresponding to the velocity impacts of 2.5 mph to 30 mph, as shown in Table 11.3. The boundary conditions and the loading are as follow. These impacts were applied to the frontal region of the head. The inferior section of the neck of the model was restrained. Half symmetric boundary conditions were applied on the plane of symmetry of the model. The head/neck model and its boundary condition and loading are shown in Figure 11.24. In the first study, the frontal head of the 3D model was subjected to an impact corresponding to was 2.5 MPH (1.1m/s), i.e., displacement of 0.022 meter in 20ms. The model was then subjected to a series of impacts corresponding to 2.5 MPH to 27 MPH,

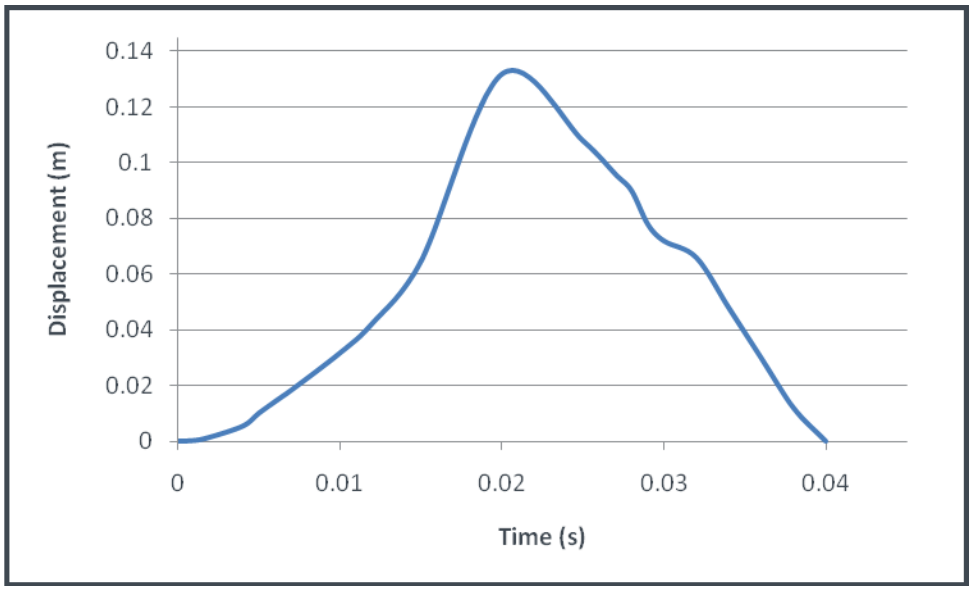

Figure 11.23 Velocity impact profile corresponding to 15mph (6.7m/s).

	Velocity (mph)											
	v=1.1	v=5	v=7.5	v=10	v=12.5	v=15	v=17.5	v=20	v=22.5	v=25	v=27.5	v=30
Time (s)	Displacement (m)											
0.00	0	0	0	0	0	0	0	0	0	0	0	0
0.00	0.00005	0.0001	0.00015	0.0002	0.00025	0.0003	0.00035	0.0004	0.00045	0.0005	0.00055	0.0006
0.00	0.00026	0.00052	0.00078	0.00104	0.0013	0.00156	0.00182	0.00208	0.00234	0.0026	0.00286	0.00312
0.00	0.00092	0.00184	0.00276	0.00368	0.0046	0.00552	0.00644	0.00736	0.00828	0.0092	0.01012	0.01104
0.01	0.0017	0.0034	0.0051	0.0068	0.0085	0.0102	0.0119	0.0136	0.0153	0.017	0.0187	0.0204
0.01	0.0024	0.0048	0.0072	0.0096	0.012	0.0144	0.0168	0.0192	0.0216	0.024	0.0264	0.0288
0.01	0.00308	0.00616	0.00924	0.01232	0.0154	0.01848	0.02156	0.02464	0.02772	0.0308	0.03388	0.03696
0.01	0.0053	0.0106	0.0159	0.0212	0.0265	0.0318	0.0371	0.0424	0.0477	0.053	0.0583	0.0636
0.01	0.00708	0.01416	0.02124	0.02832	0.0354	0.04248	0.04956	0.05664	0.06372	0.0708	0.07788	0.08496
0.02	0.0108	0.0216	0.0324	0.0432	0.054	0.0648	0.0756	0.0864	0.0972	0.108	0.1188	0.1296
0.02	0.022	0.044	0.066	0.088	0.11	0.132	0.154	0.176	0.198	0.202	0.242	0.264
0.03	0.018	0.036	0.054	0.072	0.09	0.108	0.126	0.144	0.162	0.18	0.198	0.216
0.03	0.016	0.032	0.048	0.064	0.08	0.096	0.112	0.128	0.144	0.16	0.176	0.192
0.03	0.015	0.03	0.045	0.06	0.075	0.09	0.105	0.12	0.135	0.15	0.165	0.18
0.03	0.013	0.026	0.039	0.052	0.065	0.078	0.091	0.104	0.117	0.13	0.143	0.156
0.03	0.012	0.024	0.036	0.048	0.06	0.072	0.084	0.096	0.108	0.12	0.132	0.144
0.03	0.011	0.022	0.033	0.044	0.055	0.066	0.077	0.088	0.099	0.11	0.121	0.132
0.03	0.008	0.016	0.024	0.032	0.04	0.048	0.056	0.064	0.072	0.08	0.088	0.096
0.04	0.005	0.01	0.015	0.02	0.025	0.03	0.035	0.04	0.045	0.05	0.055	0.06
0.04	0.002	0.004	0.006	0.008	0.01	0.012	0.014	0.016	0.018	0.02	0.022	0.024
0.04	0	0	0	0	0	0	0	0	0	0	0	0

Table 11.3 Applied velocity impact on 3D head model.

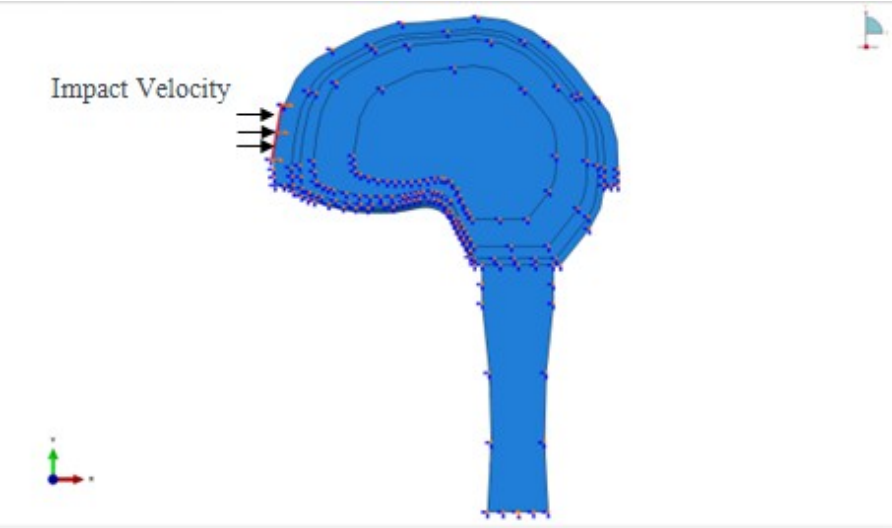

Figure 11.24 Boundary conditions applied to the frontal head of the 3D model.

11.3.2 Result blunt impact analyses

Figure 11.25 shows the strain variation of the middle of the brain for all 12 cases. This Figure reveals that as the impact speed increases, the strain in the brain also increases with a profound peak values. The maximum value of the strain corresponding to each case was determines and the maximum strain-velocity curve was plotted. Figure 11.26 shows that if the applied impact velocity to the head varies from 2.5 MPH to 27 MPH, the maximum strain increase from 2% to 20%.

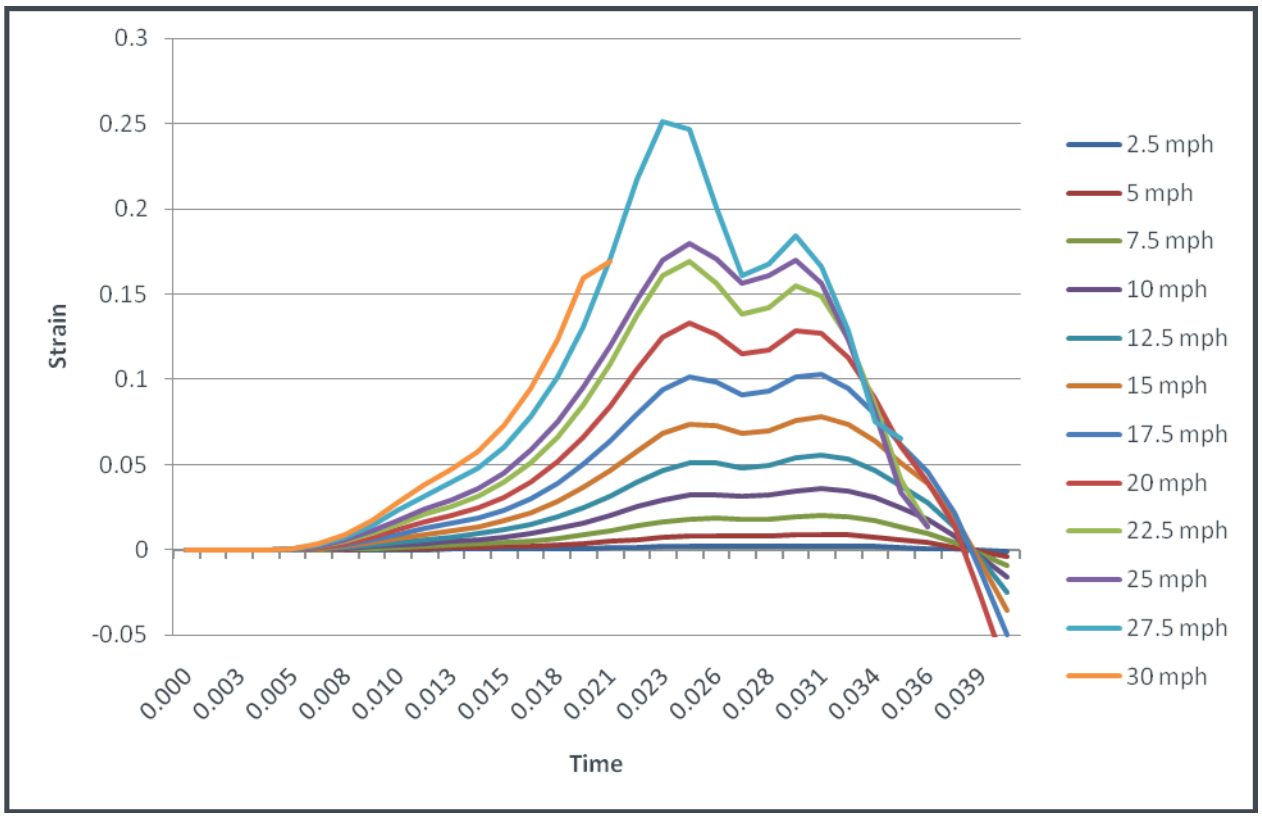

Figure 11.25 Strain in the brain corresponding to 12 different cases of velocity impact.

11.3.3 Conclusion

Animal and human experimental studies are always limited to mild angular accelerations or impacts. Validated 3D finite element models are an important tools for investigator to provide accurate result for more severe impacts when human or animal studies of these impacts are not allowed.

In this section the validated 3D head model was subjected to the wide range of velocity impacts and the relationship between the applied velocity and the strain in the brain was analyzed.

In their studies meany et al. (1995) and Bayly et al. (1977) indicated that, different types of the TBI occur if the axon of the neuron nerve in the brain stretches more that 10%-15%. That is, the myelin sheath around the axon nerve will be damaged and in that case these nerve tissues are not able to recover and heal themselves. This usually is the stage when TBI will occur in severe cases.

These analyses reveal that the velocity impact on the frontal head is proportional with the maximum strain in the brain. With the increase in velocity of the impact the likelihood TBI is increased as shown in Figure 11.26.

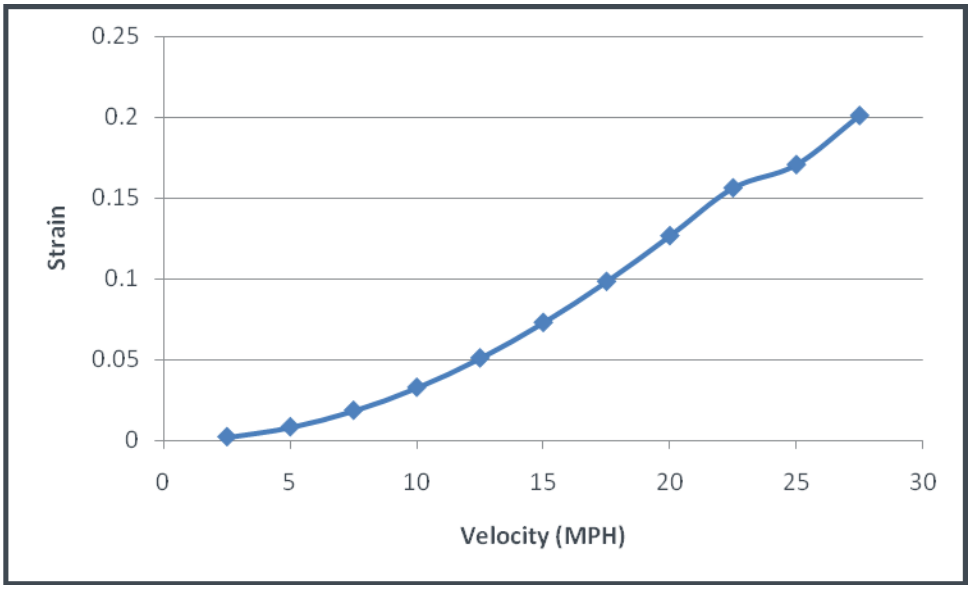

Figure 11.26 Variation of the strain in the brain as a function of impact velocity to the head.

CHAPTER 12 Discussion and Conclusion

12 DISCUSSION AND CONCLUSION

The goal of this study was to investigate the transmission of head impacts to the brain, using histology (experimental) and modeling methods of the subarachnoid space, as it relates to the strain in the brain leading to traumatic brain injury. That is, to quantify the relationship between the range of magnitude of external impacts and the strain in the brain which could cause concussion or TBI. This goal was accomplished though three aims.

12.1 Aim 1-Experimental study

The first aim of this study was to investigate the histology and architecture of the SAS and in particular, the trabeculae. This was accomplished through several experimental studies including, CT Scan machine, Histology sectioning, Two- Photon Microscopy (TPM), Scanning Electron Microscopy (SEM) and Transmission Electron Microscopy (TEM). It was concluded that the trabeculae are collagen based of Type I, Kierszenbaum 2007, Van Der Rest (1991), and their architectures are in the form of tree shaped rods, pillars or plates and they have a complex network.

In the first experimental study, reflected in chapter 5, the Micro CT- Scan machine was used. Several tissue samples from different regions of cadaver's brain were prepared. Since the human brain was already fixed in formaldehyde the arachnoid had collapsed on the pia mater and CSF was drained. Thus, several techniques were employed to separate the arachnoid from the pia mater and to recreate the subarachnoid space, which is approximately 2 to 3 mm in humans. The technique involved several steps including confining the region and injecting Microfil (Silicone Rubber Injection Compounds) from *flowtech*, *Inc.*, which solidifies quickly and keeps the two

layers separated. Once the SAS of the specimen was solidified it was taken to the SkyScan 1172 Micro-CT System, having 2μ resolution. We were unable to obtain very good results using Micro CT- Scan machine, as shown in Figure 5.5. This was due to the fact that trabeculae are collagen base and are transparent. The X-ray of the Micro CT-Scan was not completely absorbed by the tissue to create clear 2D images with good contrast. While we employed Mimic software to recreate the trabecula structure, because of the poor contrast and small size of these tissues, the 3D construction was not satisfactory. Although we tried different contrasting agent, we were unable to capture clearly the trabecula structures.

The second experimental study was accomplished through histology sectioning of the brain using fluorescent and bright light microscopy. Using the same method as the Micro CT Scan machine, samples of the cadaveric brain tissues that were solidified, were sliced using vibrotom machine and were dyed through the standard procedure for fluorescent and bright light microscopy. Note that since the tissue was already fixed in the formaldehyde, the micro fill did not survive the staining procedure and it was washed out during the preparation process. However, we were able to see the trabeculae structure and make a distinction between the arachnoid and the pia mater.

The third method was in vivo animal experimental study, using Two – Photon Microscopy (TPM). The TPM was used to obtain images of the SAS in a Sprague-Dawley rat. The animal was anesthetized with pentobarbital sodium injected subcutaneously. To get better images a quantity of fluorescein, a fluorescent dye, was also injected into the blood stream. At this point we bare the skull and small area about 2-3 mm in diameter was created on top of the

skull next to the sagittal suture. The animal was then prepared for TPM. The microscope was located on the top of the hole. Images were taken with the Ultima IV two-photon microscope (Prairie Technologies) and the Prairie View software was used to visualize them. The resolution was 512X512 pixels. The results obtained with the two-photon microscopy constituted a good start for the experimental study of the SAS. The fluorescent stain allowed us to locate the SAS with respect to the bone. The skull appeared as a dark space on the photographs, as shown in Figure 5.8, whereas the SAS was florescent. The space between these two structures, i.e. the bone and SAS, could be easily indentified. Indeed at various locations next to the skull an agglomeration of dark region were found. Given the scale bar, these structures seemed to have a diameter of between 100nm and 200nm. They always appeared in groups close to the skull. It was not easy to understand and interpret those results. It was speculated that the little dots could be either the trabeculae or they could be some parts of the skull as they seemed related to it. In order to further investigate these structures the next experiments were conducted.

To further investigate the histology and the architecture of the SAS trabeculae, the fourth and fifth in vivo experimental studies were performed using Electron Microscopy, SEM and TEM. These experiments were performed using Sprague-Dawley rats weighting 250-300g and 2 to 3 months old. The rats were anesthetized with pentobarbital sodium given subcutaneously (80-100 mg/kg body weight for initial anesthetization) and kept warm on a heating pad. Then, the right atrium was incised and with a sharp needle fixative solution (glutaraldehyde) was injected to the blood stream. After a few minutes through the blood circulation, the blood vessels of the SAS were solidified. The animal was then sacrificed and samples of the brain tissue were prepared for the Scanning and Transmission Electron microscopy. The SEM and TEM were

much more successful and confirmed the initial discoveries of TPM. Collagen fibrils could be observed on the SEM images and small dark dots appeared on the TEM images. A new step was then achieved: we were able to better understand and identify these structures. The architecture and organization of the SAS were recognized and this was compared with the results of the study of Killer et al. (2003).

With the results obtained from SEM and TEM, a cartoon sketch of the SAS in the rat was drawn as shown in Figure 12.1.

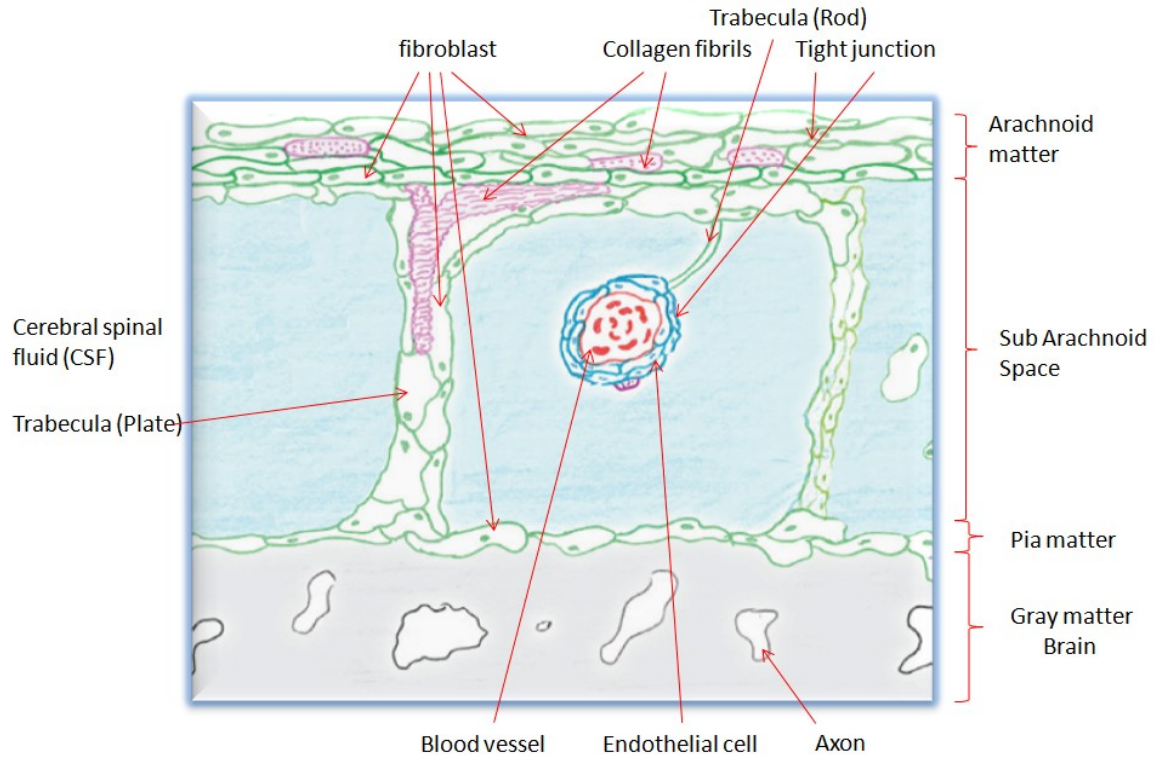

Figure 12.1 Cartoon sketch of the SAS in the rat's brain.

The experimental study revealed that the arachnoid mater was composed of about ten layers of fibroblasts cells joined together by tight junctions. Within the cells of the arachnoid,

some collagen fibrils bundles could be observed. The fibrils were produced by the fibroblasts and were providing a structural support to the arachnoid layer in addition to the support provided by the fibroblasts. The arachnoid layer appeared to be permeable on the TEM results. Some fluid was observed in the spaces between the fibroblasts. The layer at the junction with the SAS was spreading at some locations and was forming a descending trabecula from arachnoid to the pia mater in the tree-shaped architecture. This trabecula was mainly consisted of bundles of collagen fibrils wrapped together by fibroblast cells. The trabecula took the form of spreading tree-shaped, plates and also simple rods. These rods were mainly connected the blood vessels to the arachnoid/pia mater. The trabeculae were commonly connecting the external layer of fibroblasts of the blood vessels to the arachnoid or pia mater.

In addition to the rods, plates and tree-shaped architecture in some region complex networks of more randomly oriented trabeculae were also found in the SAS. These networks architecture were mainly located in the vicinity of the blood vessels and were very complex and inhomogeneous. The network of the trabeculae was actually composed of fibroblasts, collagen fibrils and extracellular matrix. Some holes/cavity could be observed in the networks to facilitate the flow of cerebrospinal fluid around the brain. Indeed the pia mater appeared to be much thinner than the arachnoid layer as it was composed of only one layer of fibroblasts. The results of this experimental study were compared and validated with a study by Killer et al. (2003). While these results are for rat it is believed that human brain has the same architecture.

12.2 Aim2-Finite element analyses

The second aim of this study as explained in chapter 7 and 8 was to create and analyze 2D and 3D local models of SAS. As the first step the mechanical property of the SAS was investigated. This step was performed through several modeling stages. The 2D and 3D local models of the SAS were created and the effect of the SAS material properties on transferring the external load to the brain was investigated. From the result of this chapter it was concluded that the load or the impact is directly transmitted to the brain if the material property of the trabecula reported by Zhang et al. (2002) , $E=21.5x10^6$ Pa, is used. That is, if the young modules reported by Zhang et al. (2002) is used for SAS material property, this region is unable to buckle under the impact load and causes directly the deformation of the brain. However, based on our histology and the experimental work the soft tissue of the trabeculae would buckle when the brain approaches the skull, thereby reducing the transmitted force to the brain. In the second set of FE analyses, the transverse, lateral and sagittal model of the human head/brain using MRI images of an adult female patient were created. Wide ranges of the mechanical properties of the trabeculae were employed. The transductions of blunt impact loads from the skull to the brain were investigated. Then the mechanical properties of the SAS trabeculae were determined to be E=1150 Pa based on the validation of the models with the experimental results of Sabet et al. (2009). The results indicated that when we use softer material properties for the trabeculae the meningeal layers absorb and damp the impact load. It is also concluded that the material properties of a trabecula can be simulated by only a tension element since the trabecula buckles with minimal compressive load.

In chapter 9, the mechanics of CSF flow through the SAS was investigated. This step was accomplished through analytical and numerical studies of a unit cell model, where a single trabecula model was created. We propose a structural model for the analysis of mechanical transduction of CSF's hydrodynamic forces through the SAS. We considered a transverse and/or lateral slice of the head where the brain is encased by the SAS. For simplicity of the analytical model we assumed that the SAS is a uniform strip of a continuum around the brain. When the head is subjected to an impact the deformation of the brain at the coup location causes the CSF to flow around the brain and stagnates at the countercoup location. In addition, our in-vivo and in-vitro studies revealed that abundant trabeculae exist in the SAS region, which create a hydrodynamic resistance force against the CSF flow similar to Darcy's permeability model. Imagine that at the CSF's stagnation point (countercoup) the SAS is cut, then the strip band around the brain is straightened out as a long channel. Therefore, the mechanics of the CSF flow through the SAS can be simulated as the flow of the CSF through a deformable channel (a long strip) when the top plane of the channel is subjected to an impact or deformation. It is assumed that the flow of the fluid through the deformable channel is governed by Darcy's permeability law, with the permeability of 3.125×10^{-10} m^2. It was determined that Darcy's model is a realistic representation of the SAS region and can explain the hydrodynamic forces of CSF through the SAS region. Also the structural model of unit cell was created to study the mechanotransduction of CSF's hydrodynamic forces through the SAS. Next, a single trabecula model was also created in order to study the buckling and recoiling phenomena of the tissue due to the velocity flow of CSF. A 2D FE model and an analytical model of a single trabecula were created and the velocity boundary conditions were applied to both the analytical and FE models. Then Abaqus software

was employed and the displacement history of the trabecula was determined. The results as shown in Figure 9.9, indicates that it takes approximately 19-20 milliseconds for the fiber to come back to its original shape in the SAS region. The results of this study confirm the validity of the proposed structural unit cell model.

As indicated in the result of our experimental studies, approximately 70% of the trabeculae are tree-shaped architecture, where the branches were attached to the arachnoid and the stems were connected to pia mater. In chapter 10, in respond to the question of the orientation of the tree-shaped and the inverted tree-shaped trabecular architcture, the mechanotransduction of the external load to the brain based on these orientations and architecture were investigated. Two basic local models i.e. one with a tree-shaped and the other with an inverted tree-shaped of a single trabecula connecting the pia mater to the arachnoid were created and analyzed. The results of the analysis of the models revealed that the strain, displacement and stress fields in the brain for the tree-shaped trabecular architecture are less than that of the inverted one. It also revealed that the tree-shaped orientation of a trabecular architecture, where the branches are attached to the arachnoid mater, provides more protection for the brain tissue when the head in subjected to a impact. One reason that the tree-shaped trabecula applies less strain in the brain is that the CSF is trapped in the branches of the inverted tree-shaped. This would increase the shear flow and thereby the pressure on the brain. Where as in the tree-shaped trabecula the stem buckles immediately and there is no additional pressure concentration in the brain. In addition in the tree-shaped trabecula, when the brain start to move toward the skull, the CSF can freely flow over the surface of the brain and applies a more

uniform and reduced pressure on the brain. The results of this study will lead to accurately modeling of the SAS and thereby determining the strain in the brain.

12.3 Aim 3- 3D Head Model

To understand our previous results in more global sense, in chapter 11, a three-dimensional (3D) model of the head-neck using magnetic resonance imaging (MRI) and Abaqus/CAE Sketch modules was created. The 3D head could be used for computer simulation of TBI. The 3D head model was validated against the experimental study of Feng et al. (2010). The validated 3D head model is a convenient tool to study the effect of the different types of the impacts to the brain. The nodal solution of the strain in the brain was plotted in the material location "a" and "b" and the relative displacement between the skull and the brain was compared with the experimental study of Feng et.al (2010).

In the experimental study of Feng et al. (2010) a human subject's head is dropped on its own gravity approximately 2 cm and the forehead comes in contact with a rubber band, that is used as a stopper. Displacement data were then obtained from this mild frontal head angular acceleration of the head and the impact with the rubber band. Tagged magnetic resonance imaging method was used to measure in vivo relative displacement between the brain and the skull of three adult male human subjects. Their experimental study provides an important set of displacement measurements in the human brain during the mild frontal skull impact. The result of Feng et.al (2010) shows that, at the four specific locations of the brain, the rotation and the displacement of these points relative to the skull is approximately 1-3 mm.

The experimental result of Feng et al. (2010) shown in Figure 11.14 and Figure 11.15 indicates two picks during the 168 ms period of the study. The first pick which occurs at about 40-60 ms is due to the time when the head has its maximum angular acceleration. This is when the forehead of the subject hits the rubber band, see Figure 11.14 and Figure 11.15. Once the elastic rubber band is stretched, it creates a rebound force pushing the head upward. Then the head of the subject separates from the rubber band fallowed by dropping down on its own gravity. This is the moment when the second pick occurs. Note that in our 3D head model, we did not consider the rebound force of the rubber band as it refers to the second pick. It is important to indicate that the time lag after the first pick, between experiment and our FEM results is due to the secondary force of the rubber that is not considered in our FE model.

The result of 3D head model validation indicates that the proposed young modulus's of 1000 Pa for the SAS is a reliable and appropriate value. The proposed value of E, also suggest that, the SAS material is soft and absorbs the brain's movement. This confirms our hypothesis about the functionality of the SAS which act as a damper and a shock absorber of the brain.

In chapter 8, 2D models of different material type for SAS, i.e. soft solid, fluid, porous material and Darcy permeability were considered. To further investigate these result in chapter 11 three different materials for SAS were proposed. The material properties of each material type i.e. soft solid, fluid and porous material were analyzed and compared with study of Feng et al. (2010). The relative displacement between the skull and the brain for each material type was compared with the experimental study of Feng et al. (2010). The displacements for all three SAS material models were in good agreement with the experiment as shown in Figure 11.22. That is,

if one decides to use soft solid, fluid or porous materials to model the SAS, in local or global FE analyses, the properties found in this study are appropriate for modeling investigations.

Finally in last section of chapter 11 the 3D head model was subjected to the wide range of velocity impacts and the relationship between the applied velocities and the strain in the brain was analyzed. In their studies Meany et al. (1995) and Bayly et al. (1977) indicated that different types of the TBI occur if the axon of the neuron nerve in the brain stretches more that 10%-15%. That is, the myelin sheath around the axon nerve will be damaged and in that case these nerve tissues are not capable to recover and heal themselves. This usually is the stage when TBI will occur in severe cases.

These analyses reveal that the velocity impact on the frontal head is proportional with the maximum strain in the brain and thereby different type of TBI. It has been conclude that, 12%-17% of the stain in the brain which is corresponding to the velocity impacts of 17-27 MPH, is less than the 20% threshold of brain injury (TBI) addressed in the literature, Meany et al. (1995) and Bayly et al. (2003). It is concluded that if the head is subjected to an impact velocity of less than 17 MPH the strain in the brain is below the threshold of TBI.

CHAPTER 13 Future Work

13 FUTURE WORK

This thesis reveals that the material properties of the meningeal layer is a significant factor in determining the strain in the brain and therefore understanding different types of the brain/ head injuries. Therefore, the future investigation of this study involves using Darcy's permeability as a material property for the SAS in the 3D head model, and applies various velocities impact. The histology and the architectures of the SAS, in particular the trabeculae, also need to be improved. These studies may be accomplished through the following steps:

1) Samples from different species need to be investigated to compare the structure and architecture of the SAS among unlike species, i.e human, bovine and rat (Figure 13.1 to Figure 13.3).
2) More investigation is needed for modeling of the SAS as a Darcy's permeability.
3) The velocity impact can be applied on the 3D head model using porous material and Darcy's permeability for SAS.

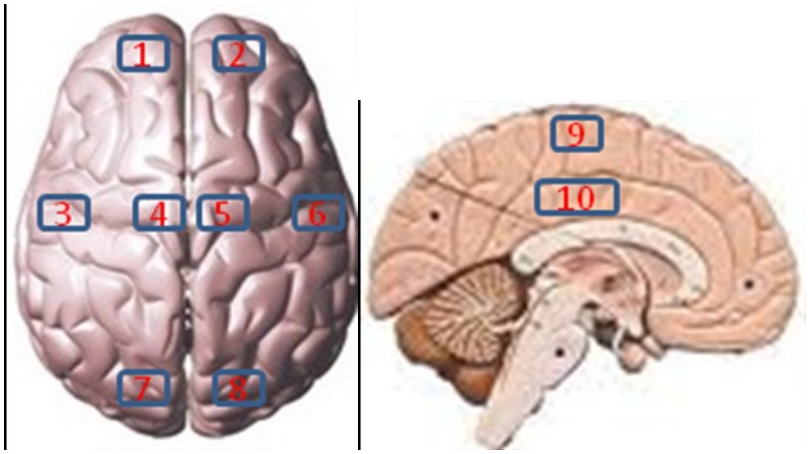

Figure 13.1 Cadaver sample from different section of the human brain.

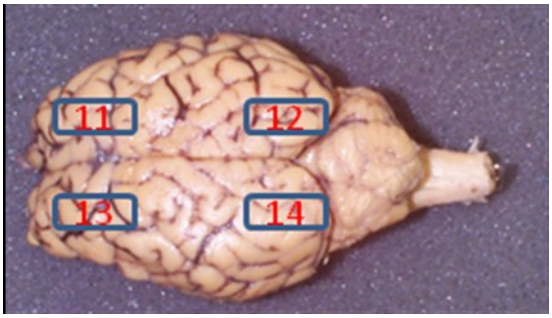

Figure 13.2 Cadaver sample from different section of the bovine brain.

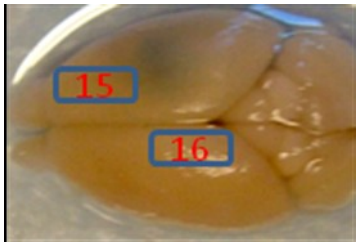

Figure 13.3 Cadaver sample from different section of the rat brain.

APPENDIX 1

HEMATOXYLIN & EOSIN STAINING PROTOCOL

Prior to staining, slides must be baked for at least two hours at a minimum temperature of 70^{o} C to inhibit detachment of sections during the staining procedure.

STAINING PROCEDURE

1. Stain in Weigert's Hematoxylin, working solution, for 6 minutes.

2. Drain slides.

3. Differentiate in 70% Acid-Ethanol, pH 2.5, two changes, three quick dips each.

4. Differentiate in 70% Acid-DI, pH 2.5, two changes, three quick dips each.

5. Wash in running tap water for 15 minutes. Drain excess water from slides.

6. Stain in working Eosin-Phloxine solution for 2 minutes.

7. Drain slides.

8. Differentiate and dehydrate in 95% ethanol, two changes, 30 seconds each.

9. Completely dehydrate in 100% ethanol, three changes, three quick dips each.

10. Clear in Histoclear, two changes, one minute each.

11. Fresh Histoclear and coverslip with mounting medium.

RESULTS

Nuclei – deep blue-violet

Chromatin – blue-black

Nucleoli – varying shades of orange-pink to red-violet, depending on cell type.

Cytoplasm – varying shades of pink and orange

Collagen – pale pink

Muscle – deep pink

Source: FWRI HISTOLOGY

APPENDIX 2

SEM sample preparation protocol

Rinse the brain obtained from the perfusion-fixation under the hood in distilled water. Rinse about 5 times, let the sample in distilled water about 1-2 minutes each time. Take care to always keep the sample wet in a minimum amount of solutions.

Cut the sample into small sections or pieces with a razor blade. To get sharp sections use the razor only once on each edge and cut in one top to bottom movement, avoid saw-like movements. Usually the rat brain is cut in coronal sections, but sagittal sections also work. For the safety, the sections should be cut under the hood. The sections are placed in a small basket. Place the basket in a 100ml tube and dehydrate the sections. In another tube, prepare the alcohol solutions by first adding the required amount of alcohol and then filling the tube up to 100ml with water. The samples are dehydrated in graded series of ethanol: 25%, 50%, 70%, 80%, 90%, 100%, 3-5 minutes each time. The water-free sections are then dried following the critical point drying technique. The sections are rinsed 7 times in liquid CO2, each time for 3-5 minutes. Mount the sections on an SEM pin using double coated carbon tape. Store the samples at 60 °C for 2 hours or longer. Coat the samples with gold/palladium right before observing them in the SEM.

TEM sample preparation protocol

Prepare the primary fixer by mixing 5 ml of 0.2 M sodium cacodylate buffer pH 7.2 with 3 ml of 10% glutaraldehyde and 2 ml of 16% paraformaldehyde. In a separate vial, prepare the secondary fixer by mixing 2 ml of 4% osmium tetroxide with 2 ml of sodium cacodylate buffer, pH 7.2. After the samples are fixed for 2 hours minimum in glutaraldehyde 5%, we take them under the hood and rinse them with sodium cacodylate buffer, 2-3 times for about 5 minutes. For the TEM the samples need to be 1mm square big. Therefore we had to choose which region of the brain would be cut and in which direction we would cut. We chose to first extract a stripe from the supersagittal sinus by making a few milimiters apart on each side of the sinus. Then this strip was shortened following a transverse plane and the 1-by-1mm strap was shopped into small

squares. The pieces were obtained by using a razor blade and cutting only once with each edge of the blade.

As we are dealing with brain tissues that are really soft, it's better if the fixative penetrates the tissue well so that when decrease the damages when performing the next steps. To help the fixative to infiltrate the tissue we used acrolein, a chemical used in tear gas. We immersed the TEM samples in this chemical for 1 hour on ice (this is the minimal required time). This chemical is EXTREMELY dangerous so it's absolutely required to work under the hood. After that step the samples have turned black. Then we took off the tear gas and added the secondary fixer, the 2% osmium tetroxide and kept the samples on ice. This step was still performed under the hood. After 30 minutes we removed the osmium tetroxide by sucking it up, and we rinsed the samples 3 times with distilled water under the hood. Each time the samples stay for about 5 minutes in distilled water. Once the samples are washed one doesn't need to work under the hood anymore. After that step we followed the protocol provided on the CCNY EM website. Dehydrate the tissue in a graded series of acetone or ethanol, 5 min each time (20%, 30%, 40%, 50%, 60%, 70%, 80%, 90%, 100%,100%). You may work outside of the hood for this step. If you used acetone proceed to the next step. If you used alcohol, rinse your tissue in propylene oxide two times, 5 minutes each time, use the hood and gloves for this step, also use glass pipettes and vials --propylene oxide will dissolve most plastics.

In a 50 ml Corning tube, prepare 100% resin: 20 ml of Embed 812, 10 ml of DDSA, and 12 ml of NMA. Mix vigorously for 3-5 min and let it sit for 10 min. Prepare 30% resin by mixing 3 ml of freshly prepared resin and 7 ml of solvent (acentone or propylene oxide). Similarly prepare 50%, 70%, and 90% resin. If your cells are in acetone, your resin dilutions should be prepared in acetone, similarly, if your cells are in propylene oxide, your resin dilutions should be prepared in propylene oxide.

Infiltrate the cells with increasing concentration of resin (30%, 50%, 70%, 90%, 100%, 100%), 1-3 hr each time and keep on a blood mixer or a rotor shaker. Prepare a fresh batch of resin as described in step 8, mix well, let the air bubbles out by placing under vacuum (25 inches of mercury for 20 min), then add 70 ul of DMP-30 and mix throughly without introducing bubbles.

Transfer each pellet to the bottom of a Beem capsule. Fill the capsule ¾ of the way with freshly prepared resin with DMP-30. Place the Beem capsules under a vacuum (25 inches of mercury for 30-60 min) to remove bubbles. Place samples in a 60oC oven for 3 days. Remove the plastic mold, and place back in the oven for one more day. Remove samples from the oven and keep in a dry place.

Remarks:

Always keep the samples wet in a minimal amount of solution.

Think ahead, prepare the material you need or open the bottles you need before your hands are full with samples, pipettes, etc.

Think about cleanliness, don't touch any bottle with the tip of the pipette. If so, discard it.

Change gloves as often as you think it is needed.

APPENDIX 3

Gomori's trichrome staining protocol

PRINCIPLE:

Gomori's one-step trichrome is a staining procedure that combines the plasma stain (chromotrope 2R) and connective fiber stain (fast green FCF) in a phosphotungstic acid solution to which glacial acetic acid has been added.

SPECIMEN REQUIRED:

Snap frozen human striated muscle. (Use the isopentane freezing method previously described.)

METHOD:

Fixation: None, use snap frozen tissue.

Technique: Cut 10 - 16 micron (12 μm) sections in cryostat from snap frozen biopsy. Attach one or more sections to a No.1½, 22 mm square coverslip.

Equipment:

Ceramic staining rack - Thomas Scientific #8542-E40

Columbia staining dish - Thomas Scientific #8542-C12

Columbia staining dish(jar) - Thomas Scientific #8542-E30

Forceps

Latex gloves

REAGENTS:

1) Glacial Acetic Acid -Fisher A507-500, CORROSIVE store at room temperature

2) Chromotrope 2R - Sigma C3143, IRRITANT, store at room temperature

3) Deionized water

4) Fast Green FCF - certified, Sigma F7258, GLOVES AND MASK REQUIRED, store at room temperature

5) Harris Hematoxylin Stain, acidified, - Lerner Laboratories * #1931382, store at room

6) Permount - Fisher SP15-100, FLAMMABLE HEALTH HAZARD

7) Phosphotungstic acid, free acid, - Sigma P4006, CORROSIVE, store at room temperature

8) Reagent alcohol, ACS - histochemical Fisher A962-4, or HPLC A995 FLAMMABLE, TOXIC, TERATOGENIC, store at room temperature in flammable cabinet

9) Xylenes - Fisher #HC700-1GAL, FLAMMABLE, store room temperature in flammable cabinet)

SOLUTIONS:

I. Gomori's trichrome stain

Chromotrope 2R 0.6 g

Fast green FCF 0.3 g

Phosphotungstic acid 0.6 g

Deionized water 100 ml

Acetic acid, glacial 1.0 ml

Adjust pH of the above mixture to 3.4 using 1 N NaOH

Store at room temperature, prepare weekly

2. Acetic acid, ~0.2 %

Deionized water 1000 ml

Acetic acid, glacial 2 ml

3. Alcohol 50 %

Reagent alcohol ~50 ml

Deionized water ~50 ml

4. Alcohol 70 %

Reagent alcohol ~70 ml

Deionized water ~30 ml

5. Alcohol 80 %

Reagent alcohol ~80ml

Deionized water ~20 ml

6. Alcohol 95 %

Reagent alcohol ~95 ml

Deionized water ~ 5 ml

STAINING PROCEDURE:

Place the cover slip with section in a ceramic staining rack (Thomas Scientific #8542-E40).

Immerse sections in Harris Hematoxylin for 5 minutes.

Wash with tap water until the water is clear.

Immerse sections in Gomori trichrome stain for 10 minutes.

Differentiate using 0.2% acetic acid. A few dips should be sufficient.

14 REFERENCES

Aimedieu P, Grebe, R, Idy-Peretti I. 2001. Study of brain white matter anisotropy. In: 23rd Annual EMBS International Conference

Anzelius A (1943). The Effect of an Impact on a Spherical Liquid Mass. Acta Pathol. Microbiol. Scand. (Suppl.) 48:153-159.

Al-Bsharat AS, Hardy WN, Yang KH, Khalil TB, Tashman S, King AI (1999). Brain/Skull Relative Displacement Magnitude Due to Blunt Head Impact: New Experimental Data and Model. Stapp Car Crash Conference, 43:99SC22.

Al-Bsharat AS, Zhou C, Yang KH, Khalil TB, King AI (1999). Intracranial Pressure In The Human Head Due To Frontal Impact Based On A Finite Element Model. Proc. 1999 Bioengineering Conference, BED ASME, 42:113-114.

Alcolado JC, Moore IE, Weller RO (1986). Calcification In The Human Choroid Plexus, Meningiomas And Pineal Gland. Neuropathology and Applied Neurobiology, 12:235-250.

Arbogast KB and Margulies SS (1997). Regional Differences in Mechanical Properties of the Porcine Central Nervous System. Stapp Car Crash Conference, 41:973336.

Bandak, F.A and Eppinger, R.H. (1995) A three dimensional finite element analysis of the human brain under combined rotational and translational acceleration. Proc. 38th Stapp car crash conference.

Banadak, F.A., Zhang, A.X., Tannous, R.E., Dimasi, F., Masiello, P., Eppinger, R., (2001) Simon; a simulated injury monitor; application to head injury assessment. ESV 17th International Technical Conference on Enhanced Safty of Vehicles, NHTSA, Washington, DC.

Bayly P.V. Cohen T.S. Leister E.P. Ajo D. Leuthardt E. and Genin G.M. (2005), Deformation of the human brain induced by Mild acceleration J Neurotrauma. 22(8): 845–856.

Bilston, L.E., Liu, Z., Phan- Thien, N.(1998) Linear viscoelastic properties of bovine brain 263tissue in shear. Biorheology 34(6), 377-385

Broglio, S. P., Schnebel, B., Sosnoff, J. J., Shin, S., Fend, X., He, X., and Zimmerman, J., 2010, "Biomechanical Properties of Concussions in High School Football," Med Sci Sports Exerc, 42(11),

CDC 2011, www.cdc.gov

Darvish, K. J.R. Crandall (2001), J of Medical Engineering & Physics, 23:633–645.

Darvish, K., and Stone, J. (2004) Relationship of Decreased Brain Tissue Viscoelasticity to Traumatic Axonal Injury Following Traumatic Brain Injury, Proceedings for the 7th International Neurotrama Synposium, Adelaide, Australia.

Darvish, K., Shafieian, M., Laksari, K., Barabadi, B., Parenti, C., (2008) Experimental and Computational Analysis of Brain Deformations in Linear Head Impact, Proceeding of ASME International Mechanical Engineering Congress and Exposition.

Darvish, K. (2009) Comparison between the Dynamic Moduli of Fully Non-Linear and Quasilinear Viscoelastic Materials, International Journal of Non-Linear Mechanics, In Press

De Jager and Sadegh A.(1994) A Three-dimensional Head-Neck Model: Validation for Frontal and Lateral Impacts. Society of Automotive Engineers. SAE paper No. 942211.

Drew, W. E. (2004). The contrecoup-coup phenomenon: a new understanding of the mechanism of closed head injury. Neurocritical Care, 1, 385-390.

Engin AE and Wang H (1970). A mathematical model to determine viscoelastic behavior of in vivo primate. Journal of Biomechanics, 3:283-296.

Elkin, B. S., Azeloglu, E. U., Costa, K. D., and Morrison III, B. (2007) Mechanical heterogeneity of the rat hippocampus measured by AFM indentation, J Neurotrauma. 2007 May;24(5):812-22.

Estes, M.S and McElaney, J.H.(1970) Response of brain tissue of compressive loading. ASME, No. 70- BHF-13

Fallenstin, G.T., Hulce, V.D., and Melvin, J.W. (1969a) Dynamic matrial properties of human brain tissue. J. Biomachanics 2, 217-226

Faul M, Xu L, Wald MM, Coronado VG. (2010) Traumatic brain injury in the United States: emergency department visits, hospitalizations, and deaths. Atlanta (GA): Centers for Disease Control and Prevention, National Center for Injury Prevention and Control

Feng Y, Abney TM, Okamoto RJ, Pless RB, Genin GM, Bayly PV. (2010) Relative brain displacement and deformation during constrained mild frontal head impact. J R Soc Interface. 2010 Dec 6;7(53):1677-88.

Finnie and S. Sangani and A. Acrivos, (2004) Slow flow past periodic arrays of cylinders with application to heat transfer. International Journal of Multiphase Flow8(3): 193-206

Frederickson G.R. (1991) The Subdural Space Interpreted as a cellular Layer of Meninges, The Anatomical Record, 230:38-51

Hardy WN, Foster CD, King AI, Tashman S (1997). INVESTIGATION OF BRAIN INJURY KINEMATICS: INTRODUCTION OF A NEW TECHNIQUE. Crashworthiness, Occupant Pretection, BED 38 ASME, 225:241-254.

Hardy WN, Foster CD, Mason MJ, Yang KH, King AI, Tashman S (2001). Investigation of Head Injury Mechnisms Using Neutral Density Technology and High-Speed Biplaner X-Ray. *Stapp Car Crash Conference,* 45:2001-22-0016.

Hardy, W. N., Mason, M. J., Foster, C. D., Shah, C. S., Kopacz, J. M., Yang, K. H., King, A. I., Bishop, J., Bey, M., Anderst, W., and Tashman, S., 2007, "A Study of the Response of the Human Cadaver Head to Impact," Stapp Car Crash J, 51, pp. 17-80.

Hong Zou, James P. Schmiedeler, Warren N. Hardy (2006) Separating brain motion into rigid body displacement and deformation under low-severity impacts. Journal of Biomechanics Volume 40, Issue 6 , Pages 1183-1191, 2007

Holbourn AHS (1945). The Mechanics of Brain Injury. *Brithish Medical Bulletin,* 3:147-149.

Ibrahim, Nicole G, (2010)In Situ Deformations in the Immature Brain During Rapid Rotations, J. Biomech. Eng. 132,

Galford, J.E., and McElhaney, J.H. (1969) A Viscoelastic Study of Scalp, Brain, And Dura. J. Biomechanics 3, 211-221.

Greenwald, R. M., Gwin, J. T., Chu, J. J., and Crisco, J. J., 2008, Head Impact Severity Measures for Evaluating Mild Traumatic Brain Injury Risk Exposure, Neurosurgery, 62(4), pp. 789-98; discussion798.

Guo P, Weinstein A. M, and Weinbaum S. (2000) A hydrodynamic mechanosensory hypothesis for brush border microvilli. Am J Phy. Renal Physiol 279(4):F698-712.

Gupta S, Soellinger M, Boesiger P, Poulikakos D, Kurtcuoglu V. (2009) Three-dimensional computational modeling of subject-specific cerebrospinal fluid flow in the subarachnoid space. J Biomech Eng. 131(2):021010.

Guskiewicz, K. M., Mihalik, J. P., Shankar, V., Marshall, S. W.,Crowell, D. H., Oliaro, S. M., Ciocca, M. F., and Hooker, D. N., 2007, Measurement of Head Impacts in Collegiate Football Players: Relationship between Head Impact Biomechanics and Acute Clinical Outcome after Concussion, Neurosurgery, 61(6), pp. 1244-53.

Kierszenbaum L. Abraham (2007), *Histology and Cell Biology an Introduction to Pathology*, Second edition, ISBN 0-323-04527-8

Killer HE, Laeng H R, Flammer J, Groscurth P. (2003) Architecture of arachnoid trabeculae, pillars, and septa in the subarachnoid space of the human optic nerve, Br J Ophthalmol; 87:777–81.

Killer H. E, Jaggi GP, Flammer J, Miller NR, Huber AR. (2006). The optic nerve: a new window into cerebrospinal fluid composition. 129(Pt 4):1027-30.

Kleiven S and Hardy WN (2002). Correlation of an FE Model of the Human Head with Local Brain Motion-Consequences for Injury Protect. *Stapp,* 46:2002-22-0007.

Kleiven, S. (2007) Predictors for Traumatic Brain Injury Evaluated through Accident Reconstruction. Stapp Car Crash Journal 21: 81-114

Koeneman, J.B. (1966) Viscoelastic properties of brain tissue. Case institute of thechnology

Kozeny, J (1927) Ueber kapillare leitung des wassers im boden, Sitzungsberichte der Akademie der Wissenschaften in Wien, (136): 271-306.

Levchakov, A., Linder-Ganz, E., Raghupathi, R., Margulies, S.S., and Gefen, A. (2006) Computational studies of strain exposures in neonate and mature rat brains during closed head impact. J. Neurotrauma 23(10):1570-1580

Meaney David F., Douglas H.Smith, David I.Shreiber, Allisson C.Bain, Reid T. Miller, Doug T. Ross, and Thomas A. Gennarelli (1995). biomechanics analisis of exprimental diffuse axonal injury. J neurotrauma, 12: 689-695

Mehdizadeh. S, Mehdi Khoshgoftar, Siamak Najarian, Farhad Farmanzad and Seyyed Amir Hooshiar Ahmadi (2008). Comparison between Brain Tissue Gray and White Matters in Tension including necking phenomenon. American Journal of Applied Sciences, 5(12): 1701-1706

Miller K and Chinzei K (1997). CONSTITUTIVE MODELING OF BRAIN TISSUE: EXPERIMENT AND THEORY. Journal of Biomechanics, 30(11,12):1115-1121.

Miller RT, Margulies SS, Leoni M, Nonaka M, Chen X, Smith DH, Meaney DF (1998). Finite Element Modeling Approaches for Predicting Injury in an Experimental Model of Severe Diffuse Axonal Injury. Stapp Car Crash Conference, 43:983154.

Miller K (1999). Constitutive model of brain tissue suitable for finite element analysis of surgical procedures. Journal of Biomechanics, 32:531-537.

Miller K, Chinzei K, Orssengo G, Bednarz P (2000). Mechanical properties of brain tissue in-vivo: experiment and computer simulation. Journal of Biomechanics, 33:1369-1376

Miller K and Chinzei K (2002). Mechanical properties of brain tissue in tension. Journal of Biomechanics, 35:483-490.

Moss W. C, King M. J, Blackman E. G (2009). Skull Flexure from Blast Waves: A Mechanism for Brain Injury with Implications for Helmet Design, Physical Review Letters

Nahum AM, Smith R (1976). An experimental model for closed head impact injury. Stapp Car Crash Conference, 20:760825.

Nahum AM, Smith R, Ward CC (1977). Intracranial Pressure Dynamics During Head Impact. Stapp Car Crash Conference, 21:770922.

Noback C.. Strominger N. L, Demarest Robert J., David A. Ruggiero (2005). The Human Nervous System. Humana Press. p. 93.ISBN 978-1588290403

Nicolle, S., Lounis, M., Willinger, R. (2004) Shear properties of brain tissue over a frequency range relevant for automotive impact situations: New experimental results. 48th Stapp Car Crash Journal: 239-258.

Ommaya AK, Yarnell P, Hirsch AE, Harris EH (1967). Scaling of Experimental Data on Cerebral Concussion in Sub-Human Primates to Concussion Threshold for Man. Stapp Car Crash Conference, 11:670906.

Ommaya AK, Grubb RL, Naumann RA (1971). Coup and contre-coup injury: observations on the mechanics of visible brain injuries in the rhesus monkey. Journal of Neurosurgery, 35:503-516.

Ommaya AK, Gennarelli TA (1974). Cerebral concussion and traumatic unconsciousness: correlation of experimental and clinical observation on blunt injuries. *Brain*, 97:633-654.

Ono K, Kikuchi A, Nakamura M, Kobayashi H, Nakamura N (1980). Human Head Tolerance to Sagittal Impact Reliable Estimation Deduced from Experimental Head Injury Using Subhuman Primates and Human Cadaver Skulls. Stapp Car Crash Conference, 24:801303.

Prange M. and Margulies S., (2002) Regional, directional and age-dependent properties of brain undergoing large deformation, Journal of Biomechanical Engineering **124,** pp. 244–253

Rao V, Lyketsos C. Neuropsychiatric Sequelae of Traumatic Brain Injury. Psychosomatics 41 (2): 95– 103, 2000

Rowson S, Duma SM. (2011) Development of the STAR Evaluation System for Football Helmets: Integrating Player Head Impact Exposure and Risk of Concussion. Ann Biomed Eng. 39(8):2130-40

Ruan JS, Khalil TB, King AI (1993). Finite Element Modeling of Direct Head Impact. *Stapp Car Crash Conference*, 37:933114.

Schachenmayr. W and R. L. Friede (1978) The origin ofsubdural neomembranes. II. Fine structural of neomembranes. Am J Pathol. 92(1): 69–84

Sabet, A., Bayly, P.V.T.S. Cohen, E.P. Leister, D. Ajo, E. Leuthardt, and G.M. Genin (2005) Deformation of the human brain induced by mild acceleration, J Neurotrauma, 22(8): 845–856

Saladin, Kenneth (2007). *Anatomy and Physiology: The Unity of Form and Function*. McGraw Hill. p. 520. ISBN 978-0-07-287506-5.

Saboori, P and Sadegh, A., (2009). Effect of Mechanical Properties of SAS Trabeculae in transferring Loads to the Brain. Proceedings of the International Mech. Engr. Congress and Exposition, (IMECE), BED/ASME, Lake Buena Vista Florida

Saboori, P. and Sadegh, A.,(2010a). Trabeculae Histology and Architecture for Modeling of Traumatic Brain Injuries. Junior Scientific Conference (JSC), Vienna, Austria

Saboori, P., Germanier, C. and Sadegh, A., (2010b). Mechanics of CSF flow through trabecular architecture in the Brain" The 26th Southern Biomedical engineering Conference (SBEC), College Park, Maryland

Saboori, P. and Sadegh, A.,(2010c). Histology and Trabecular architecture of the brain for modeling of Subarachnoid Space. Summer Bioengineering Conference (SBC2010-19379), Naples, Florida

Saboori, P. and Sadegh, A., (2010d). Modeling of Subarachnoid Space and Trabeculae Architecture as it Relates to TBI. 16th US National Congress of Theoretical and Applied Mechanics (USNCTAM2010-887), State College Pennsylvania

Saboori, P. and Sadegh, A., (2010e). The effect of SAS materials and modeling in transferring impact loads to the brain. Proceedings of the International Mech. Engr. Congress and Exposition, (IMECE), Vancouver, British Colombia

Saboori, P. Sadegh A. (2011a). Architecture and Histology of The Sub Arachnoid Space Trabeculae in The Brain .BMES 2011.2011 Hartford, CT

Saboori, P. Sadegh A. (2011b). Effect Of Trabecular Architecture On Transferring Load/Impact To The Brain: A Local Model Of Single Trabecula. SBC 2011, Farmington, Pennsylvania, USA

Saboori, P. Sadegh A. (2011c). Mechanotransduction of External Load to the Brain: The Effect of Trabecular Architecture.ABS 2011, Long Beach, CA.

Saboori, P. Sadegh A. (2011d.) Brain Subarachnoid Space Architecture: Histological approach. IMECE 2011, Hyatt regency Denver and Colorado convection center.

Schachenmayr W. and Friede R. L. (1978). The origin of subdural neomembranes. I. Fine structure of the dura-arachnoid interface in man. Am J Pathol. 1978 July; 92(1): 53–68.

Kleiven S and Holst H (2002). Cosequences of Reduced Brain Volume Following Imoact in Prediction of Subdural Hematoma Evaluated with Numerical Techniques. Injury Prevention, 3:303-310.

Takhounts, E.G., Eppinger, R.H., Campbell, J.Q., Tannous, R.E., Powe , E.D., Shook, L.S. (2003a) On the development of the SIMon finite element head model. Stapp car Crash Journal 47: 107-133

Takhounts, E.G., Crandall, J.R., Darvish, K.K. (2003b) On the importance of nonlinearity of brain tissue under large deformation. Stapp car Crash Journal 47: 79-92

Takhounts EG, Ridella SA, Hasija V, Tannous RE, Campbell JQ, Malone D, Danelson K, Stitzel J, Rowson S, Duma S.(2008) Investigation of traumatic brain injuries using the next generation of simulated injury monitor (SIMon) finite element head model. Stapp Car Crash J. 2008 Nov;52:1-3

Trosseille X, Tarriere C, Lavaste F, Guillon F, Domont A (1992). Development of a F.E.M. of the Human Head According to a Specific Test Protocol. *Stapp Car Crash Conference*, 36:922527.

Truskey G, Yuan F, Katz D. (2003) Transport Phenomena in Biological Systems. Prentice Hall.

Van Der Rest M, Garrone R. (1991) Collagen family of proteins. Institute of Biology and Chemistry of Proteins (CNRS-UPR 412), Villeurbanne, France; Ecole Normale Sup#{233}rieure de Lyon, Lyon, France; and University {233} Claude Bernard, Lyon, France.

www. drrobertamoran.com

www.en.wikipedia.org

www.face-and-emotion.com

www. medical-dictionary.thefreedictionary.com

www. tree.com

www.vanat.cvm.umn.edu

www. wikieducator.org

Weinbaum S , Zhang X, Han Y, Vink H, Cowin C. S**,** (2002). Mechanotransduction and flow across the endothelial glycocalyx. PNAS 100(13): 7988-7995

Jin X, Lee JB, Leung LY, Zhang L, Yang KH, King AI. (2006). Biomech. Response of the Bovine Pia-Arachnoid Complex to Tensile Loading at Varying Strain-Rates. Stapp 50: 637-649.

Zhang ET, Inman CBE, Weller RO (1990). Interrelationship of the pia mater and the perivascular (Virchow-Robin) spaces in the human cerebrum. *Journal of Anatomy*,170: 111-123.

Zhang ET, Richards HK, Kida S, Weller RO (1992). Directional and compartmentalized drainage if interstitial fluid and cerebrospinal fluid from the rat brain. Acta:Neuropathology, 83: 233-239.

Zhang L, Yang KH, Dwarampudi R, Omori K, Li T, Chang K, Hardy WN, Khalil TB, King AI (2001a). Recent Advances in Brain Injury Research: A New Human Head Model Development and Validation. *Stapp Car Crash Conference,* 45: 2001-22-0017.

Zhang L, Yang KH, King AI (2001b). Biomechanics of neurotrauma. *Neurological Research,* 23: 144-156.

Zhang L, Yang KH, King AI (2001c). Comparison of Brain Responses Between Frontal and Lateral Impacts by Finite Element Modeling. *Journal of Neurotrauma,* 18: 21-30.

Zhang L, Bae J, Hardy WN, Monson KL, Manley GT, Goldsmith W, Yang KH, King AI (2002). Computational Study of the Contribution of the Vasculature on the Dynamic Response of the Brain. *Stapp Car Crash Conference,* 46: 2002-22-0008.

Zhang L, Yang KH, King AI, Viani D (2003). A NEW BIOMECHANICAL PREDICTOR FOR MILD TRAUMATIC BRAIN INJURY - A PRELIMINARY FINDING. Summer Bioengineering Conference June 25-29, 137-138.

Zhang QH, Teo, EC, Ng HW (2005). Development and Validation of A C0-C7 FE Complex for Biomechanical Study. Journal of Biomechanical Engineering, 127:729-735.

Zoghi M., Sadegh, A, Watkins, C. and Dan Dunlap (2008) Biodynamics Model For Operator Head Injury In Stand-Up Lift Trucks", Int. J. of Computer Methods in Biomechanics and Biomedical Engineering, Vol. 11 No. 4, pp 397-405.

Zoghi M, Sadegh A, (2009). Global/Local Head Models to Analyze Cerebral Blood Vessel Rupture Leading to ASDH and SAH" , Int. J. of Computer Methods in Biomechanics and Biomedical Engineering, vol. 12, issue 1, pp1-12.

Zoghi M., Sadegh, A, (2010). Equivalent Fluid Model for CSF and SAS Trabeculae Using Head/Brain Damping", Int. J. of Biomedical Engineering and Technology, Vol. 4 No. 3.

Zhou C, Khalil TB, King AI (1995). A New Model Comparing Impact Responses of the Homogeneous and Inhomogeneous Human Brain. Stapp Car Crash Conference, 39: 952741.